

**INVESTIGATION OF MODEL UPDATING TECHNIQUES AND THEIR
APPLICATIONS TO AIRCRAFT STRUCTURES**

**A THESIS SUBMITTED TO
THE GRADUATE SCHOOL OF NATURAL AND APPLIED SCIENCES
OF
MIDDLE EAST TECHNICAL UNIVERSITY**

BY

MUSTAFA TUĞRUL KOZAK

**IN PARTIAL FULFILLMENT OF THE REQUIREMENTS
FOR
THE DEGREE OF MASTER OF SCIENCE
IN
MECHANICAL ENGINEERING**

SEPTEMBER 2006

Approval of the Graduate School of Natural and Applied Sciences

Prof. Dr. Canan ÖZGEN
Director

I certify that this thesis satisfies all the requirements as a thesis for the degree of Master of Science.

Prof. Dr. Kemal İDER
Head of Department

This is to certify that we have read this thesis and that in our opinion it is fully adequate, in scope and quality, as a thesis for the degree of Master of Science.

Dr. Mutlu D. CÖMERT
Co-Supervisor

Prof. Dr. H. Nevzat ÖZGÜVEN
Supervisor

Examining Committee Members

Prof. Dr. Y. Samim ÜNLÜSOY (METU, ME) _____

Prof. Dr. H. Nevzat ÖZGÜVEN (METU, ME) _____

Dr. Mutlu D. CÖMERT (TÜBİTAK-SAGE) _____

Dr. Yiğit YAZICIOĞLU (METU, ME) _____

Prof. Dr. Yavuz YAMAN (METU, AEE) _____

I hereby declare that all information in this document has been obtained and presented in accordance with academic rules and ethical conduct. I also declare that, as required by these rules and conduct, I have fully cited and referenced all material and results that are not original to this work.

Name, Last Name: Mustafa Tuğrul KOZAK

Signature :

ABSTRACT

INVESTIGATION OF MODEL UPDATING TECHNIQUES AND THEIR APPLICATIONS TO AIRCRAFT STRUCTURES

KOZAK, Mustafa Tuğrul

M.S., Department of Mechanical Engineering

Supervisor: Prof. Dr. H. Nevzat ÖZGÜVEN

Co-Supervisor: Dr. Mutlu D. CÖMERT

September 2006, 140 pages

Mathematical models that are built in order to simulate the behavior of structures, most often, tend to respond differently than the actual structures in their initial state. In order to use the mathematical models and their computational outputs instead of testing the real structure under every possible case, it is mandatory to have a mathematical model that reflects the characteristics of the actual structure in the best possible way. In this thesis, the so called model updating techniques used for updating the mathematical models in order to make them respond in the way the actual structures do are investigated.

Case studies using computationally generated test data are performed using the direct and indirect modal updating techniques with the software developed for each method investigated. After investigating the direct and indirect modal updating techniques, two of them, one using frequency response functions and the other using modal sensitivities, are determined to be the most suitable ones for aircraft structures. A generic software is developed for the technique using modal sensitivities. A modal test is carried out on a scaled aircraft model. The test data is

used for updating of the finite element model of the scaled aircraft using the modal sensitivities and the usability of the method is thus evaluated. The finite element model of a real aircraft using the modal test data is also updated using the modal sensitivities.

A new error localization technique and a model updating routine are also proposed in this thesis. This modal updating routine is used with several case studies using computationally generated test data and it is concluded that it is capable of updating the mathematical models even with incomplete measured data.

Keywords: Modal Correlation, Modal Sensitivity, Mode Expansion, Model Reduction, Model Updating, Structural Dynamic Aircraft Finite Element Models, Structural Dynamics.

ÖZ

MODEL GÜNCELLEME TEKNİKLERİ VE BU TEKNİKLERİN HAVACILIK YAPILARINA UYGULAMALARI

KOZAK, Mustafa Tuğrul

Yüksek Lisans, Makina Mühendisliği Bölümü

Tez Yöneticisi: Prof. Dr. H. Nevzat ÖZGÜVEN

Ortak Tez Yöneticisi: Dr. Mutlu D. CÖMERT

Eylül 2006, 140 sayfa

Gerçek mühendislik yapılarının davranışlarını benzetebilmek için hazırlanan matematiksel modellerin ilk halleri çoğunlukla yapının davranışlarını gerçekçi biçimde yansıtmazlar. Gerçek yapının olası her koşul altında test edilmesi yerine, hazırlanan matematiksel modelleri ve bu modellerin çıktılarını kullanabilmek için, yapının davranışlarını mümkün olan en iyi şekilde yansıtan bir matematik modele gereksinim vardır. Bu tezde, matematiksel modeller üzerinde değişiklikler yaparak bu modellerin davranışlarını gerçek yapının davranışlarıyla örtüştürmeye çalışan model güncelleme yöntemleri incelenmiştir.

Doğrudan ve dolaylı model güncelleme yöntemleri, sayısal olarak türetilen test verileri ve hazırlanan kodlar kullanılarak incelenmiştir. Doğrudan ve dolaylı model güncelleme yöntemlerinin incelenmesi sonucunda, frekans tepki fonksiyonlarını ve modal duyarlılık değerlerini kullanan iki model güncelleme yönteminin havacılık yapılarının matematiksel modellerinin güncellenmesi için en uygun yöntemler olduğu sonucuna varılmıştır. Modal duyarlılık değerlerini kullanan model güncelleme yöntemi için genel kullanıma yönelik bir yazılım geliştirilmiştir.

Küçük ölçekli bir uçak modeline modal test uygulanmıştır. Bu testten elde edilen veriler, hazırlanan sonlu eleman modelinin modal duyarlılık değerlerini kullanan model güncelleme yöntemiyle güncellenmesinde ve bu sayede yöntemin uygunluğunun değerlendirilmesinde kullanılmıştır. Gerçek bir uçağın modal titreşim testi sonuçları kullanılarak, uçağın sonlu eleman modeli güncellenmiştir.

Bu tez kapsamında ayrıca yeni bir hata yeri tespit tekniği ve model güncelleme yöntemi de geliştirilmiştir. Bu yöntemin sayısal olarak türetilen test verileri ile kullanıldığı model güncelleme çalışmaları sonucunda, yöntemin ölçülen verilerin eksik olması durumunda dahi model güncelleme işlevini yerine getirdiği saptanmıştır.

Anahtar Kelimeler: Modal Duyarlılık, Modal Örtüştürme, Model Güncelleme, Model İndirgeme, Modal Veri Genişletme, Uçak Yapısal Dinamik Sonlu Eleman Modeli, Yapısal Dinamik.

To My Country TÜRKİYE, to my family and to my fiancée

ACKNOWLEDGEMENTS

I would like to express my sincere appreciation to my supervisor Prof. Dr. H. Nevzat ÖZGÜVEN and to my co-supervisor Dr. Mutlu D. CÖMERT for their precious guidance throughout this study.

The work in this thesis was performed for the practical research objectives of TÜBİTAK-SAGE. I wish to thank to TÜBİTAK-SAGE administration for allowing me to make this investigation and TÜBİTAK-SAGE for unfolding the computational and testing capabilities.

I would like to extend my special thanks to Mr. Erdiñ Nuri YILDIZ, Mr. Sertaç KÖKSAL and Mr. Fatih BÜKE for their cooperation in testing and programming stages.

Enormous thanks go to my parents Fatma Perizat KOZAK and Orhan KOZAK and my brother Yavuz KOZAK for their incredible support, trust, understanding to me and their precious encouragement throughout my all life and education. I also would like to thank to Miss Özge GÖKÇE, who will be my counterpart for the rest of my life, for her encouragement from the first sight.

At last, but not the least, I would like to send my thanks to my brothers in Middle East Technical University American Football Team METU FALCONS, with whom I have spilled sweat, tear and blood; have experienced triumph, championships and losses.

TABLE OF CONTENTS

PLAGIARISM.....	iii
ABSTRACT.....	iv
ÖZ.....	vi
ACKNOWLEDGEMENTS.....	ix
TABLE OF CONTENTS.....	x
LIST OF TABLES.....	xii
LIST OF FIGURES.....	xiii
NOMENCLATURE.....	xviii
ABBREVIATIONS.....	xix
 CHAPTERS	
1 INTRODUCTION.....	1
1.1 OBJECTIVES OF THE THESIS.....	1
1.2 BACKGROUND.....	1
1.3 SCOPE OF THE THESIS.....	8
2 OVERVIEW OF TECHNIQUES REQUIRED IN MODEL UPDATING METHODS.....	10
2.1 FINITE ELEMENT MODEL REDUCTION AND EXPERIMENTAL MODAL DATA EXPANSION.....	10
2.1.1 Finite Element Model Reduction.....	11
2.1.2 Expansion of Measured Modal Data.....	20
2.2 COMPARISON AND CORRELATION TECHNIQUES.....	26
2.2.1 Direct Comparisons.....	26
2.2.2 The Modal Assurance Criterion.....	27
2.2.3 The Coordinate Modal Assurance Criterion.....	28
2.2.4 Orthogonality Methods.....	28
3 THEORY OF MODEL UPDATING METHODS.....	30
3.1 DIRECT METHODS.....	30
3.1.1 Methods Using Lagrange Multipliers.....	31
3.1.2 Error Matrix Methods.....	34
3.1.3 Direct Matrix Updating.....	35
3.1.4 Matrix Mixing Methods.....	36
3.2 INDIRECT METHODS.....	37
3.2.1 Eigendynamic Constraint Method.....	37
3.2.2 Inverse Eigensensitivity Method.....	39
3.2.3 Response Function Method.....	46
3.2.4 Model Updating Based on MCI Minimization.....	49

4 SOFTWARE DEVELOPED.....	56
4.1 DETAILS OF THE SOFTWARE.....	56
5 CASE STUDIES.....	60
5.1 CASE STUDIES ON A SIX DOF SPRING MASS SYSTEM.....	60
5.1.1 Point FRF Results for Updating with the Method Using Lagrange Multipliers.....	62
5.1.2 Point FRF Results for Updating with the Error Matrix Methods.....	63
As this method ignores the 2 nd and higher order error terms, the obtained results are not exact ones.....	63
5.1.3 Point FRF Results for Updating with the Direct Matrix Updating Method	63
5.1.4 Point FRF Results for Updating with the Matrix Mixing Method.....	64
5.1.5 Point FRF Results for Updating with the Response Function Method	65
5.1.6 Point FRF Results for Updating with the MCI Minimization Method .	67
5.2 CASE STUDIES ON A 20 DOF FREE-FREE COMPOSITE BEAM USING THE MCI MINIMIZATION METHOD.....	71
5.3 CASE STUDY ON A SCALED AIRCRAFT MODEL USING THE INVERSE EIGENSENSITIVITY METHOD.....	77
5.4 CASE STUDIES ON AN AIRCRAFT MODEL (REAL LARGE STRUCTURE) USING THE INVERSE EIGENSENSITIVITY METHOD.....	99
5.4.1 Updating the Model of the Empty Aircraft.....	99
5.4.2 Updating of the Fully Loaded Aircraft.....	104
6 DISCUSSION, CONCLUSIONS AND RECOMMENDATIONS FOR FUTURE WORK.....	111
6.1 DISCUSSION.....	111
6.1.1 Discussion on Case Studies Performed Using Direct Methods.....	111
6.1.2 Discussion on Case Studies Performed Using with Miscorrelation Index (MCI) Minimization.....	112
6.1.3 Discussion on the Updating of the Scaled Aircraft Finite Element Model	113
6.1.4 Discussion on the Updating of the Real Aircraft Finite Element Model	114
6.2 CONCLUSIONS.....	115
6.3 RECOMMENDATIONS FOR FUTURE WORK.....	117
 REFERENCES.....	 118
 APPENDICES.....	 122
APPENDIX A.....	122
APPENDIX B.....	124
APPENDIX C.....	128

LIST OF TABLES

Table 1. Stiffness and Mass Values for Original Analytical and Pseudo-Experimental Model.....	61
Table 2. Experimental and Analytical Natural Frequencies and Initial Errors in the Natural Frequencies of the 6 DOF Spring-Mass System	61
Table 3. Geometric Parameters for Original Analytical and Pseudo-Experimental Model (mm)	71
Table 4. Material Property Ratios (Experimental/Analytical) for Original Analytical to Pseudo-Experimental Model	72
Table 5. Measurement Points and Directions.....	80
Table 6. Excitation Points and Directions.....	81
Table 7. Data Acquisition Details for Modal Testing of GARTEUR SM-AG19 Test-Bed	82
Table 8. MPC Element Details	87
Table 9. Material Properties Used in the Finite Element Model	88
Table 10. Experimental Modes and Correlating Original Finite Element Model's Modes.....	89
Table 11. Experimental Modes and Correlating Updated Theoretical Modes from the Finite Element Model.....	98
Table 12. Possible Parameters for which Sensitivities can be Calculated	131
Table 13. Settings for Modal Sensitivity Analysis.....	138

LIST OF FIGURES

Figure 1. Linear Estimation on a Single Variable Function.....	40
Figure 2. Flowchart for Updating MSC Nastran Models Using Inverse Eigensensitivity Method.....	45
Figure 3. Flowchart for the Response Function Method.....	48
Figure 4. Flowchart for the Inverse Eigensensitivity Analysis with the Software Generated.....	59
Figure 5. Spring-Mass System Used in Case Studies.....	60
Figure 6. Point Receptance (DOF of Mass 1) Plots (Experimental, Theoretical, Updated) Solved by Lagrange Multipliers Method for Error in Mass Matrix Only (No Error in Stiffness Matrix).....	62
Figure 7. Point Receptance (DOF of Mass 1) Plots (Experimental, Theoretical, Updated) Solved by Lagrange Multipliers Method for Error in Stiffness Matrix Only (No Error in Mass Matrix).....	62
Figure 8. Point Receptance (DOF of Mass 1) Plots (Experimental, Theoretical, Updated) Solved by Error Matrix Method.....	63
Figure 9. Point Receptance (DOF of Mass 1) Plots (Experimental, Theoretical, Updated) Solved by Direct Matrix Updating Method.....	64
Figure 10. Point Receptance (DOF of Mass 1) Plots (Experimental, Theoretical, Updated) Solved by Matrix Mixing Method.....	64
Figure 11. FRF Plots of Experimental, Original and Updated Models when Excitation and Response are at 1 st DOF.....	65
Figure 12. FRF Plots of Experimental, Original and Updated Models when Excitation and Response are at 2 nd DOF.....	65
Figure 13. FRF Plots of Experimental, Original and Updated Models when Excitation and Response are at 3 rd DOF.....	66
Figure 14. FRF Plots of Experimental, Original and Updated Models when Excitation and Response are at 4 th DOF.....	66
Figure 15. FRF Plots of Experimental, Original and Updated Models when Excitation and Response are at 5 th DOF.....	66
Figure 16. FRF Plots of Experimental, Original and Updated Models when Excitation and Response are at 6 th DOF.....	67

Figure 17. Absolute Maxima of MCI Values at All DOF's	68
Figure 18. Convergence of Updating Parameters	68
Figure 19. FRF Plots of Experimental, Original and Updated Models when Excitation and Response are at 1 st DOF	69
Figure 20. FRF Plots of Experimental, Original and Updated Models when Excitation and Response are at 2 nd DOF	69
Figure 21. FRF Plots of Experimental, Original and Updated Models when Excitation and Response are at 3 rd DOF	69
Figure 22. FRF Plots of Experimental, Original and Updated Models when Excitation and Response are at 4 th DOF	70
Figure 23. FRF Plots of Experimental, Original and Updated Models when Excitation and Response are at 5 th DOF	70
Figure 24. FRF Plots of Experimental, Original and Updated Models when Excitation and Response are at 6 th DOF	70
Figure 25. Illustration of the Beam Model Used in Second Case Study.....	72
Figure 26. The Absolute Maxima of the Starting MCI Values at All DOF's for an Elastic Cord Stiffness of 100 N/m.....	73
Figure 27. The Absolute Maxima of the Starting MCI Values at All DOF's for an Elastic Cord Stiffness of 1000 N/m.....	73
Figure 28. FRF Plots of the Experimental, the Original and the Updated Models when Excitation is at 9 th DOF and Response is at 1 st DOF for an Elastic Cord Stiffness of 100 N/m	74
Figure 29. FRF Plots of the Experimental, the Original and the Updated Models when Excitation is at 9 th DOF and Response is at 19 th DOF for an Elastic Cord Stiffness of 100 N/m	75
Figure 30. FRF Plots of the Experimental, the Original and the Updated Models when Excitation is at 9 th DOF and Response is at 9 th DOF for an Elastic Cord Stiffness of 100 N/m	75
Figure 31. FRF Plots of the Experimental, the Original and the Updated Models when Excitation is at 9 th DOF and Response is at 1 st DOF for an Elastic Cord Stiffness of 1000 N/m	75
Figure 32. FRF Plots of the Experimental, the Original and the Updated Models when Excitation is at 9 th DOF and Response is at 19 th DOF for an Elastic Cord Stiffness of 1000 N/m	76

Figure 33. FRF Plots of the Experimental, the Original and the Updated Models when Excitation is at 9 th DOF and Response is at 9 th DOF for an Elastic Cord Stiffness of 1000 N/m	76
Figure 34. The Absolute Maximum of the Final MCI Values at All DOF's for an Elastic Cord Stiffness of 100 N/m.....	77
Figure 35. The Absolute Maximum of the Final MCI Values at All DOF's for an Elastic Cord Stiffness of 1000 N/m.....	77
Figure 36. Test-Bed Tested in TÜBİTAK-SAGE.....	78
Figure 37. The Dimensions and Locations of the Aluminum Plates in GARTEUR SM-AG19 Test-Bed (Dimensions in mm)	79
Figure 38. Hooks for Elastic Cords.....	80
Figure 39. Excitation and Measurement Points and Coordinate Axes	80
Figure 40. Detailed Photographs of Modal Testing Setup.....	82
Figure 41. A Screenshot From LMS Modal Testing Software (Excitation and Measurement on z- Axis of Point 34)	83
Figure 42. Stability Diagram From POLYMAX	84
Figure 43. Visual Representations of the First 10 Modes Obtained From POLYMAX	85
Figure 44. Finite Element Mesh of the Test-Bed Structure (3-D View)	86
Figure 45. The Locations of the Strips in the Finite Element Model.....	86
Figure 46. MPC Elements in The Model.....	87
Figure 47. MAC Matrix between the Experimental Model and the Original Finite Element Model.....	88
Figure 48. Natural Frequency Comparison between the Experimental Model and the Original Finite Element Model	89
Figure 49. Visual Representations of the First 10 Modes Obtained From the Original Finite Element Model	91
Figure 50. Variation of Parameter Values through the Updating Procedure	92
Figure 51. MAC Matrix between the Updated Finite Element Model and the Experimental Model.....	93
Figure 52. Natural Frequency Comparison between the Updated Finite Element Model and the Experimental Model	93
Figure 53. Eigenvector Graphs for 1st Correlating Mode Pair.....	94
Figure 54. Eigenvector Graphs for 2nd Correlating Mode Pair	94

Figure 55. Eigenvector Graphs for 3rd Correlating Mode Pair	94
Figure 56. Eigenvector Graphs for 4th Correlating Mode Pair	94
Figure 57. Eigenvector Graphs for 5th Correlating Mode Pair	95
Figure 58. Eigenvector Graphs for 6th Correlating Mode Pair	95
Figure 59. Eigenvector Graphs for 7th Correlating Mode Pair	95
Figure 60. Eigenvector Graphs for 8th Correlating Mode Pair	95
Figure 61. Eigenvector Graphs for 9th Correlating Mode Pair	96
Figure 62. Eigenvector Graphs for 10th Correlating Mode Pair	96
Figure 63. Point FRF Values of Node 1 in z- Direction for the Experimental, the Analytical and the Updated Models	96
Figure 64. Visual Representations of the First 10 Modes Obtained From the Updated Finite Element Model	97
Figure 65. The Natural Frequency Graph for Experimental-Experimental and Experimental-Analytical Model Modes	100
Figure 66. MAC Matrix before Updating Procedure	100
Figure 67. The Natural Frequency Graph for Experimental-Experimental and Experimental-Analytical Model Modes (for Correlating Pairs)	101
Figure 68. MAC Matrix After Updating Procedure	101
Figure 69. Eigenvector Graphs for 1st Correlating Mode Pair.....	102
Figure 70. Eigenvector Graphs for 2nd Correlating Mode Pair	102
Figure 71. Eigenvector Graphs for 3rd Correlating Mode Pair	102
Figure 72. Eigenvector Graphs for 4th Correlating Mode Pair	103
Figure 73. Eigenvector Graphs for 5th Correlating Mode Pair	103
Figure 74. Eigenvector Graphs for 6th Correlating Mode Pair	103
Figure 75. Point FRF Curves for the Empty Aircraft: Measured (Experimental) and Calculated (Analytical and Updated Models) at the Right and the Left Wing Tips.....	104
Figure 76. The Natural Frequency Graph for Experimental-Experimental and Experimental-Analytical Model Modes	105
Figure 77. MAC Matrix before Updating Procedure	105
Figure 78. The Natural Frequency Graph for Experimental-Experimental and Experimental-Analytical Model Modes (for Correlating Pairs)	106
Figure 79. MAC Matrix after Updating Procedure	106
Figure 80. Eigenvector Graphs for 1st Correlating Mode Pair.....	107

Figure 81. Eigenvector Graphs for 2nd Correlating Mode Pair	107
Figure 82. Eigenvector Graphs for 3rd Correlating Mode Pair	107
Figure 83. Eigenvector Graphs for 4th Correlating Mode Pair	107
Figure 84. Eigenvector Graphs for 5th Correlating Mode Pair	108
Figure 85. Point FRF Curves for the Fully Loaded Aircraft: Measured (Experimental) and Calculated (Analytical and Updated Models) at the Right and the Left Wing Tips.....	109
Figure 86. “ <i>Model Variables</i> ” Submenu in MSC PATRAN 2004 r2 GUI.....	130
Figure 87. The Screen in MSC PATRAN 2004 r2 GUI in which Beam Dimensions can be Set as Parameters	131
Figure 88. The Screen on which Material Properties are Defined as Design Variables in MSC PATRAN 2004 r2 GUI.....	132
Figure 89. Location of “ <i>Design Study</i> ” Submenu Under MSC PATRAN 2004 r2 .	133
Figure 90. The Screen that Appears After Selection of “ <i>Design Study</i> ” in MSC PATRAN 2004 r2 GUI	133
Figure 91. The Screen for Selection of Updating Parameters.....	134
Figure 92. The Screen on which Design Objective is Set in MSC PATRAN 2004 r2 GUI	135
Figure 93. The Screen on which Natural Frequency is Set as a Modal Response for Sensitivity Calculations in MSC PATRAN 2004 r2 GUI	136
Figure 94. The Screen on which Mode Number, Mode Shape, Node and Degree of Freedom are Selected for Defining Eigenvector as a Modal Response for Sensitivity Calculations in MSC PATRAN 2004 r2 GUI.....	137
Figure 95. The Screen on which Analysis Settings are Done for a Modal Sensitivity Analysis in MSC PATRAN 2004 r2 GUI	137
Figure 96. Example File Format for Weight Sensitivity Values.....	138
Figure 97. Example File Format for Natural Frequency Sensitivity Values	139
Figure 98. Example File Format for Eigenvector Sensitivity Values.....	140

NOMENCLATURE

$\{F\}$	Forcing vector
i	Unit imaginary number
$[I]$	Identity matrix
$[K]$	Stiffness matrix
$[K_R]$	Reduced Stiffness matrix
$[M]$	Mass matrix
$[M_R]$	Reduced Mass matrix
$\{x\}$	Displacement vector
$\left\{\begin{matrix} \ddot{x} \\ x \end{matrix}\right\}$	Acceleration vector
$[\alpha]$	Receptance matrix of original system
$[\Delta M]$	Updating mass matrix
$[\Delta K]$	Updating stiffness matrix
$[\Delta C]$	Updating viscous damping matrix
$[\gamma]$	Receptance matrix of updated system
$\{\phi\}$	Mass normalized undamped modal matrix
$\{\omega\}$	Excitation frequency
$[]^T$	Transpose of a matrix

ABBREVIATIONS

FRF	Frequency Response Function
DOF	Degree of Freedom
IRS	Improved Reduced System
SEREP	System Equivalent Reduction Expansion Process
MCI	Miscorrelation Index

CHAPTER 1

INTRODUCTION

1.1 OBJECTIVES OF THE THESIS

The main objective of this work is to investigate the methods for correlating structural dynamic mathematical models to experimental data and correcting them, namely model updating techniques.

A significant number of works have been published and many model updating techniques have been proposed in the last twenty years. However, there are no exact or generally-applicable methods that ensure the model updating procedure to succeed. This study is an attempt to:

- Investigate the current model updating techniques and compare their performances under the same conditions
- Check the applicability of the current methods for updating of structural dynamic finite element models of aircraft and determine the most suitable one.
- Update a real aircraft model with most suitable (current) updating techniques
- Introduce a new error localization technique and a model updating method

1.2 BACKGROUND

The dynamic characteristic of a structure is a demanding knowledge in order to predict the response it will give during operation if the structure is under forces that vary with time continuously. The dynamic behavior of a structure can be obtained by using any or both of the two main methodologies, namely analytical and experimental. The analytical approach handles the problem by using a

mathematical model that represents the dynamic characteristics of the real structure. The experimental model is obtained by exciting the system (or using operational excitation) and measuring the corresponding responses. The most popular way for obtaining the analytical model is using the finite element method, where a continuous system is expressed by discrete parts (having dimensions larger than an infinitesimally small part) moving with known shape functions. The finite element method was originated in the field of structural analysis and was developed in the aerospace industry.

The finite element method can simply be explained by dividing the actual physical structure (for the case of structural analysis) into small elements. Each element can be thought of as a simple unit, the behavior of which can be analyzed by approximations on its displacement field (shape functions). After the elements and their functions have been chosen, the matrices, containing the properties of individual elements, must be determined. For this task, one of the following four approaches may be used: the direct approach, the variational approach, the weighted variational approach, or the energy balance approach [1]. The next step is to assemble all the element properties. The outcome of this action is the composed mass and stiffness matrices of dimension N , where N is the number of degrees of freedom in the model. The choice of N depends on the analysis and it should be large enough to minimize the discretization errors. The number of degrees of freedom and the mass and stiffness matrices of a structure can vary from one analysis to another, and from one element type to another. In any case, an accurate representation of damping matrices is not yet possible. The most common approach is building a proportional damping matrix that is based on experimentally-derived modal damping factors. The resulting mathematical model is a set of equations that may or may not accurately represent the actual structure's responses. The inaccuracies or uncertainties that may be present in finite element models can be divided into two categories:

- discretization errors,
- modeling errors.

The first category includes the errors that arise because of using numerical techniques. The most critical one is the discretization error which arises from

describing a continuous structure by a finite number of individual elements. The magnitude of this error depends on the finite element mesh quality and on the efficiency of the element shape functions [1]. Formulation errors arise from choosing elements that do not behave in the way the real structure behaves on the elemental scale.

The second category includes the modeling errors arising from the assumptions made by the analyst. These include the choice of elements to represent a given geometry (these errors generally occur because of the choice of incorrect element types; usually choosing elements having undesired shape functions), omission of some details, uncertainties coming from the boundary conditions that can not be defined by the embedded boundary conditions available in the FE code, etc. Although some of these errors will primarily create elemental (i.e. local) level errors, others will affect the global eigenparameters.

The coarsest possible mesh that gives satisfactory results should be obtained in order to have a balance between the discretization errors and computational effort. While having the minimum possible number of elements, the results of the finite element model should be similar to the one having a finer mesh. A quick and effective way of testing the finite element model, whether it has the minimum possible number of elements is as follows: First of all, the structure is divided into parts having a fine mesh density and the eigenvalues and eigenvectors are examined. After this point, the structure is modeled with a coarser mesh and the results are checked again. If the results of the fine and coarse meshed models fit each other, the structure can be modeled with even a coarser mesh density until the results get out of the bounds of the analyst's tolerance band. If, on the other hand, the first coarse model gives miscorrelated results compared with the original fine meshed model, the coarse model can not be used and the structure should be modeled with more elements until a good correlation is achieved.

The second way of examining the dynamic properties of a structure is testing and having an experimental model. Due to lack of confidence in analytical models, actual dynamic testing of structures has become a classical procedure to verify an existing finite element model or adjust it to match test results. For nearly four decades, modal testing has been a fast developing technique in the experimental evaluation of the dynamic properties. The data from a modal test has several uses:

- to verify finite element or other mathematical models,
- to predict the effects of a design change by structural coupling,
- to provide a basis for model updating.

Modal testing basically consists of two steps: Data acquisition and data analysis for the extraction of modal parameters such as natural frequencies, mode shapes and damping ratios. Modal testing is the action of exciting a structure with known forcing amplitudes and frequencies and acquisition of the resulting response of the structure. There are two main methods for exciting a structure. The structure can either be excited by an impact hammer or a shaker which is connected to the structure through a push rod (stinger). Sometimes more than one shaker may be used to excite the structure. Transducers, which are made from piezoelectric materials (materials yielding electrical potentials with deformation), are generally used to measure both the response and the excitation force on the structure. The response can be measured at one or more points, usually by accelerometers, which are connected to a data acquisition device. After the measurements have been performed, modal identification is accomplished in order to find the modal properties of the system. This area has been extensively developed and various techniques for identifying modal models from FRF data have been proposed (some of which have been implemented in a wide variety of commercial modal analysis software). Further details on the theoretical and practical aspects of vibration measurement techniques can be found in the works of Ewins [2], Maia and Silva *et al.* [3].

Just like analytical modeling, modal testing has also a number of problems:

- The number of accelerometers is limited, thus the size of the experimental model is almost always less than that of the analytical model.
- Yet, it is not possible to measure some degrees of freedom, such as rotational and internal ones (for example the structural parts under the structural skin of the wing of an aircraft).
- The number of extracted modes is limited by the frequency range.

- The modal analysis usually yields complex mode shapes while the theoretical model usually uses proportional damping, thus yielding normal modes only.
- Measured data are contaminated by a certain level of noise. Some modes of the structure may not be excited during the test or, even if excited, some modes may not be identified.
- Clamped boundary conditions are very difficult to achieve while free-free boundary conditions are subject to suspension effects, yielding rigid body modes having eigenvalues not equal to zero.
- The test structure may exhibit non-linearities while the analytical model usually assumes linearity.

The sources of error arising from the two modeling approaches are explained above. Each effect brings a certain amount of error into the model yielding differences in the dynamic characteristics reflected by the experimental and analytical models. Considering the modal test data as more reliable, the analytical model of the structure may be updated by using the data obtained from the modal test. This approach, known as model updating, tries to fit the analytical responses to the experimental ones by applying **numerical** changes to the original (or previous, if an iterative approach is used) analytical system matrices i.e., the mass, stiffness and, if taken into account, damping matrices.

Because of the different limitations and assumptions in the two approaches, the finite element model and the experimental modal model have different advantages and disadvantages. The finite element model provides information on dynamic behavior of the mathematical structure while the experimentally-derived model contains information from the actual structure.

Updating of an analytical model can be performed by applying changes to some specific elements (if an effective error localization technique is applied and erroneous elements are identified) or in a global sense (if the error is scattered).

The first model updating techniques were based on using the experimental modal data and updating the mathematical model directly. These methods can be

regarded as a class of system identification procedures rather than model updating schemes in indirect model updating methods. System parameters in the form of mass, stiffness and damping are extracted from the measured data and implemented in the original mathematical model.

Pioneers in indirect model updating methods have used different forms of constraints for building the updating matrices. Bar-Itzhack and Baruch [4] assumed that the original analytical mass matrix contained no error and made the updating on the stiffness matrix using Lagrange multipliers and orthogonality of the eigenvectors.

Berman [5] tried also to update the mass matrix. He used the same constraints (symmetricity and orthogonality constraints). Caesar [6] tried to update the free-free conditioned mathematical models by following the same approach as Berman. He introduced force equilibrium and rigid body modes as additional constraints in order to update the free-free models.

Sidhu and Ewins [7] have introduced the Error Matrix Method, which updates the analytical models directly. The experimental modal data is used in order to extract the experimental matrices, and the difference between those and the analytical system matrices are defined as error matrices. The resulting error is assumed to be approximated by binomial expansion. This condition leads the method not to be an exact one as the second and higher order terms in error are neglected. Gypsin [8] have proved that this method loses accuracy in case of incomplete modes. Expansion yields a model that has a connectivity character different than the original model which can yield physically meaningless system matrices. Link [9] and Caesar [10] used the analytical mode shapes for the missing experimental data.

Link *et al.* [11] proposed a direct model updating method known as Matrix Mixing Method which uses orthogonality conditions and performs updating on both analytical mass and stiffness matrices.

The use of FRF data instead of modal data brought new advantages. Since the modal data are extracted from the FRF data, there are no errors that would come

from the modal parameter extraction (modal analysis) stage. Moreover, there are much more points for building the updating equations which can improve stability. This means that the problem can be made more overdetermined (a system of equations having more equations than unknowns) compared to the modal data based model updating techniques.

Lin and Ewins [12], Larsson and Sas [13], Lammens [14] have proposed application of FRF data for updating the analytical models. Visser and İmregün [15], [16] dealt with the problem of coordinate incompleteness and introduced a new scheme for building the resulting set of linear equations. They proposed using the analytical FRF data for incomplete degrees of freedom and discarded those equations in the final solution.

The response function method [12] is an indirect method which tries to correlate the experimental and analytical FRF data for the selected updating frequencies. Although it seems that the number of equations will be a multiple of the frequency points of the experimental data, there is almost no way to include all the frequency points as there will be contamination on the experimental FRF data for some higher frequency points and linear dependency of some equations built by using different frequency points.

A frequency response based model updating method which also uses the sensitivities of dynamic stiffness matrices has also been proposed [3].

Fox and Kapoor [17] used the first order sensitivities of modal data with respect to the selected updating parameters which is the origin of the Inverse Eigensensitivity Method. This method needs a number of corresponding modes (both in the experimental and analytical models) to be identified. The pairing of the experimental and analytical modes can be made by visual inspection (by animating the mode shapes) or by numerical means such as MAC matrix. As there will be possible frequency errors between correlated modes, there can also be some shifts in the ranking of some modes. The procedure needs pairing of correlated modes after each iteration step and computations will end until desired convergence has been accomplished.

The updating parameters are chosen after an investigation on their numerical values. In order to have rapidly converging systems, parameters with the highest sensitivity values are chosen as the updating parameters.

Göge [18] worked on the Inverse Eigensensitivity Method and applied this method to the data and finite element model obtained from a real commercial aircraft. He chose the Young's Modulus and area moments of inertia of some dimensionally long/large parts (which have higher sensitivities) and accomplished model updating of the real aircraft.

İmregün and Visser [19] summarized the model updating techniques with their possible areas of application.

Mottershead *et al.* [20] proposed the ways for obtaining the best updating parameters in a work on an aluminum space frame model.

There are also a number of MSc and PhD thesis studies accomplished in the Imperial College of Science and Medicine ([1], [21], [22]) and an MSc thesis presented in the Middle East Technical University by Karaman [23].

Ewins [2], Maia, Silva *et al.* [3] have included chapters on model updating in their books on modal analysis. Also, a book that is completely on Model Updating has been written by Friswell and Mottershead [24].

1.3 SCOPE OF THE THESIS

Chapter 2 includes the current methods on preliminary model updating actions, namely model reduction, modal data expansion and correlation techniques.

Chapter 3 focuses on the methods of model updating and summarizes the methods under two basic categories:

- Direct Model Updating Methods
- Indirect Model Updating Methods

Strengths and weaknesses of the current methods are discussed in the same chapter. A new error localization technique and model updating method named as “Miscorrelation Index Minimization Technique” are also given in this chapter.

Chapter 4 gives the details of the computer code generated.

Chapter 5 includes the case studies performed by using seven different model updating methods investigated in order to draw an objective comparison among them. A six degree of freedom mass-spring system is solved with all of these methods (except the Inverse Eigensensitivity Method) in order to investigate the performance of the methods. Two case studies based on real experimental data (one of which is from a real aircraft) are solved with the Inverse Eigensensitivity Method. Finally, case studies to study the robustness of the MisCorrelation Index (MCI) minimization technique are also given in this chapter.

Chapter 6 is the one containing the discussions and conclusions based on the case studies of Chapter 5. Recommendations for future researchers are also given in this chapter.

Basic information on least squares regression for a set of linear equations, procedures for inserting system matrices in MSC Nastran and the instructions that should be followed in MSC Patran GUI in order to obtain the sensitivity values from MSC Nastran are given in Appendix A, Appendix B and Appendix C, respectively.

CHAPTER 2

OVERVIEW OF TECHNIQUES REQUIRED IN MODEL UPDATING METHODS

2.1 FINITE ELEMENT MODEL REDUCTION AND EXPERIMENTAL MODAL DATA EXPANSION

The finite element model updating will hardly ever start as soon as the modal data is obtained. Some computations should be done before the model updating stage in order to correlate the degrees of freedom in the analytical and experimental models that are compared.

Before starting the updating procedure, it is favorable to compare the analytical and experimental data sets to obtain insight as to whether both sets are in reasonable agreement so that updating is at all possible. Unfortunately, there will be an incompatibility in the size of the analytical and experimental models to be correlated.

There are two main differences between analytical and experimental models

- Insufficient number of modes
- Insufficient number of measured degrees of freedom.

The former insufficiency arises from the limited bandwidth of data acquisition. This brings a limitation on the frequency range of the experimental data.

The latter problem can be handled by either of the following two approaches:

- Reduction (condensation) of the large analytical model's slave (non-measured) degrees of freedom without perturbing the modal and spatial properties of the structure. In practice, although the kinetic energy or

potential energy is retained, or both compromised, original system connectivity is lost.

- Expansion of the smaller model to match the larger counterpart.

Due to the fact that some degrees of freedom (apart from rotational ones) can not be measured and to the difficulty in handling the rotational degrees of freedom, the experimental model is usually expanded over the finite element data (not to lose data arising from the degrees of freedom mentioned above). However, if the number of the original finite element degrees of freedom that are in relation to the measured degrees of freedom is not large, then dilution of the modal test data and loss of local properties arise. If such a case is to be handled, reduction of the finite element model should be preferred [3].

In the following sections, reduction of the finite element model and expansion of the experimental model are discussed in detail.

2.1.1 Finite Element Model Reduction

The aim of finite element model reduction is to bring the size of the analytical model's spatial matrices to the same as that of the experimental model. In other words, if n measurement locations are used for data acquisition, the linear degrees of freedom in the analytical model should also be n (if no expansion is carried out), where the degrees of freedom kept must be in accordance with the experimental counterparts.

There are three popular reduction techniques in the literature:

- Guyan (static) reduction.
- IRS (Improved Reduction System).
- SEREP (System Equivalent Reduction Expansion Process).

2.1.1.1 Guyan Reduction

This method, also known as “Static Condensation” has been proposed by Guyan [25] and is one of the most popular reduction techniques (embedded in some commercial model updating and FE codes). The method can be summarized as follows:

For a linear system, the equation of motion can be written as

$$[K]\{x\} = \{F\} \quad (2.1)$$

where

$[K]$, $\{x\}$ and $\{F\}$ denote the stiffness matrix, the displacement vector and the forcing vector respectively.

If the forcing on the system is not applied to all the degrees of freedom, then the matrices and vectors can be partitioned as

$$\begin{bmatrix} [K_{ss}] & [K_{sp}] \\ [K_{ps}] & [K_{pp}] \end{bmatrix} \begin{Bmatrix} \{x_s\} \\ \{x_p\} \end{Bmatrix} = \begin{Bmatrix} \{0\} \\ \{F_p\} \end{Bmatrix} \quad (2.2)$$

where indices s and p denote slave and primary, respectively. That is, the degrees of freedom with forcing are called as the primary ones while the rest are called as slave degrees of freedom. For the case of modal testing, the term primary denotes the degrees of freedom at which measurement is done and the term slave refers to the remaining degrees of freedom.

From the system of equations given in Eq. (2.2), the following equation can be written by using the first row

$$[K_{ss}]\{x_s\} + [K_{sp}]\{x_p\} = \{0\} \quad (2.3)$$

or by equating the terms, the following expression can be obtained:

$$[K_{ss}]\{x_s\} = -[K_{sp}]\{x_p\} \quad (2.4)$$

Leaving the slave degrees of freedom alone, $\{x_s\}$ can be solved as

$$\{x_s\} = -[K_{ss}]^{-1}[K_{sp}]\{x_p\} \quad (2.5)$$

Rewriting the displacement vector and equation Eq. (2.2) in terms of $\{x_p\}$

$$\{x\} = \begin{Bmatrix} \{x_s\} \\ \{x_p\} \end{Bmatrix} = \begin{bmatrix} -[K_{ss}]^{-1}[K_{sp}] \\ [I] \end{bmatrix} \{x_p\} \quad (2.6)$$

one obtains the transformation matrix $[T]$ that relates the whole degrees of freedom in the model to the primary degrees of freedom. That is,

$$\{x\} = [T]\{x_p\} \quad (2.7)$$

and

$$\{x\}^T = \{x_p\}^T [T]^T \quad (2.8)$$

with

$$[T] = \begin{bmatrix} -[K_{ss}]^{-1}[K_{sp}] \\ [I] \end{bmatrix} \quad (2.9)$$

The potential and kinetic energy relations can be written as follows:

$$PE = \frac{1}{2} \{x\}^T [K] \{x\} \quad (2.10)$$

$$KE = \frac{1}{2} \left\{ \dot{x} \right\}^T [M] \left\{ \dot{x} \right\} \quad (2.11)$$

one can substitute $\{x\}$ and $\left\{ \dot{x} \right\}$ with $\{x_p\}$ and $\left\{ \dot{x}_p \right\}$ having

$$PE = \frac{1}{2} \{x_p\}^T [T]^T [K] [T] \{x_p\} \quad (2.12)$$

$$KE = \frac{1}{2} \left\{ \dot{x}_p \right\}^T [T]^T [M] [T] \left\{ \dot{x}_p \right\} \quad (2.13)$$

For the reduced system to have the same potential and kinetic energy values as the original system, the mass and stiffness matrices of the reduced system should be taken as

$$[K_{GR}] = [T]^T [K] [T] \quad (2.14)$$

$$[M_{GR}] = [T]^T [M] [T] \quad (2.15)$$

So, the resulting eigenvalue problem becomes

$$[[K_{GR}] - \omega^2 [M_{GR}]] \{u_p\} = \{0\} \quad (2.16)$$

yielding ω_r and $\{u_p\}^r$, where the mode shape vector $\{\varphi\}^r$ is obtained from

$$\{\varphi\}^r = [T] \{u_p\}^r \quad (2.17)$$

As the formulation omits the inertial effects (this is the reason why the method is called as static condensation), the selection of the primary degrees of freedom becomes very important. Poor results will be obtained by the choice of “incorrect” sets of degrees of freedom [1]. The omitted degrees of freedom should have mass effects of lower magnitude than the kept ones.

2.1.1.2 Improved Reduction System

Including the inertial effects to the system that is described in Guyan's reduction Method, Improved Reduction System proposed by O'Callahan [26], forms the equation of motion as

$$\left(\begin{bmatrix} [K_{ss}] & [K_{sp}] \\ [K_{ps}] & [K_{pp}] \end{bmatrix} - \omega^2 \begin{bmatrix} [M_{ss}] & [M_{sp}] \\ [M_{ps}] & [M_{pp}] \end{bmatrix} \right) \begin{Bmatrix} \{x_s\} \\ \{x_p\} \end{Bmatrix} = \begin{Bmatrix} \{0\} \\ \{0\} \end{Bmatrix} \quad (2.18)$$

where, the equality holds for ω values equal to the natural frequencies of the system. Taking the upper row of the partitioned set of equations yields

$$[[K_{ss}] - \omega^2 [M_{ss}]] \{x_s\} = -[[K_{sp}] - \omega^2 [M_{sp}]] \{x_p\} \quad (2.19)$$

$$\{x_s\} = -[[K_{ss}] - \omega^2 [M_{ss}]]^{-1} [[K_{sp}] - \omega^2 [M_{sp}]] \{x_p\} \quad (2.20)$$

$$\{x_s\} = -[[I] - \omega^2 [K_{ss}]^{-1} [M_{ss}]]^{-1} [K_{ss}]^{-1} [[K_{sp}] - \omega^2 [M_{sp}]] \{x_p\} \quad (2.21)$$

By using the binomial theorem,

$$[[I] - \omega^2 [K_{ss}]^{-1} [M_{ss}]]^{-1} = [[I] + \omega^2 [K_{ss}]^{-1} [M_{ss}] + O(\omega^4)] \quad (2.22)$$

$$\{x_s\} = -[K_{ss}]^{-1} [[I] + \omega^2 [K_{ss}]^{-1} [M_{ss}] + O(\omega^4)] [[K_{sp}] - \omega^2 [M_{sp}]] \{x_p\} \quad (2.23)$$

$$\{x_s\} = -[K_{ss}]^{-1} [[K_{sp}] - \omega^2 ([M_{sp}] + [K_{ss}]^{-1} [M_{ss}] [K_{sp}]) + O(\omega^4)] \{x_p\} \quad (2.24)$$

where the ω^4 terms are considered in the error term which is of order four and higher.

As the equality is only valid for the natural frequencies, one can use the ω term as

$$\omega^2 [M] \{u\} = [K] \{u\} \quad (2.25)$$

or as

$$\omega^2 [M_{GR}] \{u_p\} = [K_{GR}] \{u_p\} \quad (2.26)$$

for the Guyan reduced system. Rewriting Eq. (2.26) as follows

$$\omega^2 \{u_p\} = [M_{GR}]^{-1} [K_{GR}] \{u_p\} \quad (2.27)$$

substituting ω^2 term with $[M_{GR}]^{-1} [K_{GR}]$ and omitting the ω^4 terms, Eq. (2.24) can be written as

$$\{x_s\} = -[K_{ss}]^{-1} [[K_{sp}] - ([M_{sp}] + [K_{ss}]^{-1} [M_{ss}] [K_{sp}]) [M_{GR}]^{-1} [K_{GR}]] \{x_p\} \quad (2.28)$$

In order to have Eq. (2.28) in a relatively compact form, let us call $-[[K_{ss}]^{-1} [K_{sp}]]$ as T_s and write Eq. (2.28) as follows

$$\{x_s\} = (T_s + SMT_s M_{GR}^{-1} K_{GR}) \{x_p\} \quad (2.29)$$

so that the resulting transformation matrix T_{irs} becomes

$$T_{irs} = T_s + SMT_s M_{GR}^{-1} K_{GR} \quad (2.30)$$

where T_s is

$$T_s = T_{static} = -[K_{ss}]^{-1} [K_{sp}] \quad (2.31)$$

and

$$S = \begin{bmatrix} [0] & [0] \\ [0] & [K_{ss}]^{-1} \end{bmatrix} \quad (2.32)$$

M_{GR} , K_{GR} are the Guyan reduced mass and stiffness matrices respectively.

Using an iterative approach (as the higher order terms are neglected, the solution is not exact), the transformation matrix can be obtained by

$$T_{irs,i+1} = T_s + SMT_{irs,i}M_{irs,i}^{-1}K_{irs,i} \quad (2.33)$$

where

$M_{irs,i}$ and $K_{irs,i}$ are the reduced mass and the stiffness matrices at the i^{th} iteration step, obtained as follows:

$$[K_{irs}] = [T_{irs}]^T [K] [T_{irs}] \quad (2.34)$$

$$[M_{irs}] = [T_{irs}]^T [M] [T_{irs}] \quad (2.35)$$

The procedure for the iterations is as follows,

1. The static transformation matrix in Eq. (2.31) is calculated
2. Using Eq. (2.34) and Eq. (2.35) and the static transformation matrix; $M_{irs,i}$, $K_{irs,i}$ are calculated
3. Using Eq. (2.33), $T_{irs,i+1}$ is calculated
4. The reduced mass and stiffness matrices are calculated using steps 2 and 3 until convergence is achieved.

The IRS method was developed in order to improve the Guyan reduction method. For the static case, both methods yield the same exact solution as they both use the full system stiffness matrices. However, Guyan reduction does not account for

the inertial forces so that for the dynamic case, IRS has a better the accuracy compared to the Guyan reduction method [1]. IRS uses the output of Guyan reduction as a first step and then applies a correction accounting for the inertial forces. Therefore, when the mass effects associated with the omitted degrees of freedom are significant, IRS develops better solutions than Guyan reduction does [27].

2.1.1.3 System Equivalent Reduction Expansion Process

SEREP is a transformation technique, proposed by O'Callahan and Li [28], which preserves the dynamic characteristics through the collection of a set of desired eigenmodes. The displacement vector can be expressed in terms of mode shapes and generalized coordinates as

$$\begin{Bmatrix} \{x_s\} \\ \{x_p\} \end{Bmatrix} = \begin{bmatrix} [\varphi_{ss}] & [\varphi_{sp}] \\ [\varphi_{ps}] & [\varphi_{pp}] \end{bmatrix} \begin{Bmatrix} \{u_s\} \\ \{u_p\} \end{Bmatrix} \quad (2.36)$$

The displacement vector for the primary degrees of freedom, then can be written using the lower row in Eq. (2.36) as,

$$\{x_p\} = [\varphi_{ps}] \{u_s\} + [\varphi_{pp}] \{u_p\} \quad (2.37)$$

writing Eq. (2.36) in a compact form yields,

$$\begin{Bmatrix} \{x_s\} \\ \{x_p\} \end{Bmatrix} = \begin{bmatrix} [\varphi_s] \\ [\varphi_p] \end{bmatrix} \{u\} \quad (2.38)$$

where $[\psi_s]$ and $[\psi_p]$ are the slave and primary mode shape sub-matrices, respectively.

$$\{x_p\} = [\varphi_p] \{u\} \quad (2.39)$$

$$\{u\} = [\varphi_p]^+ \{x_p\} \quad (2.40)$$

where $[\]^+$ represents the generalized inverse of a matrix.

$[\varphi_p]$ is a matrix of size $m \times p$, where m is the number of degrees of freedom and p is the number of modes, then the generalized inverses will have the form:

$$[\varphi_p]^+ = [\varphi_m^T \quad \varphi_m]^1 \varphi_m^T \text{ if } m > p \text{ and} \quad (2.41)$$

$$[\varphi_p]^+ = \varphi_m^T [\varphi_m \quad \varphi_m^T]^{-1} \text{ if } m < p \quad (2.42)$$

The displacement vector can be written in terms of only mode shapes as

$$\begin{Bmatrix} \{x_s\} \\ \{x_p\} \end{Bmatrix} = \begin{bmatrix} [\varphi_s] \\ [\varphi_p] \end{bmatrix} [\varphi_p]^+ \{x_p\} \quad (2.43)$$

From Eq. (2.43) the transformation matrix can be extracted as,

$$T_{SEREP} = \begin{bmatrix} [\varphi_s] \\ [\varphi_p] \end{bmatrix} [\varphi_p]^+ \quad (2.44)$$

The eigenvalue problem, solved with SEREP reduced system matrices, preserves the same eigenvalues and eigenvectors (for preserved degrees of freedom) for the retained modes.

To sum up the reduction techniques, no matter what procedure is used, spatial information of the finite element model will either be lost or dispersed during reduction techniques. Compared to the others, Guyan reduction is the best for comparison/correlation operations for low order modes as it preserves the low order modal properties for which inertial effects are relatively low (and because of its simplicity, it is used in many commercial software).

2.1.2 Expansion of Measured Modal Data

An alternative approach to reducing the finite element model is to expand the measured mode shapes by estimating the unmeasured degree of freedom. In general, more confidence can be placed in the expanded results by increasing the number of measurement points.

Basically, the expansion methods in the literature can be classified into 4 groups, differing by the way they approximate the unmeasured data:

- **Analytical eigenvector substitution:** This method directly substitutes the analytical slave degrees of freedom for the unmeasured data, without using the available measurements.
- **Direct data generation using the finite element model and experimental data:** The SEREP method creates a transformation matrix from the master degrees of freedom to the complete finite element coordinate system. Kidder's method [29] creates a spatial transformation formulated using the analytical mass and stiffness matrices and partitioning the generalized eigenvalue problem.
- **Indirect data generation using finite element model:** A geometric fit of the experimental data is enhanced by knowledge acquired from the finite element model.
- **Expansion of experimental data in isolation:** These methods interpolate the experimental data by fitting a continuous function through the data by means of cubic splines, surface splines or polynomial fits.

The first group of methods mentioned is based on an almost correct finite element model as it has no feedback from experimental results. The second and third group of methods use both finite element and experimental models, which can be an advantage for expanding the rotational degrees of freedom, compared to the fourth method group using only experimental data.

While using both analytical and experimental models seems to have an advantage in expanding the rotational degrees of freedom for which there exists no experimental data, a problem arises because of using the analytical model. Use of the analytical model mixes the experimental data with the analytical data for which a clear degree of confidence can not be shown. This means that the experimental data will contain the error of the analytical data.

Also, another disadvantage will be the fake correlated pairs for which expansion is applied. As the analytical and experimental models are correlated and as expanded data will carry information about the analytical model, a high degree of correlation, although not having certainty, may be observed.

Having mentioned the need for expansion and approaches in different expansion techniques, some popular methods that are frequently used are explained below.

2.1.2.1 Kidder's Method (Inverse Guyan Reduction)

This is the most commonly used expansion method [3], which is effectively derived from an inverse Guyan reduction [29]. Partitioning the generalized eigenvalue problem for the analytical model one can obtain

$$\left(\begin{bmatrix} [K_{ss}] & [K_{sp}] \\ [K_{ps}] & [K_{pp}] \end{bmatrix} - \omega_r^2 \begin{bmatrix} [M_{ss}] & [M_{sp}] \\ [M_{ps}] & [M_{pp}] \end{bmatrix} \right) \begin{Bmatrix} \{\varphi_s\}^r \\ \{\varphi_p\}^r \end{Bmatrix} = \begin{Bmatrix} \{0\} \\ \{0\} \end{Bmatrix} \quad (2.45)$$

By using the upper row of the partitioned set of equations one can write

$$\left[[K_{ss}] - \omega_r^2 [M_{ss}] \right] \{\varphi_s\}^r = - \left[[K_{sp}] - \omega_r^2 [M_{sp}] \right] \{\varphi_p\}^r \quad (2.46)$$

Then, the slave mode shape vector for the r^{th} mode can be obtained as

$$\{\varphi_s\}^r = - \left[[K_{ss}] - \omega_r^2 [M_{ss}] \right]^{-1} \left[[K_{sp}] - \omega_r^2 [M_{sp}] \right] \{\varphi_p\}^r \quad (2.47)$$

Now, in the mode shape vectors for the r^{th} mode, if p is replaced by mea representing the measured coordinates and s is replaced by exp representing the expanded coordinates, Eq. (2.47) can be rewritten as

$$\{\phi_{exp}\}^r = -\left[\left[K_{ss}\right] - \omega_r^2 \left[M_{ss}\right]\right]^{-1} \left[\left[K_{sp}\right] - \omega_r^2 \left[M_{sp}\right]\right] \{\phi_{mea}\}^r \quad (2.48)$$

By using the above relation, measured mode shapes can be expanded by using a transformation matrix including analytical spatial matrix data.

2.1.2.2 Expansion Using Analytical Modes

In this expansion method, the complete coordinates in the experimental model are generated by assuming that each mode is constructed from a linear combination of the analytical modes. In other words, the relation (transfer function) between the responses in the measured coordinates and their counterparts in the analytical model is used as a reference between the unmeasured coordinates that are present in the analytical model. So, the method assumes that the relation will be valid for the unmeasured degrees of freedom. In order to formulate the method, the following expressions can be given.

The analytical mass normalized mode shape matrix is partitioned as follows (for m measured modes and n measured degrees of freedom):

$$[\phi]_A = \begin{bmatrix} [\phi_{11}]_A & [\phi_{12}]_A \\ [\phi_{21}]_A & [\phi_{22}]_A \end{bmatrix} \begin{matrix} n \\ N-n \end{matrix} \quad (2.49)$$

$m \qquad N-m$

The expanded experimental modal data can be constructed from a linear combination of the chosen analytical modes by

$$\left\{ \begin{matrix} \{\phi_1^{exp}\}_X^r \\ \{\phi_1^{exp}\}_X^r \end{matrix} \right\} = \begin{bmatrix} [\phi_{11}]_A \\ [\phi_{21}]_A \end{bmatrix} \{v\}^r \quad (2.50)$$

$$\{\phi_1^{\text{exp}}\}_X^r = [\phi_{21}]_A \{\nu\}^r \quad (2.51)$$

$$\{\phi_2^{\text{exp}}\}_X^r = [\phi_{21}]_A \{\nu\}^r \quad (2.52)$$

where $\{\nu\}^r$ is the linearity relationship that is used for relating the analytical mode shape matrix to the r^{th} experimental one.

$$\{\nu\}^r = [\phi_{11}]_A^+ \{\phi_1\}_X^r \quad (2.53)$$

Since in general, the number of measured coordinates and the number of the measured modes will not be the same, the matrix $[\phi_{11}]_A$ will not be square. The inverse of this matrix will be calculated by using the following ways,

- If $n=m$, the pseudo-inverse in Eq. (2.53) becomes the standard inverse and $\{\phi_1^{\text{exp}}\}_X^r = \{\phi_1\}_X^r$. This means that the expanded mode fits the experimental data exactly.
- If $n>m$, a linear combination of analytical modes is found that fits the experimental data in a least-squares sense. Consequently, $\{\phi_1^{\text{exp}}\}_X^r$ is a smoothed counterpart of $\{\phi_1\}_X^r$.
- If $n<m$, then the pseudo-inverse in Eq. (2.53) is rank deficient and the solution is likely to be physically meaningless.

The rotational degree of freedom data of the analytical model can be used for expansion of the experimental data. Assume that n shows the mode shape data of the translational degrees of freedom and $N - n$ shows the mode shape data of the rotational degrees of freedom. Partitioning the analytical mode shape matrix, one obtains

$$[\phi]_A = \begin{bmatrix} [\phi_{11}]_A & [\phi_{12}]_A \\ [\phi_{21}]_A & [\phi_{22}]_A \end{bmatrix} \begin{matrix} n \\ N - n \end{matrix} \quad \begin{matrix} m \\ N - m \end{matrix} \quad (2.54)$$

Assuming also that, the translational degree of freedom data does exist in the experimental model, so

$$\{\nu\}^r = [\phi_{11}]_A^+ \{\phi_1\}_X^r \quad (2.55)$$

shows the linear relationship for the translational degrees of freedom. Then, the rotational degree of freedom data can be found by

$$\{\phi_2^{\text{exp}}\}_X^r = [\phi_{21}]_A \{\nu\}^r \quad (2.56)$$

where $[\phi_{21}]_A$ is the mode shape matrix for the rotational degrees of freedom in the finite element model and $\{\phi_2^{\text{exp}}\}_X^r$ is the mode shape vector for the rotational degrees of freedom in the experimental model for the r^{th} mode.

The success of this method is critically dependent on the selected set of analytical modes, which must include a reasonable counterpart to each experimental mode. In other words, if a relation between an experimentally obtained mode and a finite element based mode will be obtained, and if the aim is to have a relation that will reflect the real case as much as possible, then a correlated pair of experimental and analytical modes should be selected. If a mode that does not appear in the experimental model is present in the matrix $[\phi_{11}]_A$, then the relation vector $\{\nu\}^r$ will not yield a meaningful transfer function. The results of the comparison methods can drive the selection.

2.1.2.3 SEREP Expansion

Expansion using SEREP is based on the same formulation as the reduction scheme of SEREP. The difference is that, the output is not a system of space matrices but a modal one. The method uses the analytical mode shapes, partitioned in such a manner that a transformation matrix interprets the full displacement solution by using only primary mode shapes. Then, this

transformation matrix is used to expand the experimental modal data using measured mode shapes.

The partitioned form of the displacement vector, in terms of the mode shape matrix and the generalized coordinate vector is given by

$$\begin{Bmatrix} \{x_s\} \\ \{x_p\} \end{Bmatrix} = \begin{bmatrix} [\phi_s] \\ [\phi_p] \end{bmatrix} \{q\} \quad (2.57)$$

Using the primary set of equations, one obtains

$$\{x_p\} = [\phi_p] \{q\} \quad (2.58)$$

The above equation gives the relation between the primary displacements and primary mode shapes and generalized coordinates. If the generalized coordinate vector is expressed in terms of the primary mode shapes and the primary displacements as follows,

$$\{q\} = [\phi_p]^+ \{x_p\} \quad (2.59)$$

then the relation between the physical displacement set and mode shapes can be written as (by replacing the generalized displacement vector in Eq. (2.57) by Eq. (2.59))

$$\{x\} = \begin{bmatrix} [\phi_s] \\ [\phi_p] \end{bmatrix} [\phi_p]^+ \{x_p\} \quad (2.60)$$

The above equation gives the transformation matrix of SEREP as

$$T_{serep\exp} = \begin{bmatrix} [\phi_s] \\ [\phi_p] \end{bmatrix} [\phi_p]^+ \quad (2.61)$$

Unless curve fitting techniques are used, the expanded modal data will contain effects of the analytical model, which contains errors. So, although the expanded data are not fit randomly, they will not yield the exact characteristics of the experimental model. Keeping this in mind, it should be remembered that a good correlation between the expanded experimental model and the analytical model does not exactly mean that the original model is almost correct. This good correlation may be because of the analytical data that is embedded in the experimental data through the expansion process.

2.2 COMPARISON AND CORRELATION TECHNIQUES

Before starting model updating, certain comparison and correlation methods have to be applied in order to

- Detect how well the initial analytical model fits the experimental one (as well as how the updated model fits the experimental model),
- Detect the parts of the model that contain error,
- Detect which mode pairs in analytical and experimental ones are equivalent.

If the initial correlation between the analytical and experimental model were “good enough” for the frequency range of interest, then no updating action would be necessary. Unfortunately, because of the assumptions through FE modeling itself, no perfect initial correlation will be obtained; so that updating will be necessary.

This section introduces the common popular methods in the literature about model comparison and correlation techniques.

2.2.1 Direct Comparisons

Natural frequencies and mode shapes coming from analytical and experimental models can be compared directly as follows:

The natural frequencies of analytical and experimental models are plotted on the same graph. In the ideal case, one should end up with a line having a slope of 45° . Scatters from this ideal line show deficiencies in the analytical model, assuming that the experimental data are correct.

The mode shapes can be compared in a similar fashion (a method suggested by Allemang and Brown [30]), by plotting data from the two models. The slope of the best straight line passing through these data points is defined as the Modal Scaling Factor (MSF). MSF is given by,

$$MSF(\{\phi\}_X, \{\phi\}_A) = \frac{|\{\phi\}_X^T \{\phi\}_A^*|}{\{\phi\}_A^T \{\phi\}_A^*} \quad (2.62)$$

where $\{\ast\}$ indicates the complex conjugate. The MSF values should be 1 for the mode pairs that are the same (both vectorwise and magnitudewise). Any other value will indicate an error in these two terms.

2.2.2 The Modal Assurance Criterion

When modal data is used in order to update the analytical models, mode pairing is the most crucial point. Pairing of modes can be accomplished by using the Modal Assurance Criterion (MAC) proposed by Allemang and Brown [30]. The modal assurance criterion (MAC) is used to correlate the i^{th} analytical mode with the j^{th} experimental one by using the following definition

$$MAC(\{\phi_i\}_A, \{\phi_j\}_X) = \frac{|\{\phi_i\}_A^T \{\phi_j\}_X^*|^2}{\{\phi_i\}_A^T \{\phi_i\}_A^* \{\phi_j\}_X^T \{\phi_j\}_X^*} \quad (2.63)$$

MAC is a matrix and in the ideal case, the diagonal terms should be 1 (showing full correlation between the same modes), while the off-diagonal terms should all vanish (showing zero correlation between different modes).

One of the advantages of MAC is that it does not require coordinate complete experimental data, as is the case for orthogonality methods. Partitioning the analytical mode shapes is sufficient. However, MAC is known to be unreliable for localized modes, where knowledge of only a few data points is used.

MAC is a very popular correlation tool that is used in almost all commercial model updating and modal analysis software.

If the MAC values of two modes are 1 (indicating the same mode shapes) but MSF values are not, than this is an indication of a scaling (normalization) error (meaning that the MSF can be used as a means of normalization).

2.2.3 The Coordinate Modal Assurance Criterion

The Coordinate Modal Assurance Criterion (COMAC) which was proposed by Lieven and Ewins [31], gives an indication of the correlation between the two models for a given coordinate. The COMAC for coordinate i is given by,

$$COMAC(i) = \frac{\left(\sum_{r=1}^L |(\phi_i^r)_A (\phi_i^r)_X| \right)}{\sum_{r=1}^L ((\phi_i^r)_A)^2 \sum_{r=1}^L ((\phi_i^r)_X)^2} \quad (2.64)$$

A good correlation for the i^{th} coordinate indicates itself as a number close to 1, and a poor one with a number close to 0. Unlike MAC, COMAC is a vector.

Although it sounds like a perfect tool for error localization, numerical study shows that it does not go beyond some initial localization. This is because a fully numerical model containing error only in a coordinate yields COMAC values other than 1 for neighboring degrees of freedom. Using the same approach, it can be said that an error will affect the mode shapes of many degrees of freedom (if it is not a “local” one but a scattered one). So that the COMAC values for some degrees of freedom (for instance for a degree of freedom on a node of a beam element modeled exactly as the real structure) will not be 1 although they are modeled correctly.

2.2.4 Orthogonality Methods

Checking the orthogonality of analytical and experimental mode shapes can enable comparison of modal data (keeping in mind that two distinct modes will be orthogonal to each other). This can be accomplished by:

- Cross Orthogonality (proposed by Targoff [32])

$$[COM_{A,X}] = [\phi]_A^T [M]_A [\phi]_X \quad (2.65)$$

- Mixed Orthogonality

$$[MOC_{A,X}] = [\phi]_X^T [M]_A [\phi]_X \quad (2.66)$$

For well-correlated models, both checks should yield an identity matrix.

CHAPTER 3

THEORY OF MODEL UPDATING METHODS

In this section, some common model updating techniques will be reviewed. The existing techniques can be divided into two main categories considering the techniques used for solution:

- Direct methods,
- Iterative methods.

A different classification can also be made considering the input data the method uses:

- Modal data based methods,
- FRF data based methods.

The following review is based on the first set of classification.

3.1 DIRECT METHODS

The updated mathematical model is expected to behave in the way that the experimental model does for the modes measured. The direct methods search for mathematical models that match some reference data coming from the experiments.

The advantages of the direct methods can be summarized as follows:

- There is no convergence problem (as there are no iterations),
- Lower processing time (for the whole updating process),
- The resulting mathematical model fits the reference model exactly.

Although the exact fitting of the experimental model seems to yield the direct method solution as the primarily searched result, there exist some disadvantages that put the direct methods on the secondarily searched results side. These are

- High quality results and modal analysis are needed
- In order to have a mathematical model that has the same size as the original mathematical model, the mode shapes must be expanded (there will be errors coming from expansion techniques)
- The original coordinate connectivity in the analytical model will be lost and the resulting matrices will be fully populated (for example, there will be off-diagonal stiffness elements for the degrees of freedom where, in the real structure, no direct connection is present).
- The positive definiteness of the space matrices can be disturbed (if the rigid body modes are not taken into account, the resulting mathematical model will also not have the rigid body modes, indicating a wrong positive definite stiffness matrix)

After summarizing the advantages and disadvantages, the methods are introduced in detail below.

3.1.1 Methods Using Lagrange Multipliers

This method can be divided into two distinct approaches proposed by Baruch and Bar Itzhac [4] and Berman [5], where either the mass or stiffness matrix is assumed to be correct and the other one is updated.

For the mass matrix reliable case (proposed by Baruch & Bar Itzhac [4]), the aim is to minimize the function

$$\varepsilon = \left| [M]_A^{-0.5} ([K]_{AU} - [K]_A) [M]_A^{-0.5} \right| \quad (3.1)$$

by introducing the constraint equations of symmetricity and orthogonality:

$$[K]_{AU} - [K]_{AU}^T = [0] \quad (\text{stiffness matrix symmetricity condition}) \quad (3.2)$$

$$[\phi]_X^T [K]_{AU} [\phi]_X - \left[\cdot \omega_r^2 \cdot \right]_X = [0] \quad (\text{orthogonality condition}) \quad (3.3)$$

In those expressions $[M]_A$ and $[K]_A$ represent the original analytical mass and stiffness matrices, respectively. $[\phi]_X$ is the experimental mode shape matrix and $[K]_{AU}$ represents the updated analytical stiffness matrix and is given by:

$$[K]_{AU} = [K]_A + [\Delta K] \quad (3.4)$$

where (from [2])

$$\begin{aligned} [\Delta K] = & -[K]_A [\phi]_X [\phi]_X^T [M]_A - [M]_A [\phi]_X [\phi]_X^T [K]_A + [M]_A [\phi]_X [\phi]_X^T [K]_A [\phi]_X [\phi]_X^T [M]_A + \dots \\ & \dots + [M]_A [\phi]_X [\cdot \omega_r^2 \cdot]_X [\phi]_X^T [M]_A \end{aligned} \quad (3.5)$$

The mass matrix updating (assuming that the stiffness matrix is correct) can be accomplished in a similar fashion.

A similar approach was used by Berman and Nagy [33] in order to update mass and stiffness matrices simultaneously. The error function to be minimized is:

$$\varepsilon = \left| [M]_A^{-0.5} ([M]_{AU} - [M]_A) [M]_A^{-0.5} \right| \quad (3.6)$$

with the constraint equations

$$[M]_{AU} - [M]_{AU}^T = [0] \quad (\text{stiffness matrix symmetry condition}) \quad (3.7)$$

$$[\phi]_X^T [M]_{AU} [\phi]_X - [I] = [0] \quad (\text{weighted orthogonality condition}) \quad (3.8)$$

The updated mass matrix is obtained by

$$[M]_{AU} = [M]_A + [\Delta M] \quad (3.9)$$

where

$$[\Delta M] = [M]_A [\phi]_X \left([\phi]_X^T [M]_A [\phi]_X \right)^{-1} \left([I] - \left([\phi]_X^T [M]_A [\phi]_X \right) \right) \left([\phi]_X^T [M]_A [\phi]_X \right)^{-1} [\phi]_X [M]_A \quad (3.10)$$

After the updated mass matrix is calculated, the stiffness matrix can be updated by using the minimization function

$$\varepsilon = \left| [M]_A^{0.5} \left([K]_{AU} - [K]_A \right) [M]_A^{0.5} \right| \quad (3.11)$$

Using the same constraints given by Eq. (3.7), Eq. (3.8) and

$$[K]_{AU} [\phi]_X = [M]_{AU} [\phi]_X \left[\ddot{\cdot} \cdot \omega_r^2 \ddot{\cdot} \right]_X \quad (3.12)$$

the updated stiffness matrix can be written as

$$[\Delta K] = \left([\Delta] + [\Delta]^T \right) \quad (3.13)$$

where

$$[\Delta] = 0.5 [M]_A [\phi]_X \left([\phi]_X^T [K]_A [\phi]_X + \left[\ddot{\cdot} \cdot \omega_r^2 \ddot{\cdot} \right]_X \right) [\phi]_X^T [M]_A - [K]_A [\phi]_X [\phi]_X^T [M]_A \quad (3.14)$$

Caesar [6] suggested a range of methods that update the mass and stiffness matrices directly using different cost functions and constraints. He also introduced some additional constraints in order to reflect the rigid body dynamics, such as position of CG, total mass and moments of inertia. Wei [34] updated the mass and stiffness matrices simultaneously using the measured eigenvectors and orthogonality conditions with a different cost function to minimize. Fuh and Chen [35] developed a method to update a structural system with non-proportional damping. Heylen and Sas [36] reviewed the Lagrange multiplier updating methods in their work in detail.

3.1.2 Error Matrix Methods

These methods (the original formulation proposed by Sidhu and Ewins [7]) directly estimate the errors in the mass and stiffness matrices. Assuming the error is small, the error terms can be defined in terms of the analytical and experimental modal data. The error matrix for mass and stiffness matrices are defined as:

$$[\Delta M] = [M]_X - [M]_A \quad (3.15)$$

$$[\Delta K] = [K]_X - [K]_A \quad (3.16)$$

Using the orthogonality conditions $[\phi]^T [M] [\phi] = [I]$ and $[\phi]^T [K] [\phi] = [\cdot \cdot \omega_r^2 \cdot \cdot]$, the mass and stiffness matrices can be represented by the modal data as

$$[M] = ([\phi]^T)^{-1} [\phi]^{-1} \quad (3.17)$$

$$[K] = ([\phi]^T)^{-1} [\cdot \cdot \omega_r^2 \cdot \cdot] [\phi]^{-1} \quad (3.18)$$

The experimental flexibility matrix can be written as

$$[K]_X^{-1} = ([I] + [K]_A^{-1} [\Delta K] [K]_A^{-1}) \quad (3.19)$$

If the stiffness error is assumed to be small, so that the second and higher order components are omitted, the above expression can be expanded as [2]

$$[K]_X^{-1} \cong [K]_A^{-1} - [K]_A^{-1} [\Delta K] [K]_A^{-1} \quad (3.20)$$

Using the above expression, the stiffness error matrix can be written as

$$[\Delta K] = [K]_A ([K]_A^{-1} - [K]_X^{-1}) [K]_A \quad (3.21)$$

or using the modal data, the same matrix can be written as

$$[\Delta K] \cong [K]_A \left([\phi]_A \left[\cdot \cdot \omega_r^2 \cdot \cdot \right]_A^{-1} [\phi]_A^T - [\phi]_X \left[\cdot \cdot \omega_r^2 \cdot \cdot \right]_X^{-1} [\phi]_X^T \right) [K]_A \quad (3.22)$$

similarly,

$$[\Delta M] \cong [M]_A \left([\phi]_A [\phi]_A^T - [\phi]_X [\phi]_X^T \right) [M]_A \quad (3.23)$$

He and Ewins [37] expanded the work to figure out the damping properties. Zhang and Lallement [38] kept some of the second order terms in the flexibility matrix. Lieven and Ewins [39] proposed a modified version of the method which uses singular value decomposition.

3.1.3 Direct Matrix Updating

This method first performs an adjustment on the system mass matrix and uses the updated mass matrix to adjust the system stiffness matrix.

Mass and stiffness error matrices are calculated as follows ([2])

$$[\Delta M] = [M]_A [\phi]_X [m]_A^{-1} ([I] - [m]_A) [m]_A^{-1} [\phi]_X^T [M]_A \quad (3.24)$$

where

$$[m]_{m \times m} = [\phi]_{m \times N}^T [M]_{N \times N} [\phi]_{N \times m} \quad (3.25)$$

and

m: mode number (maximum tested)

N: order of the model

The corrector for the stiffness matrix is given as ([2])

$$[\Delta K] = [M]_A [\phi]_X [\phi]_X^T [K]_A [\phi]_X [\phi]_X^T [M]_A + [M]_A [\phi]_X \begin{bmatrix} \cdot \\ \cdot \\ \omega_r^2 \\ \cdot \\ \cdot \end{bmatrix}_X [\phi]_X^T [M]_A - [K]_A [\phi]_X [\phi]_X^T [M]_A - \dots \\ \dots - [M]_A [\phi]_X [\phi]_X^T [K]_A \quad (3.26)$$

The obtained result is not a unique one since no constraints are applied for the modes larger than m .

3.1.4 Matrix Mixing Methods

Using the orthogonality conditions $[\phi]^T [M] [\phi] = [I]$ and $[\phi]^T [K] [\phi] = \begin{bmatrix} \cdot \\ \cdot \\ \omega_r^2 \\ \cdot \\ \cdot \end{bmatrix}$, the flexibility matrix can be calculated using the analytical and experimental modal data as

$$[K]_{AU}^{-1} = [K]_A^{-1} + [\Delta K]^{-1} = [K]_A^{-1} + \left([\phi]_X \begin{bmatrix} \cdot \\ \cdot \\ \omega_r^2 \\ \cdot \\ \cdot \end{bmatrix}_X [\phi]_X^T - [\phi]_A \begin{bmatrix} \cdot \\ \cdot \\ \omega_r^2 \\ \cdot \\ \cdot \end{bmatrix}_A [\phi]_A^T \right) \quad (3.27)$$

Whereas the updated mass matrix can be calculated as

$$[M]_{AU}^{-1} = [M]_A^{-1} + [\Delta M]^{-1} = [M]_A^{-1} + \left([\phi]_X [\phi]_X^T - [\phi]_A [\phi]_A^T \right) \quad (3.28)$$

The expressions give exact results if the mode shape matrices are of full size (in that case the number of measured modes and the number of measured degrees of freedom are the same and equal to the number of the degrees of freedom of the analytical model). For the real case, where the order of the experimental model is less than that of the analytical model, the updating matrices (proposed by Caesar [10] and Link *et al.* [11]) for m measured modes become

$$[M]_{AU} = [M]_A^{-1} + \sum_{r=1}^m \{\phi\}_X^r \left(\{\phi\}_X^r \right)^T - \sum_{r=1}^m \{\phi\}_A^r \left(\{\phi\}_A^r \right)^T \quad (3.29)$$

$$[K]_{AU}^{-1} = [K]_A^{-1} + \sum_{r=1}^m \frac{\{\phi\}_X^r \left(\{\phi\}_X^r \right)^T}{\left(\omega_r^2 \right)_X} - \sum_{r=1}^m \frac{\{\phi\}_A^r \left(\{\phi\}_A^r \right)^T}{\left(\omega_r^2 \right)_A} \quad (3.30)$$

3.2 INDIRECT METHODS

The procedure for direct updating includes adjustment on the whole system matrices. In the indirect methods, the adjustments are made on individual elements by the calculated updating factors.

If L is the number of elements for which mass and stiffness adjustments will be made, the updating matrices for an undamped system can be expressed as

$$[\Delta M] = \sum_{i=1}^L a_i [m_i] \text{ and } [\Delta K] = \sum_{i=1}^L b_i [k_i] \quad (3.31)$$

where a_i and b_i are the updating parameters that are to be calculated and m_i and k_i represent the mass and stiffness matrices for the i^{th} element.

The resulting equation is in the form of $[A]\{p\} = \{\delta\}$, where $[A]$ is a matrix of system properties, $\{p\}$ is the updating parameter vector and $\{\delta\}$ is the error vector.

The solution can be obtained as

$$\{p\} = [A]^+ \{\delta\} \quad (3.32)$$

where $[A]^+$ is the generalized inverse of $[A]$. The values of $\{p\}$ are obtained by least-squares regression if the number of equations is larger than the number of the unknowns.

3.2.1 Eigendynamic Constraint Method

This indirect method is based on the following eigendynamic equations:

$$([K]_x - \omega_x^2 [M]_x) \{\phi^r\}_x = \{0\} \quad (3.33)$$

$$\{\phi^r\}_X^T [M]_X \{\phi^r\}_X = 1 \quad (3.34)$$

$$\{\phi^r\}_X^T [K]_X \{\phi^r\}_X = \omega_X^{r,2} \quad (3.35)$$

By applying the above equations to the system matrices, the p values are obtained. The governing set of linear equations is obtained by the following equations:

$$(\omega_X^{r,2}) [\Delta M] \{\phi^r\}_X - [\Delta K] \{\phi^r\}_X = (\omega_X^{r,2}) [M]_A \{\phi^r\}_X - [K]_A \{\phi^r\}_X \quad (3.36)$$

and

$$\{\phi^r\}_X^T [\Delta M] \{\phi^r\}_X = \{\phi^r\}_X^T [M]_A \{\phi^r\}_X - 1 \quad (3.37)$$

$$\text{where } [\Delta M] = \sum_{i=1}^L a_i [m_i] \text{ and } [\Delta K] = \sum_{i=1}^L b_i [k_i].$$

The factors that define the updating mass and stiffness matrices (ie. a_i and b_i values) are the p values. The right hand side of Eq. (3.36) and Eq. (3.37) form the vector $\{\mathcal{D}\}$ defined in Eq. (3.32). The matrix $[A]$ is formed by leaving the p values alone (from the left hand side) in Eq. (3.36) and Eq. (3.37).

This method concludes that, the conditions arising from not satisfying the eigendynamic constraints are because of the errors in the analytical system matrices. As $[\Delta M]$ and $[\Delta K]$ matrices are the updating matrices, the sources of errors are directed to the absence of these matrices.

Rearranging the above equations into a standard set of linear equations will yield the equation

$$[A_i]_{(N+1) \times 2L} \{p\}_{2L \times 1} = \{\mathcal{D}\}_{(N+1) \times 1} \quad (3.38)$$

where N is the number of the degrees of freedom in the analytical model, $2L$ is the number of the updating parameters. $[A]$ and $\{\delta\}$ are formed using the analytical spatial matrices and experimental data.

If data from experiments are available for only m modes ($m < N$), then the set of equations can be rearranged as

$$\begin{matrix} \begin{bmatrix} [A_1] \\ [A_2] \\ \vdots \\ \vdots \\ [A_m] \end{bmatrix} \\ m(N+1) \times 2L \end{matrix} \begin{matrix} \{p\} \\ 2L \times 1 \end{matrix} = \begin{matrix} \left\{ \begin{matrix} \{\delta_1\} \\ \{\delta_2\} \\ \vdots \\ \{\delta_m\} \end{matrix} \right\} \\ m(N+1) \times 1 \end{matrix} \quad (3.39)$$

which is simply in the form $[A]\{p\} = \{\delta\}$. If $m(N+1) > 2L$, then the problem is over-determined (the number of equations is larger than the number of unknowns) and a least-squares solution for $\{p\}$ can be found using the generalized inverse of a $[A]$, that is $\{p\} = [A]^+ \{\delta\}$.

3.2.2 Inverse Eigensensitivity Method

Inverse Eigensensitivity Method seeks a solution to the miscorrelation of experimental model and analytical model problem by trying to correlate the modal data of the experimental and analytical models using modal sensitivities. The basics of the method are described on a single variable function below.

The Inverse Eigensensitivity Method tries to calculate the amount of change in the selected parameters in order to reach the target values (experimental data) from the initial values (analytical data). To give an example, the target value x_1 shown in Figure 1 can be calculated as

$$x1 = x0 + \frac{(y1 - y0)}{s} \quad (3.40)$$

where $y1$ simulates the experimental modal data, $y0$ simulates analytical modal data, $x0$ simulates the initial parameter value and s simulates the modal sensitivity value.

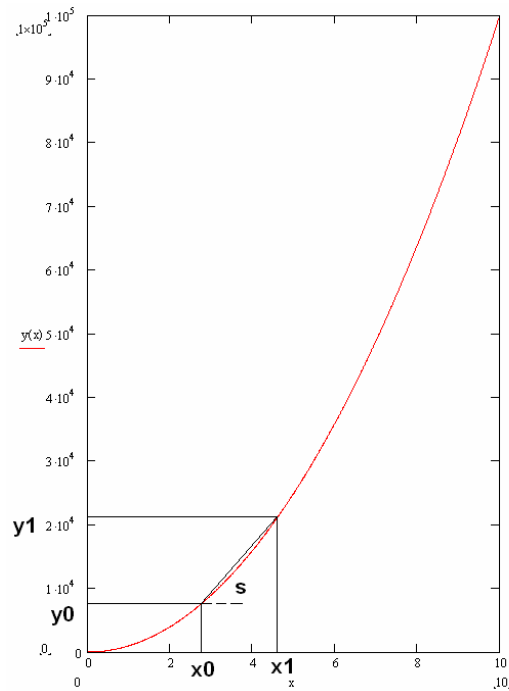


Figure 1. Linear Estimation on a Single Variable Function

If multiple parameters are used, then a set of equations can be written as

$$\{p\}_f = \{p\}_o + [S]^{-1} \begin{Bmatrix} \Delta\omega_r \\ \{\Delta\phi_r\} \end{Bmatrix} \quad (3.41)$$

In Eq. (3.41), $\{p\}_f$ is the updating parameter vector (shell thickness, Young's Modulus, density etc.), $\{p\}_o$ is the initial parameter value vector, $[S]$ is the modal

sensitivity matrix and $\begin{Bmatrix} \Delta\omega_r \\ \Delta\phi_r \end{Bmatrix}$ is the difference vector between the experimental and analytical models' modal data.

The formulation of the Inverse Eigensensitivity Method can be described in detail if the sensitivity matrix is expressed in terms of the modal data and updating parameters.

The modal data is taken as functions of updating parameters $\{p\}$ as,

$$(\omega^r)_A = f(\{p\}) \quad (3.42)$$

$$\{\phi^r\}_A = g(\{p\}) \quad (3.43)$$

In order to equate related experimental modal properties to analytical ones, experimental values (squares for natural frequencies and modal vectors themselves) are expressed using Taylor Series expansion in the following form

$$(\omega^r)_X^2 = (\omega^r)_A^2 + \sum_{i=1}^{N_p} \frac{\partial(\omega^r)_A^2}{\partial p_i} p_i + O(p_i^2) \quad (3.44)$$

$$\{\phi^r\}_X = \{\phi^r\}_A + \sum_{i=1}^{N_p} \frac{\partial\{\phi^r\}_A}{\partial p_i} p_i + O(p_i^2) \quad (3.45)$$

Linearising the above equations by assuming that the higher order terms $O(p_i^2)$ are small we obtain,

$$\Delta(\omega^r)^2 = (\omega^r)_X^2 - (\omega^r)_A^2 = \sum_{i=1}^{N_p} \frac{\partial(\omega^r)_A^2}{\partial p_i} p_i \quad (3.46)$$

$$\Delta\{\phi^r\} = \{\phi^r\}_X - \{\phi^r\}_A = \sum_{i=1}^{N_p} \frac{\partial\{\phi^r\}_A}{\partial p_i} p_i \quad (3.47)$$

The difference in modal properties can further be expressed by distinguishing the p values. If the p values for individual stiffness and mass matrices are written explicitly, one obtains the following equations:

$$\Delta(\omega^r)^2 \cong \sum_{i=1}^{N_p/2} \frac{\partial(\omega^r)_A^2}{\partial m_i} a_i + \sum_{i=1}^{N_p/2} \frac{\partial(\omega^r)_A^2}{\partial k_i} b_i = \sum_{i=1}^{N_p} \frac{\partial(\omega^r)_A^2}{\partial p_i} p_i \quad (3.48)$$

$$\Delta\{\phi^r\} \cong \sum_{i=1}^{N_p/2} \frac{\partial\{\phi^r\}_A}{\partial m_i} a_i + \sum_{i=1}^{N_p/2} \frac{\partial\{\phi^r\}_A}{\partial k_i} b_i = \sum_{i=1}^{N_p} \frac{\partial\{\phi^r\}_A}{\partial p_i} p_i \quad (3.49)$$

In the above equations, the uncertainty arises due to the truncation of 2nd and higher terms in Taylor Series expansion.

The above equations can be written in matrix form as $[S]\{p\} = \{\Delta\}$ (the same form as $[A]\{p\} = \{\delta\}$) where,

$$[S]_{(m(N+1) \times N_p)} = \begin{bmatrix} \frac{\partial(\omega_1^r)_A^2}{\partial p_1} & \dots & \dots & \dots & \dots & \frac{\partial(\omega_1^r)_A^2}{\partial p_{N_p}} \\ \frac{\partial\{\phi\}_A^1}{\partial p_1} & \dots & \dots & \dots & \dots & \frac{\partial\{\phi\}_A^1}{\partial p_{N_p}} \\ \vdots & \dots & \dots & \dots & \dots & \vdots \\ \vdots & \dots & \dots & \dots & \dots & \vdots \\ \frac{\partial(\omega_m^r)_A^2}{\partial p_1} & \dots & \dots & \dots & \dots & \frac{\partial(\omega_m^r)_A^2}{\partial p_{N_p}} \\ \frac{\partial\{\phi\}_A^m}{\partial p_1} & \dots & \dots & \dots & \dots & \frac{\partial\{\phi\}_A^m}{\partial p_{N_p}} \end{bmatrix} \quad (3.50)$$

$$\left\{ \Delta \right\}_{(m \times (N+1))} = \begin{Bmatrix} \Delta(\omega_1)^2 \\ \{\Delta\phi\}^1 \\ \vdots \\ \vdots \\ \Delta(\omega_m)^2 \\ \{\Delta\phi\}^m \end{Bmatrix} \quad (3.51)$$

$$\left\{ p \right\}_{N_p \times 1} = \begin{Bmatrix} p_1 \\ p_2 \\ \vdots \\ \vdots \\ \vdots \\ p_{N_p} \end{Bmatrix} \quad (3.52)$$

where, N_p is the number of the updating parameters, m is the number of the correlated mode pairs and N is the number of the measured degrees of freedom.

The updating parameters are obtained as $\{p\} = [A]^+ \{\delta\}$.

In order to have the correct solution set, the sensitivity matrix should be built in the correct order. That is, the sensitivity value belonging to a specific parameter and modal data should be in the correct row and column of the coefficient matrix $[S]$.

For example, for a system of 4 parameters, 2 modes and 3 degrees of freedom the equation should be written as:

$$\begin{Bmatrix} p1 \\ p2 \\ p3 \\ p4 \end{Bmatrix}_f = \begin{Bmatrix} p1 \\ p2 \\ p3 \\ p4 \end{Bmatrix}_o + \begin{bmatrix} S_{\omega_1}^{p1} & S_{\omega_1}^{p2} & S_{\omega_1}^{p3} & S_{\omega_1}^{p4} \\ S_{\phi_1^1}^{p1} & S_{\phi_1^1}^{p2} & S_{\phi_1^1}^{p3} & S_{\phi_1^1}^{p4} \\ S_{\phi_1^2}^{p1} & S_{\phi_1^2}^{p2} & S_{\phi_1^2}^{p3} & S_{\phi_1^2}^{p4} \\ S_{\phi_1^3}^{p1} & S_{\phi_1^3}^{p2} & S_{\phi_1^3}^{p3} & S_{\phi_1^3}^{p4} \\ S_{\omega_2}^{p1} & S_{\omega_2}^{p2} & S_{\omega_2}^{p3} & S_{\omega_2}^{p4} \\ S_{\phi_2^1}^{p1} & S_{\phi_2^1}^{p2} & S_{\phi_2^1}^{p3} & S_{\phi_2^1}^{p4} \\ S_{\phi_2^2}^{p1} & S_{\phi_2^2}^{p2} & S_{\phi_2^2}^{p3} & S_{\phi_2^2}^{p4} \\ S_{\phi_2^3}^{p1} & S_{\phi_2^3}^{p2} & S_{\phi_2^3}^{p3} & S_{\phi_2^3}^{p4} \end{bmatrix}^{-1} \begin{Bmatrix} \Delta\omega_1 \\ \Delta\phi_1^1 \\ \Delta\phi_1^2 \\ \Delta\phi_1^3 \\ \Delta\omega_2 \\ \Delta\phi_2^1 \\ \Delta\phi_2^2 \\ \Delta\phi_2^3 \end{Bmatrix} \quad (3.53)$$

In the above equation, p_i is the i^{th} parameter, $S_{\omega_j}^{p_i}$ is the sensitivity of the j^{th} natural frequency with respect to the i^{th} parameter, $S_{\phi_j^k}^{p_i}$ is the sensitivity of the j^{th} mode shape at k^{th} degree of freedom with respect to the i^{th} parameter, $\Delta\omega_j$ is the difference between the j^{th} experimental natural frequency and j^{th} analytical natural frequency (should be taken in Hz if MSC Nastran output is used), $\Delta\phi_j^k$ is the difference between the j^{th} experimental mode shape data and the j^{th} analytical mode shape data at the k^{th} degree of freedom, $\{ \}_f$ is the final parameter value set and $\{ \}_o$ is the initial parameter set.

As the modal data is related to the updating parameters in a non-linear manner, mostly (if the error between analytical and experimental models are not small) an iterative solution is required.

In the application of the Inverse Eigensensitivity Method, the number of equations should be more than the number of unknowns. A least squares solution scheme is necessary in order to solve such a set of equations.

A mode that is required to be updated should appear in both experimental and analytical models. Otherwise, there will be convergence problems or an unsuccessful updating trial if there is relatively a large discrepancy between the experimental and analytical mode shape values as they belong to different modes (for example trying to correlate the first wing bending mode to the second wing bending mode of an aircraft will cause unsuccessful convergence).

The most beneficial and powerful aspect of this method is that, it does not need any model reduction and/or mode shape expansion schemes. Only the data at the measured degrees of freedom and the natural frequencies are sufficient for updating. On the other hand, as this method uses only the data at the natural frequencies, the number of equations obtained is almost always less than the number of equations obtained from response function method. This in turn, yields a limit on the number of the updating parameters (in order to have more equations than unknowns). Another disadvantage is that modes to be updated must appear in both models.

The modal sensitivities can be calculated in two ways:

- Using analytical formulations
- Introducing perturbations to the matrices and analyzing the amount of change in the modal response

The perturbation method keeps all the parameters other than the investigated one as constant and applies small changes to that parameter. It is observed that if the amount of change is kept under 0.001% of the original value, satisfactory results can be obtained; then the sensitivities are calculated according to the amount of change in the modal data.

The flowchart for Inverse Eigensensitivity Method using MSC Nastran finite element package is given in Figure 2.

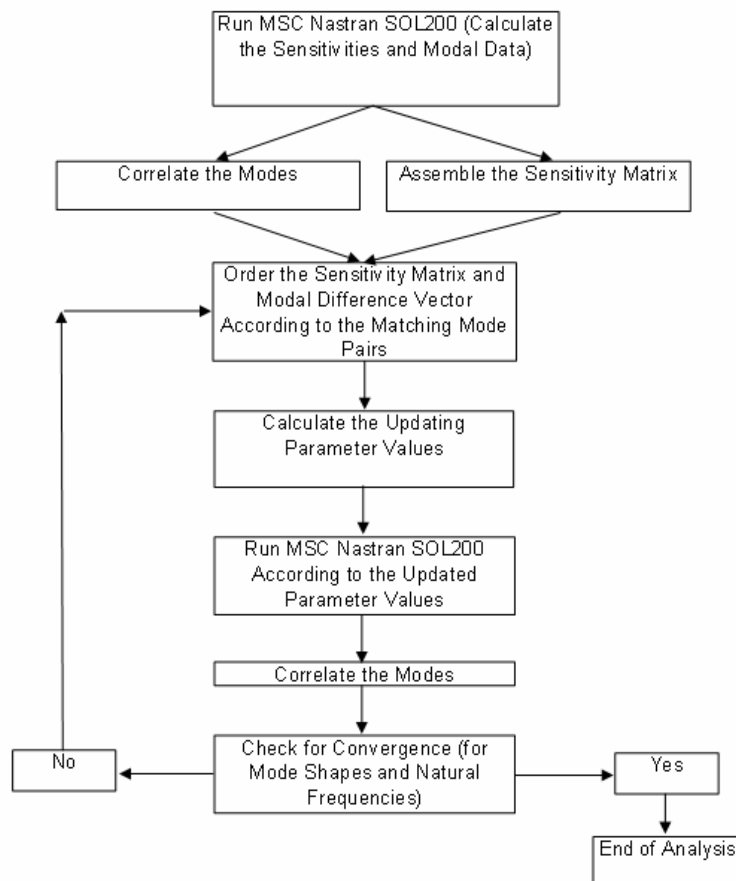


Figure 2. Flowchart for Updating MSC Nastran Models Using Inverse Eigensensitivity Method

The routine for obtaining the modal sensitivities using MSC Nastran is described in detail in Appendix D. The basics of the software using this method is given in Chapter 4.

Applications of this method to aircraft structures can be found in [40] and [18].

3.2.3 Response Function Method

The Inverse Eigensensitivity Method and the Eigendynamic Constraint Method use modal data as experimental input. However, FRF carry many more features of the response data other than do modal data. Furthermore, response data is more exact than modal data, as the latter is extracted from the former one, and the inclusion or exclusion of damping can be better handled by using response data.

The Response Function Method can be explained as follows:

Using the j^{th} column of each FRF matrix, one can write [2]

$$\{H(\omega_i)\}_A^j - \{H(\omega_i)\}_X^j = [H(\omega_i)]_A [\Delta z(\omega_i)] \{H(\omega_i)\}_X^j \quad (3.54)$$

where

$$[\Delta z(\omega_i)] = [\Delta K] - \omega_i^2 [\Delta M] + i\omega_i [\Delta C] \quad (3.55)$$

One can obtain an updating parameter vector $\{p\}$, resulting in [2]

$$[R(\omega_i)]_{m \times N_p} \{p\}_{N_p} = \{\Delta H(\omega_i)\}_n^j \quad (3.56)$$

where $[R(\omega_i)]$ is the system matrix containing the FRF properties of the analytical model and the individual stiffness and mass and damping elements, $\{\Delta H(\omega_i)\}_n^j$ is the difference between experimental and analytical FRF's, $\{p\}$ is the vector

containing the updating parameters. The above equation set can be written in the simple form $[R]\{p\} = \{\Delta\}$ or $\{p\} = [R]^+ \{\Delta\}$ which is also in the form with the equation set given in Eq. (3.32).

If response data are available for s discrete ω values, then Eq. (3.56) can be written as

$$\begin{bmatrix} [R(\omega_1)] \\ [R(\omega_2)] \\ \vdots \\ \vdots \\ \vdots \\ [R(\omega_s)] \end{bmatrix}_{sn \times 2L} \{p\}_{2L \times 1} = \begin{Bmatrix} \Delta H_j(\omega_1) \\ \Delta H_j(\omega_{21}) \\ \vdots \\ \vdots \\ \vdots \\ \Delta H_j(\omega_s) \end{Bmatrix}_{sn} \quad (3.57)$$

Determination of $[R(\omega_i)]$ depends on the assembly characteristics of the spatial matrices as the individual stiffness and mass elements written for a node depends on the connected elements.

The flowchart for the Response Function Method is given in Figure 3.

The very first obstacle that appears in using this method is rewriting the equation set into the form given in Eq. (3.56) (in calculation of the matrix $[R(\omega_i)]$). This necessitates the calculation of the matrix $[R(\omega_i)]$ by a routine instead of simple matrix multiplications as the right hand side of Eq. (3.54) does not directly yield the updating parameter vector ($\{\delta\}$ in Eq. (3.32)) and the coefficient matrix ($[A]$ in Eq. (3.32)). Routines considering the connectivity data are written for computer codes in order to have this vector and matrix.

For the model updating by using this method, the sizes of the experimental and analytical models must be the same. So, either reduction of the analytical model or expansion of the experimental model should be carried out.

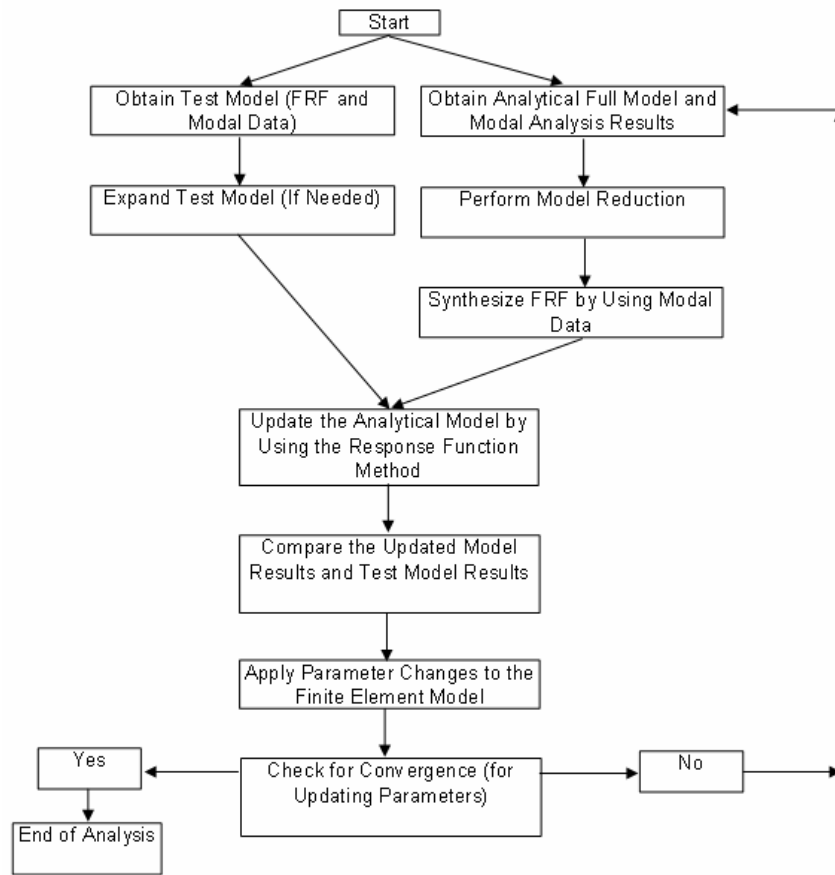


Figure 3. Flowchart for the Response Function Method

The units of the frequency response function data should be the same for the experimental and analytical models. Experimental frequency response function data is calculated by dividing the acceleration data by the forcing data ($m/s^2/N$). The analytical response function data must also be in these units (or experimental data should be converted to the units of the analytical data). Otherwise, there will be a shift that is related to the frequency even there are no errors in the analytical model.

In the response function method, as only the FRF data are used, there is no need to have the same modes in both models. However, large error values will not allow convergence even in response function method. Finally, there are no constraints on damping properties in Inverse Eigensensitivity Method; therefore it is not

possible to update damping matrices. However, in the Response Function Methods, damping matrices can also be updated

Case studies using this method with real test data can be found in [41] and [42].

3.2.4 Model Updating Based on MCI Minimization

This new error localization technique and model updating routine takes as a bases the work accomplished by Özer, Özgüven and Royston [43], where coordinates involving nonlinearity are located through a search technique. For the model updating case developed herein, instead of searching for coordinates carrying non-linearity, the uncorrelated coordinates are searched for. The resulting output is a scatter varying with frequency. Each coordinate has its own scatter. The indicator of an uncorrelated coordinate is a scatter not equal to zero at some points throughout the frequency domain. The index, pointing out the uncorrelated coordinates is named as MisCorrelation Index (MCI).

After analyzing the system and finding out the erroneous coordinates, if the analytical model carries localized errors, then updating of the analytical model by only inverting the portions including erroneous degrees of freedom would be a very efficient way instead of an updating scheme with full or partially reduced matrices. This new method, which is explained herein, uses the approach that Özer *et al.* [43] has followed for identification of structural non-linearity. In order to adapt this scheme to model updating, some simple modifications are carried out in the original formulation.

In the work of Özer, *et al.* [43], non-linearity in a structure is detected by using the receptance of the system for a low forcing level (so that the system will behave linear) and the receptances for a high forcing level. The difference between the frequency responses is attributed to the non-linearity existing in the structure. By using the differences between the frequency responses under low and high forcing levels, a number, so-called “Non-linearity Number” is formulated. The “Non-linearity Number” was used to figure out the coordinates carrying non-linearity and the degree of non-linearity. Here in this work, a similar approach is applied in model updating. Instead of searching for the difference arising from non-linearity,

the difference coming from erroneous modeling is searched for. The aim is to determine the coordinates carrying error (which is defined as the difference between experimental and analytical responses). Let us consider the equation of motion of a discrete system, which can be written as follows:

$$[M]\{\ddot{x}\} + [C]\{\dot{x}\} + [K]\{x\} = \{f\} \quad (3.58)$$

where $\{x\}$ is the displacement vector, $\{f\}$ is the forcing vector and $[M]$, $[C]$, $[K]$ are mass, viscous damping and stiffness matrices respectively.

For a harmonic excitation of $\{f\} = \{F\}e^{i\omega t}$, the equation of motion will be

$$[-\omega^2[M] + i\omega[C] + [K]]\{X\} = \{F\} \quad (3.59)$$

with ω being the excitation frequency. It is assumed that the response will also be harmonic and in the form $\{x\} = \{X\}e^{i\omega t}$. In the above expressions, $\{F\}$ and $\{X\}$ denote the magnitude vectors of forcing and displacement, respectively.

Let us define $[\Delta]$ as

$$[\Delta] = -\omega^2[\Delta M] + i\omega[\Delta C] + [\Delta K] \quad (3.60)$$

where $[\Delta M]$, $[\Delta C]$, $[\Delta K]$ are updating mass, viscous damping and stiffness matrices, respectively.

The equation of motion for the updated system under harmonic excitation will be

$$[-\omega^2[M] + i\omega[C] + [K] + [\Delta]]\{X\} = \{F\} \quad (3.61)$$

Then the receptance matrix $[\theta]$ will be

$$[\theta] = (-\omega^2[M] + i\omega[C] + [K] + [\Delta])^{-1} \quad (3.62)$$

The receptance obtained from the analytical model can be written as

$$[\alpha] = (-\omega^2[M] + i\omega[C] + [K])^{-1} \quad (3.63)$$

Using Eq. (3.62) and Eq. (3.63), updating matrix $[\Delta]$ can be obtained as

$$[\Delta] = [\theta]^{-1} - [\alpha]^{-1} \quad (3.64)$$

Post multiplying both sides of Eq. (3.64) by $[\theta]$ yields

$$[\Delta][\theta] = [I] - [Z][\theta] \quad (3.65)$$

Where $[Z]$ is the dynamic stiffness and is defined as $[Z] = [\alpha]^{-1}$.

The i^{th} column of Eq. (3.65) yields:

$$[\Delta]\{\theta^i\} = \{e^i\} - [Z]\{\theta^i\} \quad (3.66)$$

where $\{e^i\}$ is a vector of which i^{th} element is unity while all other elements are zero, $\{\theta^i\}$ is the i^{th} column of $[\theta]$. The r^{th} row of Eq. (3.66) yields:

$$[\Delta_r]\{\theta^i\} = \{\delta_{ir}\} - [Z_r]\{\theta^i\} \quad (3.67)$$

where $[\Delta_r]$ and $[Z_r]$ represent the r^{th} rows of $[\Delta]$ and $[Z]$ respectively and $\{\delta_{ir}\}$ is the Kronecker's Delta whose values are 0 except for the condition $i = r$ (the value of the element of this vector for this condition is 1).

The term $\{\delta_{ir}\} - [Z_r]\{\theta^i\}$ is called 'miscorrelation index'. If we consider the r^{th} coordinate of the system, miscorrelation index is an indication of dissimilarity

between analytical and experimental models. This term is zero if the r^{th} row of $[\Delta]$ are all zeros. Any non-zero element in the r^{th} row of $[\Delta]$ will yield a nonzero miscorrelation index for the r^{th} coordinate since

$$MCI_r(\omega) = \Delta_{r1}\theta_{1i} + \Delta_{r2}\theta_{2i} + \dots + \Delta_{rn}\theta_{ni} \quad (3.68)$$

Note that the right hand side of Eq. (3.67) will give

$$MCI_r(\omega) = \delta_{ir} - Z_{r1}\theta_{1i} - Z_{r2}\theta_{2i} - \dots - Z_{rn}\theta_{ni} \quad (3.69)$$

which is in terms of analytical dynamic stiffness matrix $[Z]$, experimental FRF vector $\{\theta^i\}$ and Kronecker's Delta.

The miscorrelation index indicates the error between the analytical and experimental models. As the need for finite element model updating arises from the error between these two models, the task is to make the errors vanish. The updating parameters for the indirect model updating methods are the parameters for which adjustments will be made in order to correct the finite element model. Instead of choosing arbitrary coordinates' parameters, one can make use of the miscorrelation number and run model updating procedures on the parameters of coordinates carrying errors.

For finding the MCI values, only a single column of the experimental FRF matrix is enough. However, for the unmeasured coordinates (assuming the degree of the analytical model is larger than that of the experimental model), one has to use the analytically calculated FRF values for unmeasured coordinates in the experimentally obtained FRF vector as if they are also a part of the experimental data. This operation is necessary to avoid the numerical errors coming from coordinate incompatibility. Although unmeasured data is inserted through the measured data set, as the aim is to search for the difference between the measured coordinates and their counterparts in the analytical model, the action has no physically misleading effect.

Actually MCI is a matrix of size $Ndof \times Nfreq$ (where $Ndof$ indicates the number of coordinates and $Nfreq$ indicates the number of frequency points). As MCI matrix indicates the error between the analytical and experimental model, updating the $[Z]$ matrix in order to minimize the elements of the MCI matrix will yield the updated analytical model.

Defining the updating matrices as follows,

$$[\Delta M] = \sum_{i=1}^N m_i [M_{ind}]_i, \quad [\Delta C] = \sum_{i=1}^N c_i [C_{ind}]_i, \quad [\Delta K] = \sum_{i=1}^N k_i [K_{ind}]_i \quad (3.70)$$

the updated form of the dynamic stiffness matrix will have the form

$$[Z]_{up} = \left(-\omega^2 [M + \Delta M] + i\omega [C + \Delta C] + [K + \Delta K] \right) \quad (3.71)$$

or

$$[Z]_{up} = \left(-\omega^2 \left[M + \sum_{i=1}^N m_i [M_{ind}]_i \right] + i\omega \left[C + \sum_{i=1}^N c_i [C_{ind}]_i \right] + \left[K + \sum_{i=1}^N k_i [K_{ind}]_i \right] \right) \quad (3.72)$$

Now defining the updating MCI matrix as

$$\left([\Delta_r] \{ \theta^i \} \right)_{up} = \{ \delta_{ir} \} - [Z_r]_{up} \{ \theta^i \} \quad (3.73)$$

or in open form

$$MCI_{r_{up}}(\omega) = (\Delta_{r1} \theta_{1i})_{up} + (\Delta_{r2} \theta_{2i})_{up} + \dots + (\Delta_{rm} \theta_{ni})_{up} \quad (3.74)$$

If the response values calculated by using the updated analytical matrices are exactly the same as the experimental FRF values, then the MCI matrix calculated by Eq. (3.74) will be a null matrix of size $Ndof \times Nfreq$. So, the updating set of equations can be stated as,

$$\{\delta_{ir}\} - [Z_r]_{up} \{\theta^i\} = \{0\} \quad (3.75)$$

Partitioning the updated dynamic stiffness matrix, Eq. (3.75) can be written as

$$\{\delta_{ir}\} - \left[\left(-\omega^2 \left[M + \sum_{i=1}^N m_i [M_e]_i \right] + i\omega \left[C + \sum_{i=1}^N c_i [C_e]_i \right] + \left[K + \sum_{i=1}^N k_i [K_e]_i \right] \right) \right]_{r,up} \{\theta^i\} = \{0\} \quad (3.76)$$

Eq. (3.76) can further be simplified by using the definition of the MCI, given in Eq. (3.67) as follows,

$$\left[\left(-\omega^2 \left[\sum_{i=1}^N m_i [M_e]_i \right] + i\omega \left[\sum_{i=1}^N c_i [C_e]_i \right] + \left[\sum_{i=1}^N k_i [K_e]_i \right] \right) \right]_{r,up} \{\theta^i\} = \{MCI(\omega)\} \quad (3.77)$$

Eq. (3.77) indicates that, in order to vanish the error terms in MCI, the updating matrices should have the negative effect of the original analytical matrices that cause the error. If Eq. (3.77) is written for $Nfreq$ discrete frequency points, one will have a linear equation system in the form

$$[A]\{p\} = \{\delta\} \quad (3.78)$$

which is the standard form of equation sets for indirect model updating algorithms. In Eq. (3.78), matrix $[A]$ is the coefficient matrix containing analytical system matrix and experimental FRF vector multiplications, $\{\delta\}$ is the residual vector containing the original MCI values and $\{p\}$ is the updating parameter vector containing the m_i , k_i , c_i values. If the number of frequency points are such that the system of equations is over-determined (number of equations are larger than number unknowns), then the solution should be searched in a least-squares sense.

The updating task from this point will include

- Determining the updating elements.

- Determining the updating frequency points.
- Obtaining the coefficient matrix and residual vector by using Eq. (3.77).
- Solving the linear set of equations in the form given by Eq. (3.78) by a least-squares regression.

If the experimental data is incomplete, the missing experimental frequency response can be calculated using the measured modal data and analytical system matrices. Modal data expansion is carried out in order to calculate the FRF values at missing degrees of freedom. After the least-squares solution is carried out with the expanded data, the updated analytical matrices are used to re-expand the measured data. This least-squares solution and expansion routine shall be followed until convergence is achieved for the updating parameters.

CHAPTER 4

SOFTWARE DEVELOPED

4.1 DETAILS OF THE SOFTWARE

Except the Eigendynamic Constraint Method, all of the model updating methods (namely the Lagrange Multiplier Method, the Error Matrix Method, the Direct Matrix Updating Method, the Matrix Mixing Method, the Response Function Method, the MCI Minimization Method and the Inverse Eigensensitivity Method) discussed in this study have been coded for performing the case studies to be presented in Chapter 5. However, most of the codes generated are not generic and therefore they can only be used efficiently in terms of computational time for systems containing about a hundred DOF's.

After deciding that the Inverse Eigensensitivity Method is the best for the purpose of updating aircraft finite element models (as will be discussed in Chapters 5 and 6), the software on the Inverse Eigensensitivity Method has been developed further that it can be used for large structures such as a real aircraft. This can be considered as the main software output of this thesis because of its flexibility and ease of use. The software contains two Matlab codes and two Delphi based executable files. The file names and their purposes are:

- **mod_read.exe** - Reordering the mode shapes by using the *.f06 file of MSC Nastran as an input.
- **correlate.m** - Correlating the experimental and analytical models (coded in Matlab)
- **sens_order.exe** - Reordering the sensitivity values present in the *.f06 file of MSC Nastran

- **update.m** - Calculating the updating parameter values by using the Inverse Eigensensitivity Method (coded in Matlab)

The mod_read.exe file used for reordering the mode shapes is coded in Delphi. The code simply reads the *.f06 file and writes the mode shapes obtained in six cartesian coordinates of all nodes in separate files with the related node map.

The correlate.m software needs the following inputs:

- The experimental mode shape data (the matrix saved as a text file)
- The experimental natural frequencies (vector saved as a text file)
- Analytical mode shapes (the output of the mod_read.exe)
- The node map of the analytical mode shape data (the output of mod_read.exe)
- The *.f06 file (in order to extract the analytical natural frequencies)
- The measured nodes and related degrees of freedom and the counterparts of those in the analytical model (a text file with the first column containing the experimental nodes, second column containing the experimental degrees of freedom of the nodes given in the first column, and the third containing the analytical counterparts of the first and second columns).
- The matching matrix of the modes to be correlated (the default value should be composed of two identical vectors having numerical values from 1 to n, where n is the number of the highest mode in concern).

The software called correlate.m first orders the new set of analytical mode shapes at the measured degrees of freedom. This mode shape matrix is then used to calculate and plot the MAC matrix for which the definition is given in Sections 2.2.1 and 2.2.2.

The analytical natural frequencies are directly read by correlate.m from the *.f06 file and they are plotted against the experimental ones read from an external text file.

The user should decide the matching mode pairs in the first run either by examining the MAC matrix or the display of the mode shapes (from modal analysis

software) and change the matching matrix accordingly. A run after this point will correlate the correct mode pairs and the outputs obtained since the text files will contain these data. The outputs of these software are:

- MAC matrix and natural frequency comparison graphs.
- Analytical mode shape matrix at the measured degrees of freedom (of the order of the experimental mode shape matrix) written in a text file.
- Analytical natural frequency vector written in a text file.

The outputs of `correlate.m` software are needed by the model updating code `update.m`, which uses the modal sensitivities calculated from MSC Nastran. The modal sensitivities are given in a text file in a formatted way. However, the format of the result file containing the sensitivity values is not directly usable. In order to overcome this, the Delphi based executable file `sens_order.exe`, is used to reorder the sensitivity values given in the *.f06 file.

The *.f06 file shall contain the weight sensitivity values, sensitivity values for a single natural frequency, sensitivity values for mode shapes (no limitations in number) at a single natural frequency. If several other modes are investigated, several runs should be made using MSC Nastran and each output file should be ordered differently.

After the sensitivity values are ordered in text files, the following inputs which are obtained from the Nastran output and bulk data files have to be given in order to calculate the updating parameters.

- The initial values of the parameters and their orders in the output file
- The order of the modal responses in the output file

The software `update.m` reads and writes the sensitivity values that are placed in different text files into a single matrix. Then using the equations given in Section 3.2.2 and using one of the two solver possibilities available, the new values of the updating parameters are calculated. The possible solver types are as below:

CHAPTER 5

CASE STUDIES

5.1 CASE STUDIES ON A SIX DOF SPRING MASS SYSTEM

The spring-mass system analyzed by Kabe [44] is used to demonstrate the application and accuracy of each updating technique discussed in this thesis (the Lagrange Multiplier Method, the Error Matrix Method, the Direct Matrix Updating Method, the Matrix Mixing Method, the Response Function Method, the MCI Minimization Method). The system considered is shown in Figure 5 while the stiffness values of the springs and the masses are tabulated in Table 1.

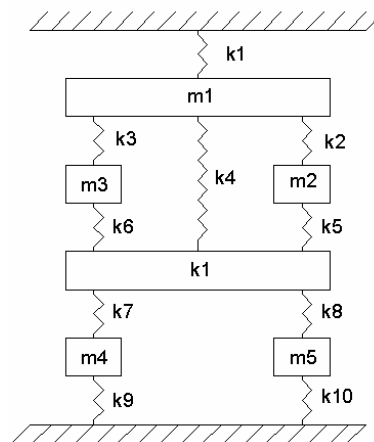


Figure 5. Spring-Mass System Used in Case Studies

Table 1. Stiffness and Mass Values for Original Analytical and Pseudo-Experimental Model

Parameter	Pseudo-Experimental Model (Actual Values)	Original Analytical Model Value (Incorrect Values)
k1	3800 (N/m)	3000 (N/m)
k2	1900 (N/m)	1500 (N/m)
k3	400 (N/m)	1000 (N/m)
k4	3100 (N/m)	2000 (N/m)
k5	1500 (N/m)	1100 (N/m)
k6	1300 (N/m)	1400 (N/m)
k7	1400 (N/m)	1250 (N/m)
k8	6500 (N/m)	5000 (N/m)
k9	2200 (N/m)	3000 (N/m)
k10	1600 (N/m)	1000 (N/m)
m1	0.9 (kg)	1.0 (kg)
m2	1.1 (kg)	1.5 (kg)
m3	1.2 (kg)	1.2 (kg)
m4	1.8 (kg)	2.0 (kg)
m5	2.4 (kg)	2.5 (kg)
m6	1.6 (kg)	1.1 (kg)

Table 2. Experimental and Analytical Natural Frequencies and Initial Errors in the Natural Frequencies of the 6 DOF Spring-Mass System

Mode Number	Experimental Natural Frequency (Hz)	Analytical Natural Frequency (Hz)	Initial % Error in Natural Frequencies
1	3.9	3.8	3.7
2	6.0	6.7	-11.1
3	6.6	7.4	-11.7
4	9.2	7.9	13.3
5	15.2	13.8	8.9
6	17.7	15.6	11.7

5.1.1 Point FRF Results for Updating with the Method Using Lagrange Multipliers

Results (point FRF plots for the degree of freedom of mass 1) obtained by using Eq. (3.5) and Eq. (3.10) are given in Figure 6 and Figure 7. For the given plots, there are no errors in the stiffness matrix and in the mass matrix respectively. Direct Methods are not investigated as candidates for methods that will be used for real structures; therefore no noise has been added to the experimental data and this case is solved only for demonstration.

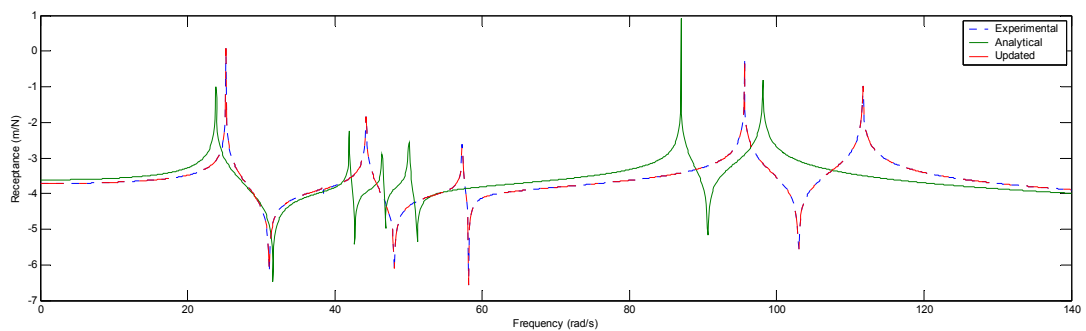


Figure 6. Point Receptance (DOF of Mass 1) Plots (Experimental, Theoretical, Updated) Solved by Lagrange Multipliers Method for Error in Mass Matrix Only (No Error in Stiffness Matrix)

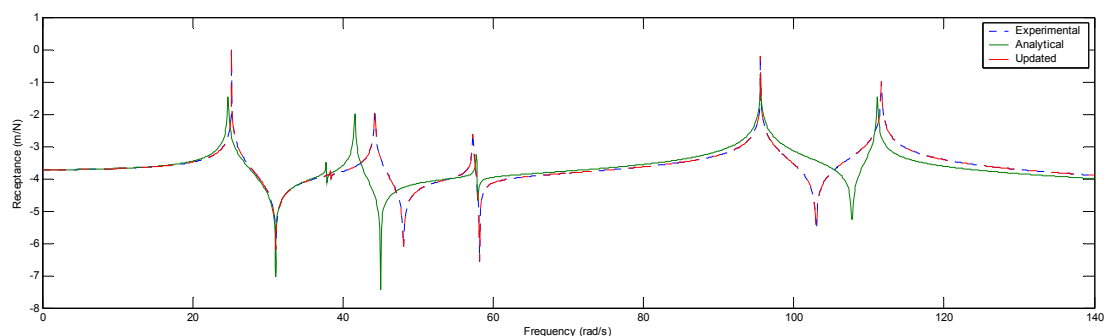


Figure 7. Point Receptance (DOF of Mass 1) Plots (Experimental, Theoretical, Updated) Solved by Lagrange Multipliers Method for Error in Stiffness Matrix Only (No Error in Mass Matrix)

The updated results for both cases are exactly the same as the experimental results as the method is a direct one using the analytical matrices.

5.1.2 Point FRF Results for Updating with the Error Matrix Methods

Point FRF plot for the mass-spring system updated using the Error Matrix Method is given in Figure 8. Direct Methods are not investigated as candidates for methods that will be used for real structures; therefore no noise has been added to the experimental data and this case is solved only for demonstration.

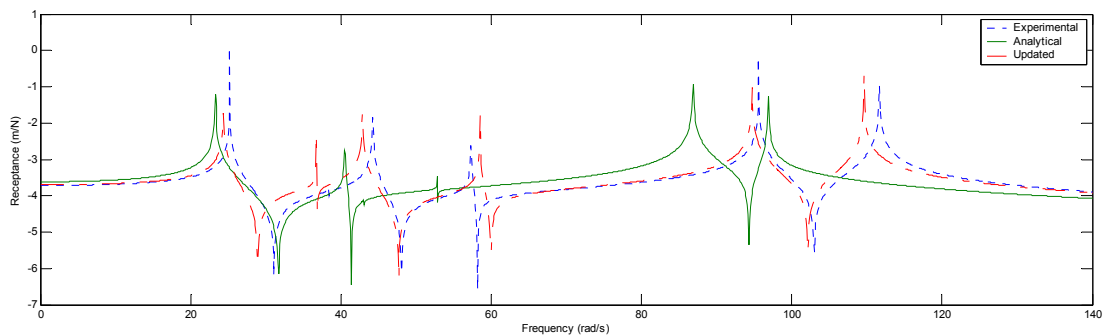


Figure 8. Point Receptance (DOF of Mass 1) Plots (Experimental, Theoretical, Updated) Solved by Error Matrix Method

As this method ignores the 2nd and higher order error terms, the obtained results are not exact ones.

5.1.3 Point FRF Results for Updating with the Direct Matrix Updating Method

Point FRF plot for the mass-spring system updated using the Direct Matrix Updating Method is given in Figure 9. Direct Methods are not investigated as candidates for methods that will be used for real structures; therefore no noise has been added to the experimental data and this case is solved only for demonstration.

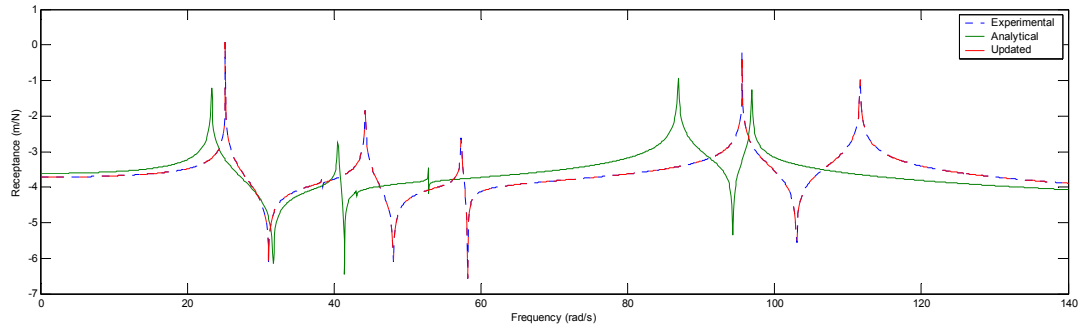


Figure 9. Point Receptance (DOF of Mass 1) Plots (Experimental, Theoretical, Updated) Solved by Direct Matrix Updating Method

The updated results are exactly the same as the experimental results as the method is a direct one using the analytical matrices.

5.1.4 Point FRF Results for Updating with the Matrix Mixing Method

Point FRF plot for the mass-spring system updated using the Matrix Mixing Method is given Figure 10. In this example, FRF's are assumed to be measured at all degrees of freedom. Direct Methods are not investigated as candidates for methods that will be used for real structures; therefore no noise has been added to the experimental data and this case is solved only for demonstration.

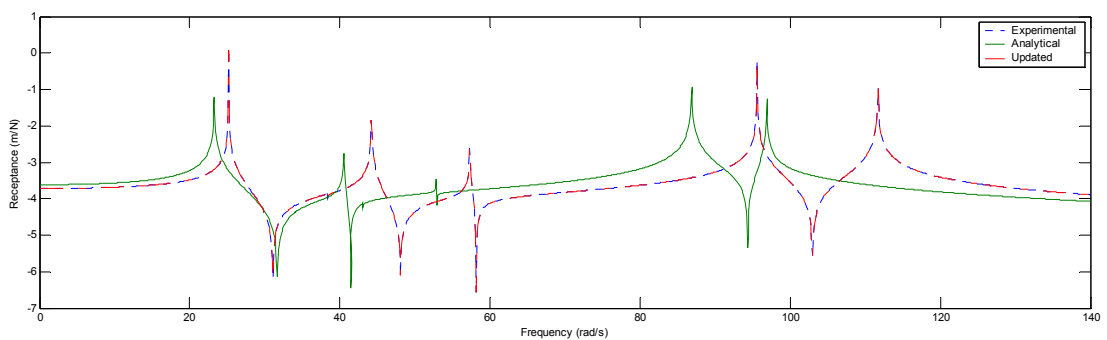


Figure 10. Point Receptance (DOF of Mass 1) Plots (Experimental, Theoretical, Updated) Solved by Matrix Mixing Method

The updated results are exactly the same as the experimental results as the method is a direct one using the analytical matrices.

5.1.5 Point FRF Results for Updating with the Response Function Method

Point FRF plot for the mass-spring system updated using the Response Function Method is given in Figure 11-Figure 16. The FRF values of the pseudo-experimental model are polluted (random noise of maximum 5%) in order to simulate the experimental noise. Also, the experimental model has viscous damping (the dampers are placed at spring locations and their values are 0.0003 times of spring constant values) while the original analytical model contains no damping.

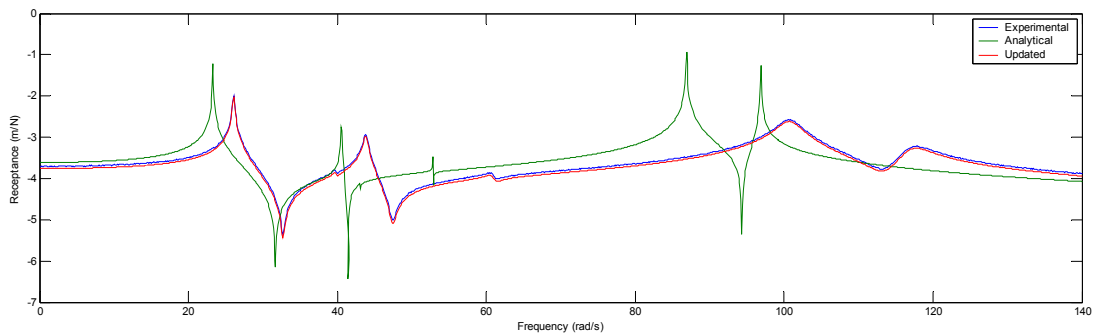


Figure 11. FRF Plots of Experimental, Original and Updated Models when Excitation and Response are at 1st DOF

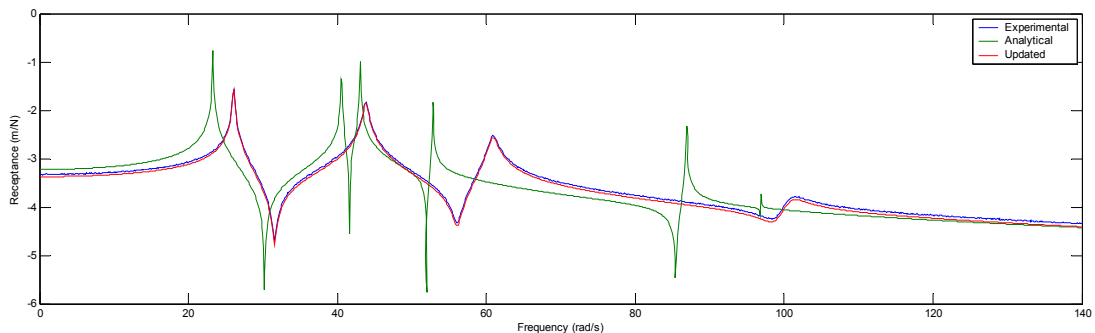


Figure 12. FRF Plots of Experimental, Original and Updated Models when Excitation and Response are at 2nd DOF

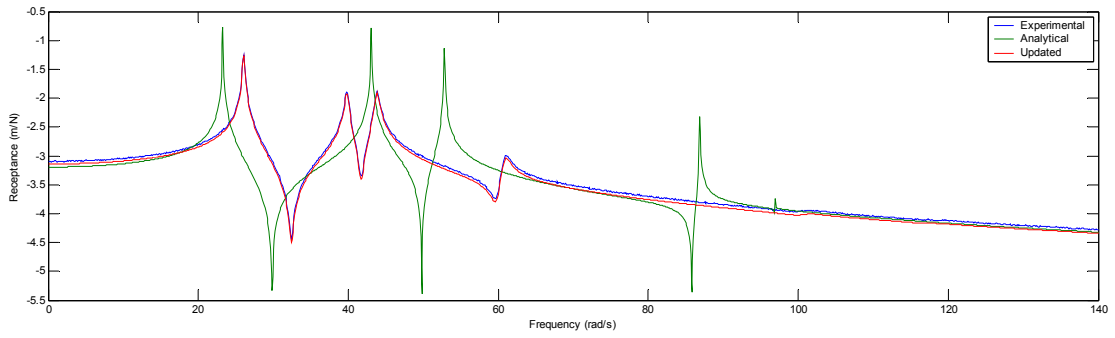


Figure 13. FRF Plots of Experimental, Original and Updated Models when Excitation and Response are at 3rd DOF

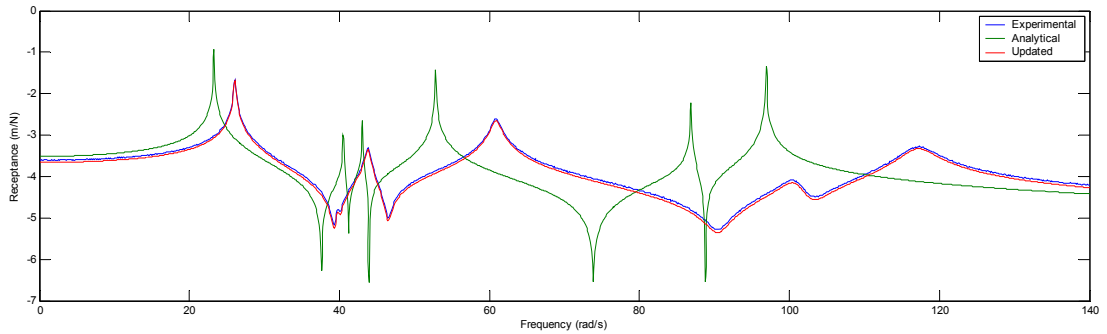


Figure 14. FRF Plots of Experimental, Original and Updated Models when Excitation and Response are at 4th DOF

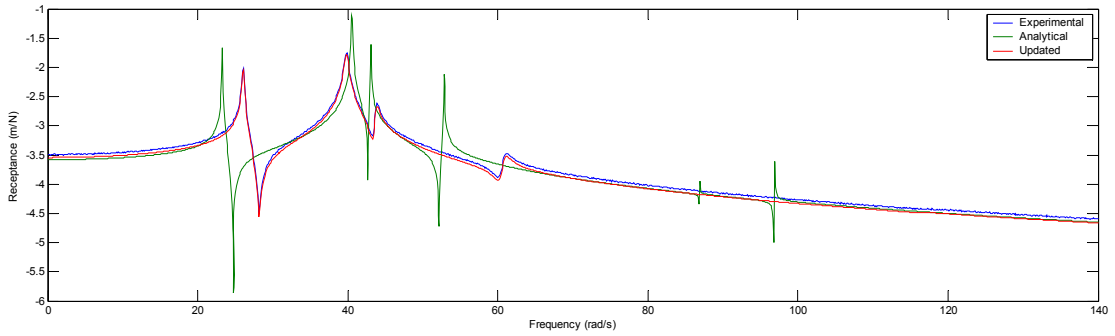


Figure 15. FRF Plots of Experimental, Original and Updated Models when Excitation and Response are at 5th DOF

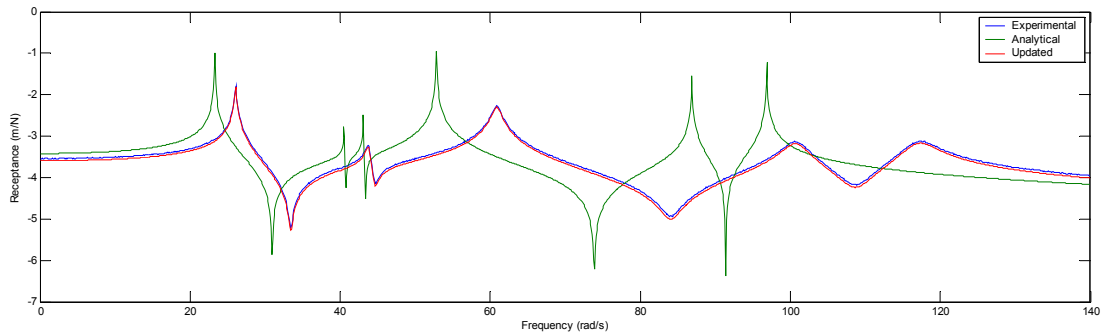


Figure 16. FRF Plots of Experimental, Original and Updated Models when Excitation and Response are at 6th DOF

About 1400 frequency points (a sweep from 0.1 Hz to 140 Hz with 0.1 Hz increments) are used as updating frequencies. Although the experimental model contains a random error level of 5%, the updating procedure can exactly update the original model. The method can also update damping matrix whether the initial model contains damping or not.

5.1.6 Point FRF Results for Updating with the MCI Minimization Method

Point FRF plots for the mass-spring system updated using the MCI Minimization Method is given in Figure 19-Figure 24. The FRF values of the pseudo-experimental model are polluted in order to simulate the experimental noise. The pseudo-experimental model is constructed using the responses that are assumed to be measured from coordinates 2, 3 and 4. The rest of the frequency responses are calculated using expanded modal data. This case study is performed in order to see the capability of the method under noisy and incomplete experimental model. In total, 16 parameters are searched for updating (10 spring constants and 6 mass values). The absolute maximum values of MCI values at each iteration and convergence plot are given in Figure 17 and Figure 18 respectively. The pseudo-experimental, analytical and updated models' point receptance plots (after convergence) are given in Figure 19-Figure 24.

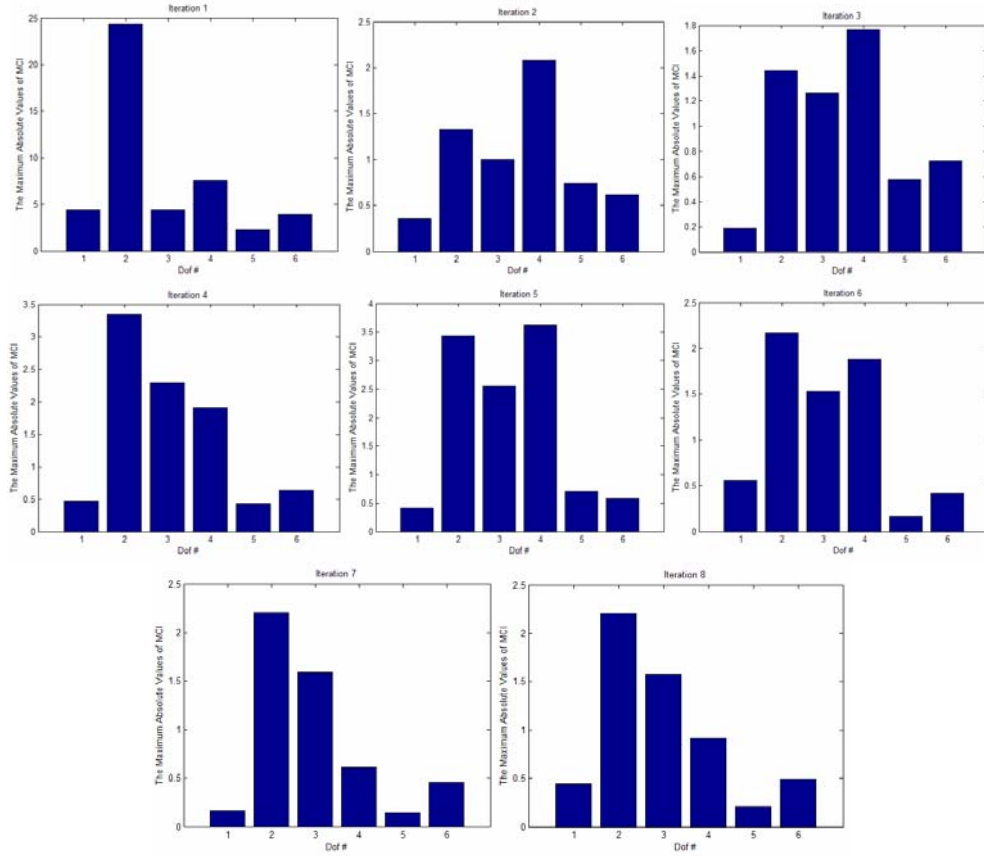


Figure 17. Absolute Maxima of MCI Values at All DOF's

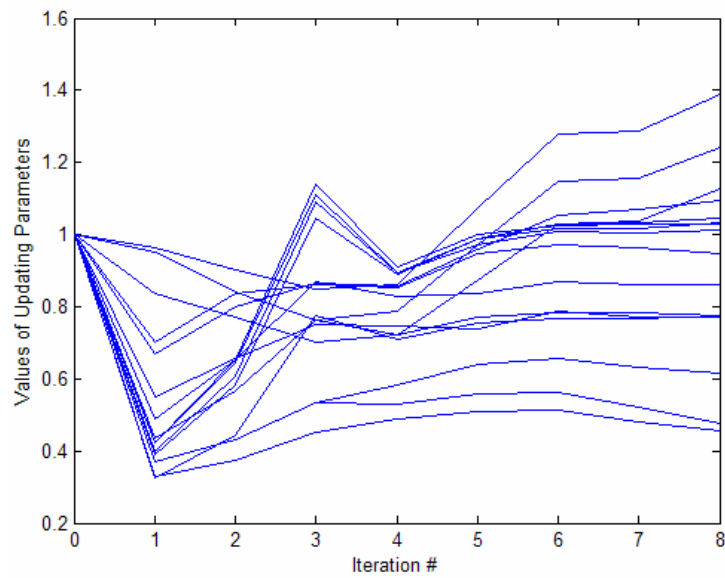


Figure 18. Convergence of Updating Parameters

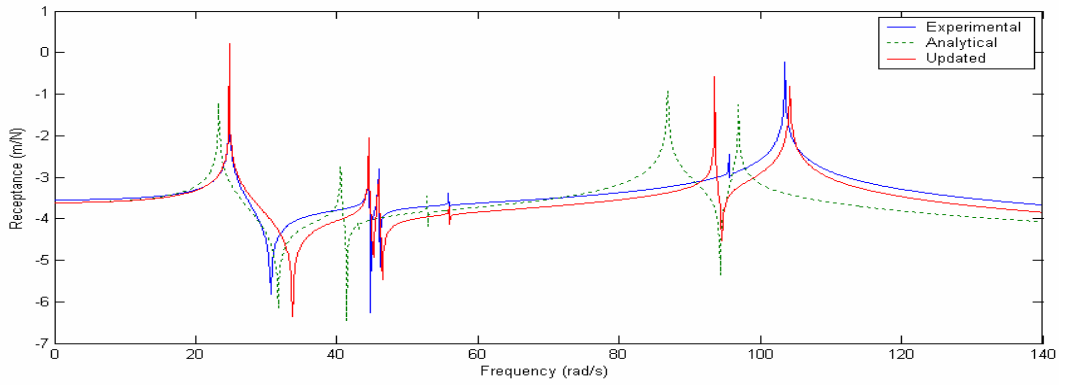


Figure 19. FRF Plots of Experimental, Original and Updated Models when Excitation and Response are at 1st DOF

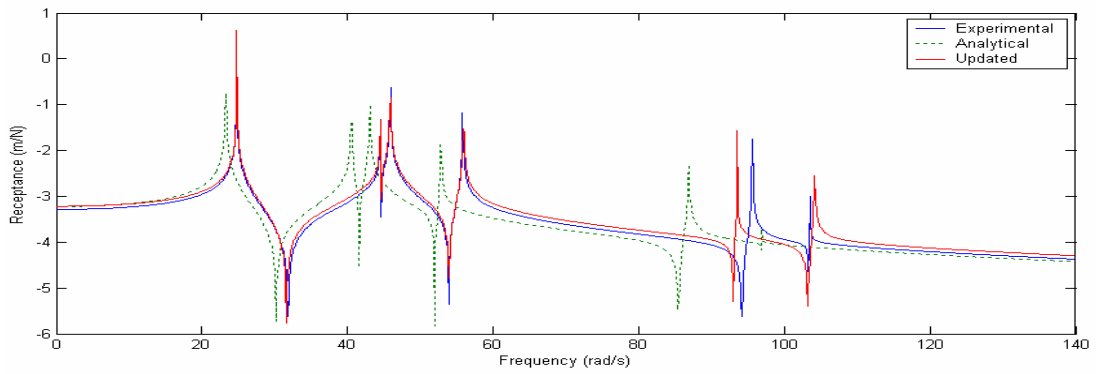


Figure 20. FRF Plots of Experimental, Original and Updated Models when Excitation and Response are at 2nd DOF

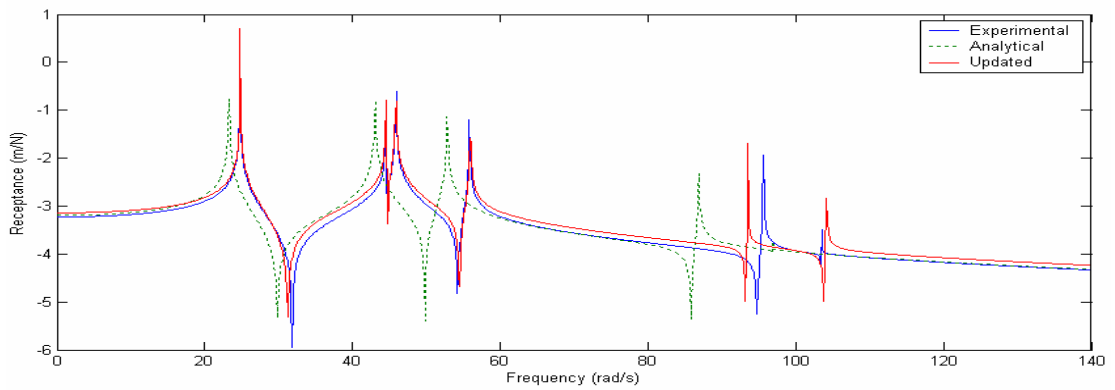


Figure 21. FRF Plots of Experimental, Original and Updated Models when Excitation and Response are at 3rd DOF

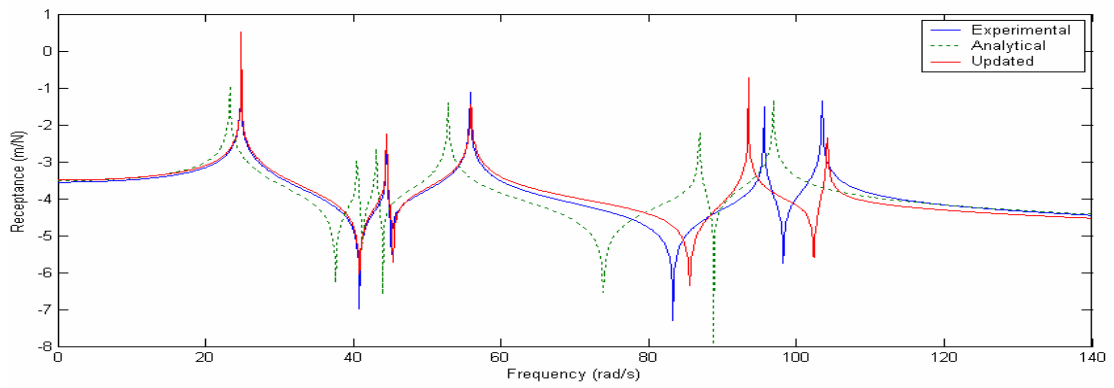


Figure 22. FRF Plots of Experimental, Original and Updated Models when Excitation and Response are at 4th DOF

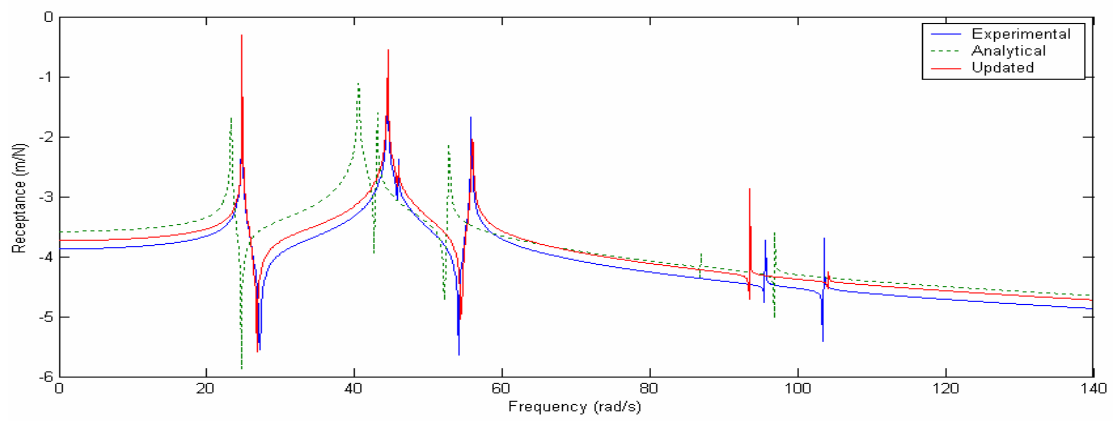


Figure 23. FRF Plots of Experimental, Original and Updated Models when Excitation and Response are at 5th DOF

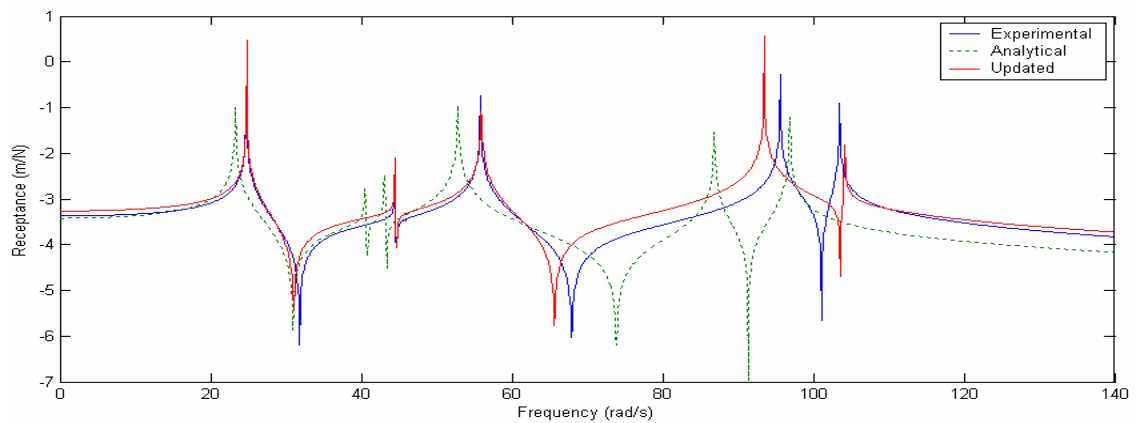


Figure 24. FRF Plots of Experimental, Original and Updated Models when Excitation and Response are at 6th DOF

The method expands the experimental data and searches for the updated solution with expanded experimental data. As the expansion process uses analytical matrices that are updated after each iteration, the expanded data are also updated. This expansion and updating procedure continues till convergence at updating parameter values is achieved.

5.2 CASE STUDIES ON A 20 DOF FREE-FREE COMPOSITE BEAM USING THE MCI MINIMIZATION METHOD

The beam structure analyzed in the second case study is shown in Figure 25 and the physical properties of the analytical model and the pseudo-experimental model are given in Table 3 and Table 4.

Table 3. Geometric Parameters for Original Analytical and Pseudo-Experimental Model (mm)

Element # / Geometric Parameter	Outer Diameter (Experimental Model)	Inner Diameter (Experimental Model)	Outer Diameter (Analytical Model)	Inner Diameter (Analytical Model)
1	10.50	8.40	10.00	8.00
2	10.20	8.30	9.00	8.00
3	10.00	8.00	9.00	8.00
4	9.10	6.20	9.00	6.00
5	9.90	6.12	9.00	6.00
6	9.10	6.11	9.00	6.00
7	7.20	5.56	7.00	5.50
8	7.10	5.43	7.00	5.50
9	7.40	5.12	7.00	5.50

The structure is modeled by using beam elements with 2 DOF at each node. There are in total 9 beam elements in the model. The pseudo-experimental model is suspended with soft cords at nodes 1 and 10. The stiffness values of these cords are added to the related diagonal term of the matrices of the elements having these nodes.

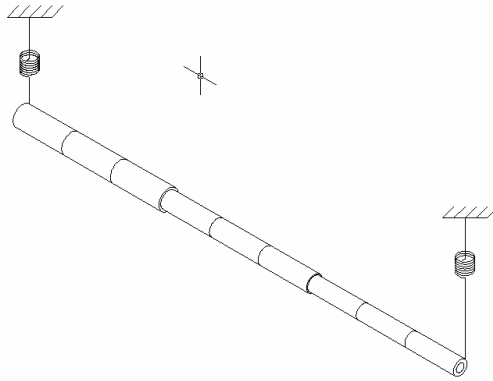


Figure 25. Illustration of the Beam Model Used in Second Case Study

Table 4. Material Property Ratios (Experimental/Analytical) for Original Analytical to Pseudo-Experimental Model

Element #	Young's Modulus Ratio	Mass Density Ratio	Ratio for Poisson's Ratio
1	1.20	1.05	1.50
2	1.20	1.05	1.50
3	1.20	1.05	1.50
4	1.05	0.98	0.80
5	1.05	0.98	0.80
6	1.05	0.98	0.80
7	0.96	1.00	1.20
8	0.96	1.00	1.20
9	0.96	1.00	1.20

It is assumed that responses from all the degrees of freedom are available and the excitation is applied at the 5th node. No artificial noise is applied to the pseudo-experimental response.

The starting MCI plots of the pseudo-experimental models having 100 N/m and 1000 N/m elastic cords are given in Figure 26 and Figure 27 respectively.

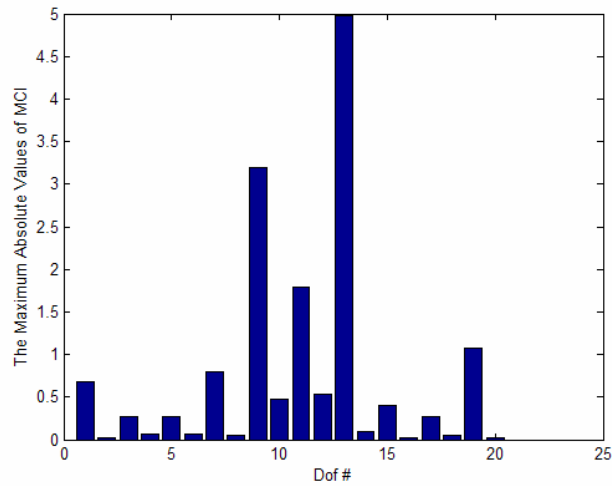


Figure 26. The Absolute Maxima of the Starting MCI Values at All DOF's for an Elastic Cord Stiffness of 100 N/m

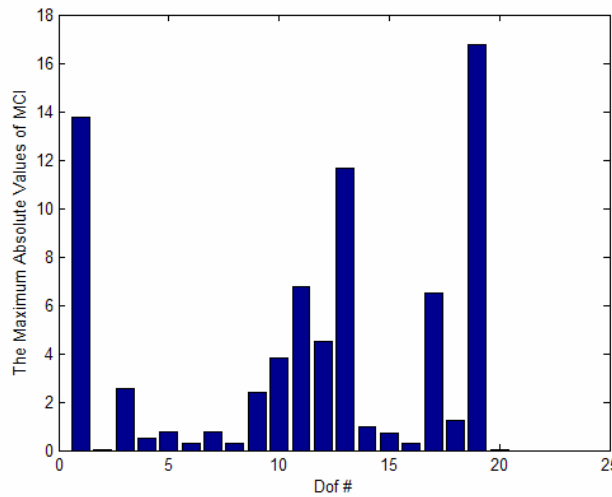


Figure 27. The Absolute Maxima of the Starting MCI Values at All DOF's for an Elastic Cord Stiffness of 1000 N/m

The elastic cords affect the rigid body modes, so if the updating frequencies are selected away from the low frequency band (0-20 rad/s for this case), convergent solutions are obtained. However, if the updating frequencies include those omitted frequency values, then the algorithm seeks for an analytical model that is connected to the ground. As the updating is based on finding the multipliers of the individual elements, any connection to the ground like the one in the pseudo-

experimental model can not be obtained and the relation between the pseudo-experimental and updated model responses can not be satisfied perfectly even for the larger values of frequencies. Also, the effect of the 1000N/m elastic cord on the rigid body modes is higher. So at lower frequency values, the correlation between the pseudo-experimental and analytical FRF values of data with the 100 N/m elastic cord is better than the data with the 1000 N/m elastic cord.

In Figure 28-Figure 33, the updating frequencies are taken between 40-80 rad/s (only the equations between these two frequencies are used for updating). As it can be seen from the graphs, the FRF plots of the updated model do have rigid body modes (having frequencies higher than zero) that are influenced by the cords. However, getting away from the first two elastic mode natural frequencies, close agreement between the pseudo-experimental and updated model responses are obtained.

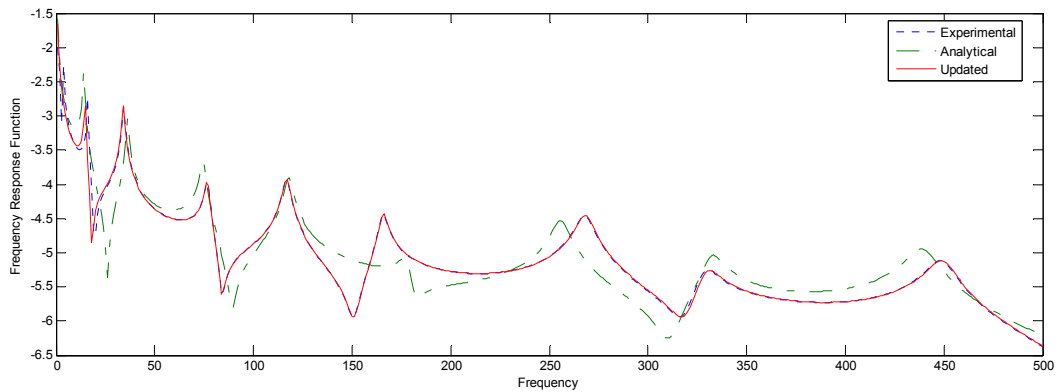


Figure 28. FRF Plots of the Experimental, the Original and the Updated Models when Excitation is at 9th DOF and Response is at 1st DOF for an Elastic Cord Stiffness of 100 N/m

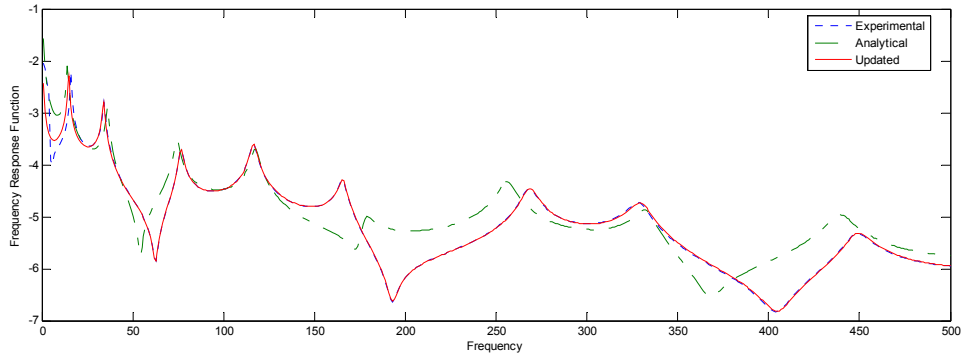


Figure 29. FRF Plots of the Experimental, the Original and the Updated Models when Excitation is at 9th DOF and Response is at 19th DOF for an Elastic Cord Stiffness of 100 N/m

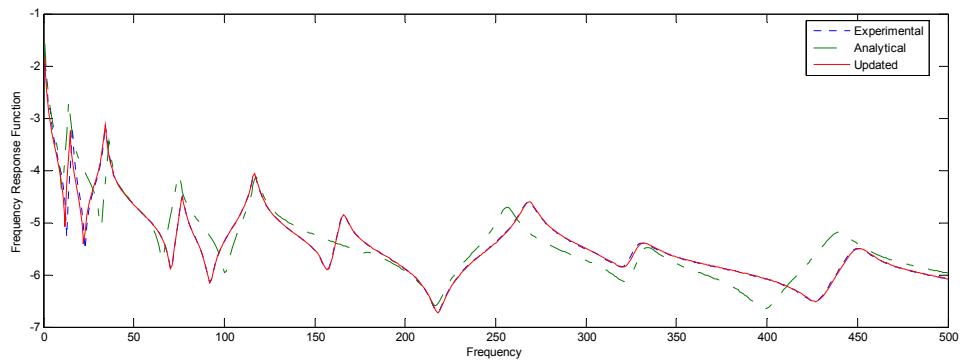


Figure 30. FRF Plots of the Experimental, the Original and the Updated Models when Excitation is at 9th DOF and Response is at 9th DOF for an Elastic Cord Stiffness of 100 N/m

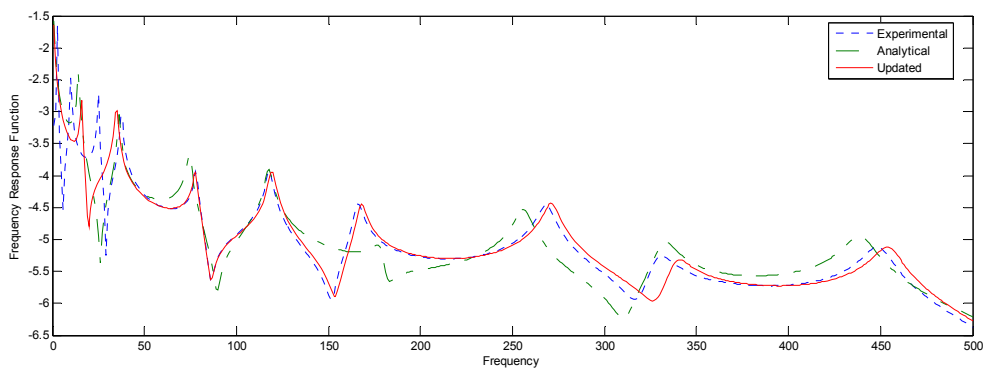


Figure 31. FRF Plots of the Experimental, the Original and the Updated Models when Excitation is at 9th DOF and Response is at 1st DOF for an Elastic Cord Stiffness of 1000 N/m

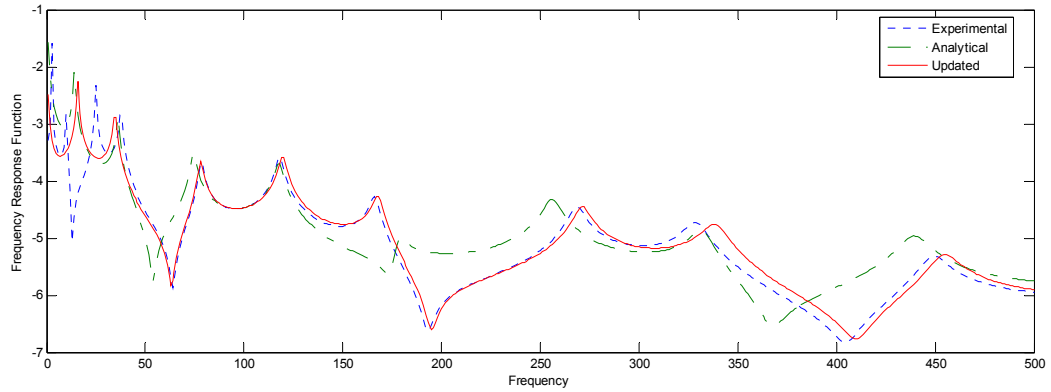


Figure 32. FRF Plots of the Experimental, the Original and the Updated Models when Excitation is at 9th DOF and Response is at 19th DOF for an Elastic Cord Stiffness of 1000 N/m

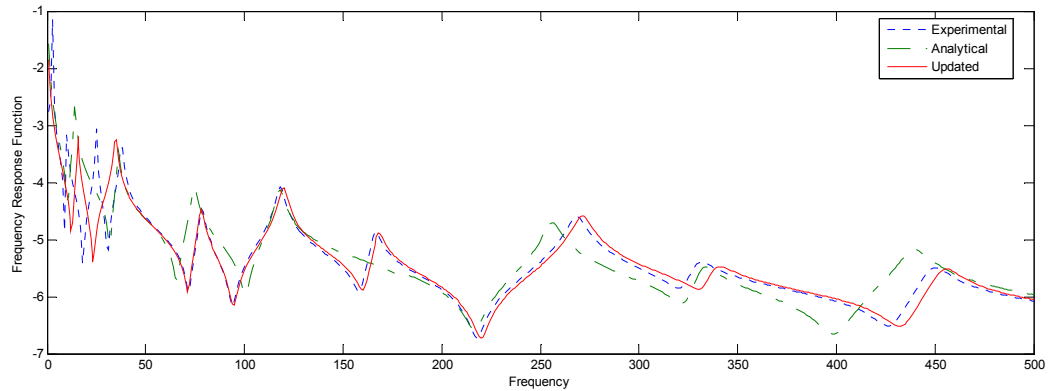


Figure 33. FRF Plots of the Experimental, the Original and the Updated Models when Excitation is at 9th DOF and Response is at 9th DOF for an Elastic Cord Stiffness of 1000 N/m

The MCI plots after applying the updating procedure are also given in Figure 34- Figure 35. As it is mentioned above, the effect of the cords could not be reflected on the updated model with an updating scheme of multiplying the individual matrices with updating parameters. So, at the end of the updating procedure, error is located only in the coordinates to which the cords are connected. For the rest of the coordinates, the updating algorithm effectively nullifies the error.

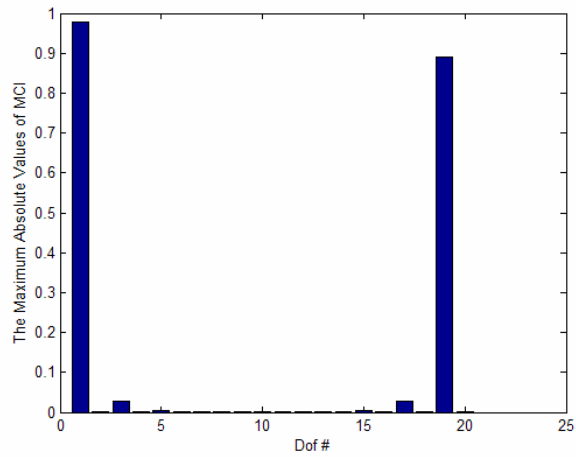


Figure 34. The Absolute Maximum of the Final MCI Values at All DOF's for an Elastic Cord Stiffness of 100 N/m

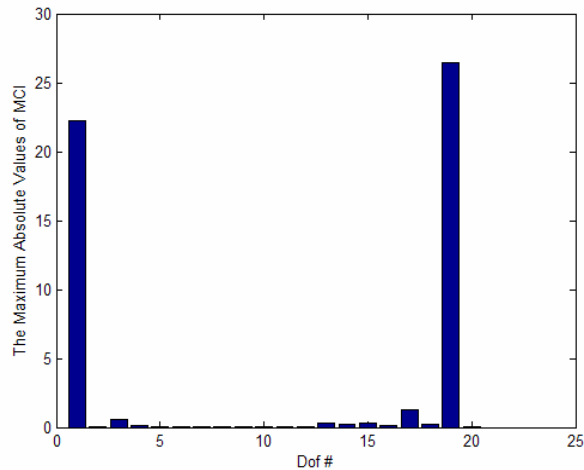


Figure 35. The Absolute Maximum of the Final MCI Values at All DOF's for an Elastic Cord Stiffness of 1000 N/m

Detailed discussions on the results obtained by MCI minimization technique on given case studies are given in 6.1.2.

5.3 CASE STUDY ON A SCALED AIRCRAFT MODEL USING THE INVERSE EIGENSENSITIVITY METHOD

Another case study on Inverse Eigensensitivity Method was conducted on a real test structure. The test-bed is a one-to-one replication in dimensions of the test-bed

designed and used by GARTEUR (Group for Aeronautical Research and Technology in Europe). The test-bed is special in the sense that, a community in Europe uses the results of the tests conducted on the same structure and continue with different or the same approaches on the same test data. The difference of the test-bed used in this thesis with the one used by GARTEUR is in the joints. For the test-bed under consideration in this thesis the wing-fuselage, fuselage-vertical stabilizer and vertical stabilizer-horizontal stabilizer are joined by welding, whereas in the original GARTEUR model these are joined by bolts. Also, in the original GARTEUR model a viscoelastic tape was placed on the upper surface of the wings, however such an additional damper was not used for the tests conducted in this thesis. The test-bed used in this thesis, which was manufactured and tested in TÜBİTAK-SAGE is shown in Figure 36.

Modal impact tests were conducted on the test bed and the results of the tests were used for model updating of the finite element model of the structure.

The dimensions of the aluminum plates and their locations are given in Figure 37 (dimensions are in millimeters).

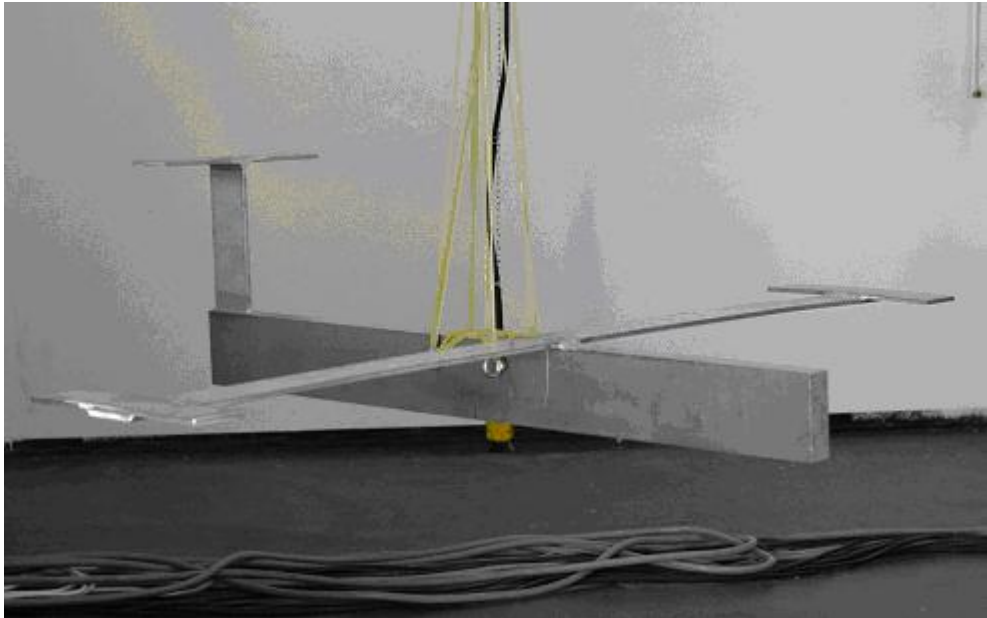


Figure 36. Test-Bed Tested in TÜBİTAK-SAGE

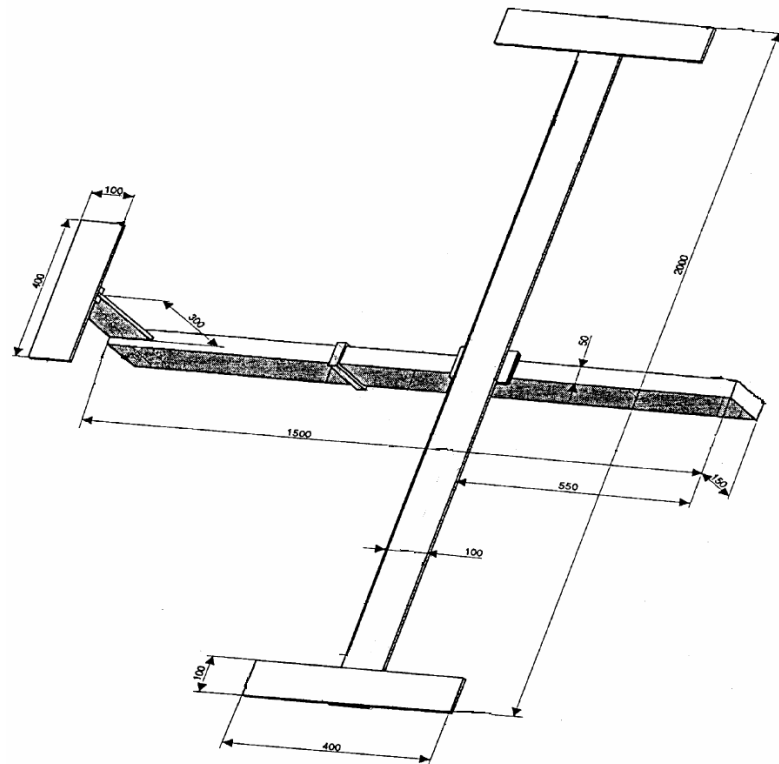


Figure 37. The Dimensions and Locations of the Aluminum Plates in GARTEUR SM-AG19 Test-Bed (Dimensions in mm)

The test-bed was hung from the hooks (for which the details are given in Figure 38) in order to obtain the free-free boundary conditions applied in the associated finite element model. The rigid body modes of the test-bed were determined to be about 1 Hz.

The modal tests were conducted by using accelerometers, a modal hammer and a modal sledge hammer. A total of 12 accelerometers, 36 impact points and 66 impact degrees of freedom were used throughout the tests. The FRF set is re-ordered by using the reciprocity rule in order to have 36 measurement and 12 excitation points. In the line model below, the nomenclature for excitation and measurement is shown. The points and degrees of freedom used for excitation and measurement are given in Table 5 and Table 6.

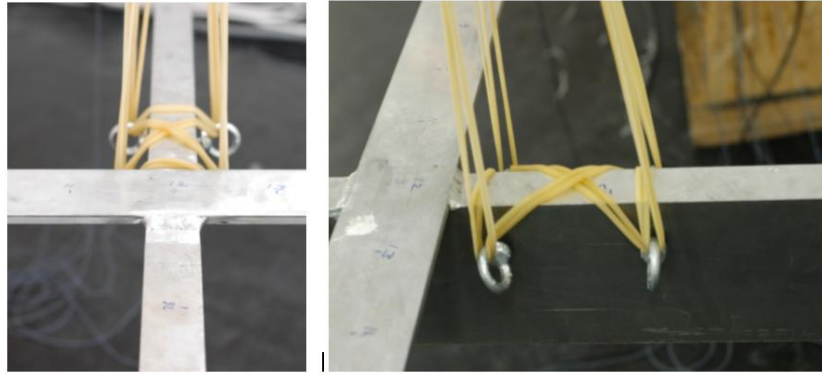


Figure 38. Hooks for Elastic Cords

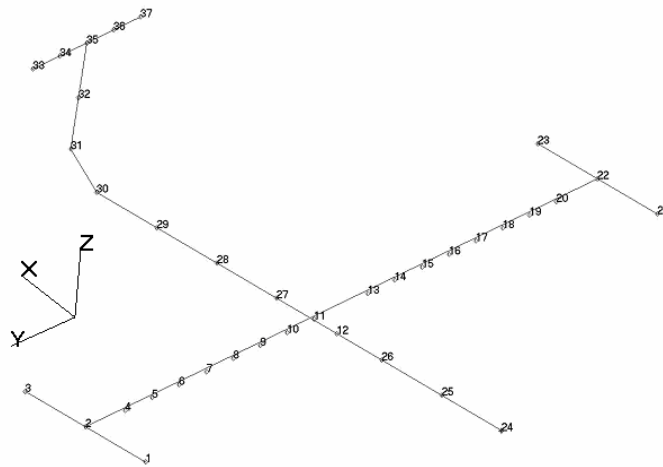


Figure 39. Excitation and Measurement Points and Coordinate Axes

Table 5. Measurement Points and Directions

Measurement Point	Degree of Freedom
1	X-, Z-
3	Z-
6	Z-
18	Z-
21	X-, Z-
23	Z-
31	y-
33	Z-
35	y-
37	Z-

Table 6. Excitation Points and Directions

Excitation Points	Degrees of Freedom	Excitation Points	Degrees of Freedom
1	x-, y-, z-	19	x-, z-
2	z-	20	x-, z-
3	x-, y-, z-	21	x-, y-, z-
4	x-, z-	22	z-
5	x-, z-	23	x-, y-, z-
6	x-, z-	24	z-
7	x-, z-	25	z-
8	x-, z-	26	z-
9	x-, z-	27	Measured by Interpolation
10	x-, z-	28	z-
11	x-, z-	29	z-
12	z-	30	z-
13	x-, z-	31	y-
14	x-, z-	32	y-
15	x-, z-	33	x-, y-, z-
16	x-, z-	34	x-, z-
17	x-, z-	35	x-, z-
18	x-, z-	36	x-, z-
		37	x-, z-

The modal hammer was saturated when the points on the fuselage were excited while the signals from the accelerometers were relatively low. In order to have high signals from the accelerometers without saturating the hammer signal, a modal sledge hammer was used to create larger impact forces for excitation of these points.

A total of 5 excitation samples were conducted for each degree of freedom excited. The excitations for which, the coherence values were thought to be low were repeated. Coherence checks were accomplished using LMS Test.Lab software.

The comparisons were based on other coherence scatters from neighboring degrees freedom through the frequency band.

Data acquisition details are tabulated in Table 7.

Table 7. Data Acquisition Details for Modal Testing of GARTEUR SM-AG19 Test-Bed

Data Acquisition Card	LMS SCADAS III
Max. Capacity of the Accelerometers (g)	50
Max. Capacity of the Modal Hammer (N)	240
Max. Capacity of the Modal Sledge Hammer (N)	22000
Accelerometer Saturation Potential (V)	5
Modal Hammer Saturation Potential (V)	2
Modal Sledge Hammer Saturation Potential (V)	5
Windowing Type	Force-Exponential
Cut-off (%)	1.5
Frequency Resolution (Hz)	1/1024
Data Acquisition Time (per hit) (s)	10.24
Number of Samples (per degree of freedom)	5

The details of accelerometers and hammers used are given in Figure 40.

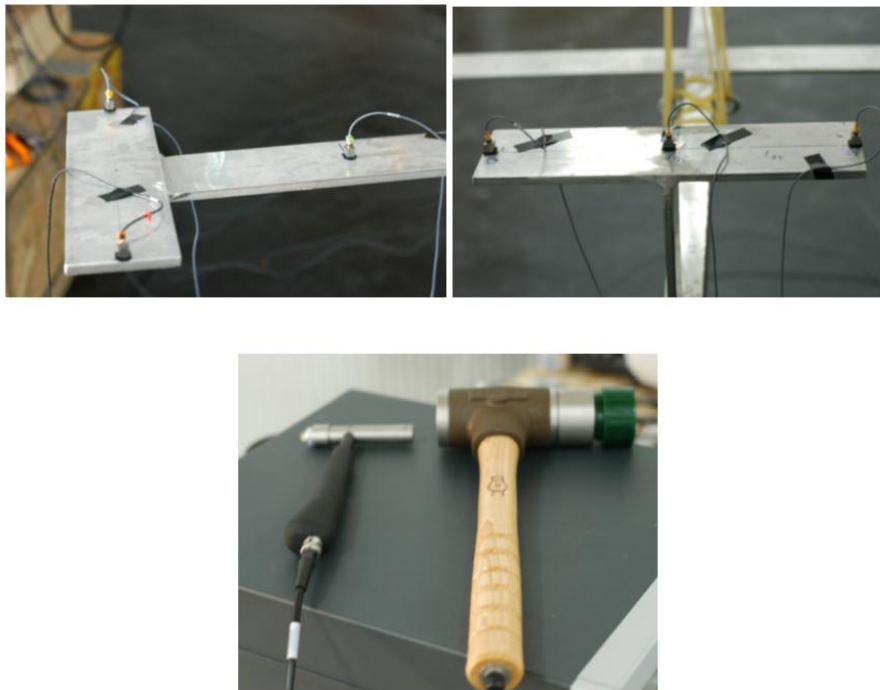


Figure 40. Detailed Photographs of Modal Testing Setup

A sample for FRF and coherence plots for a point FRF measurement from these tests is given in Figure 41 (a screenshot from modal testing software).

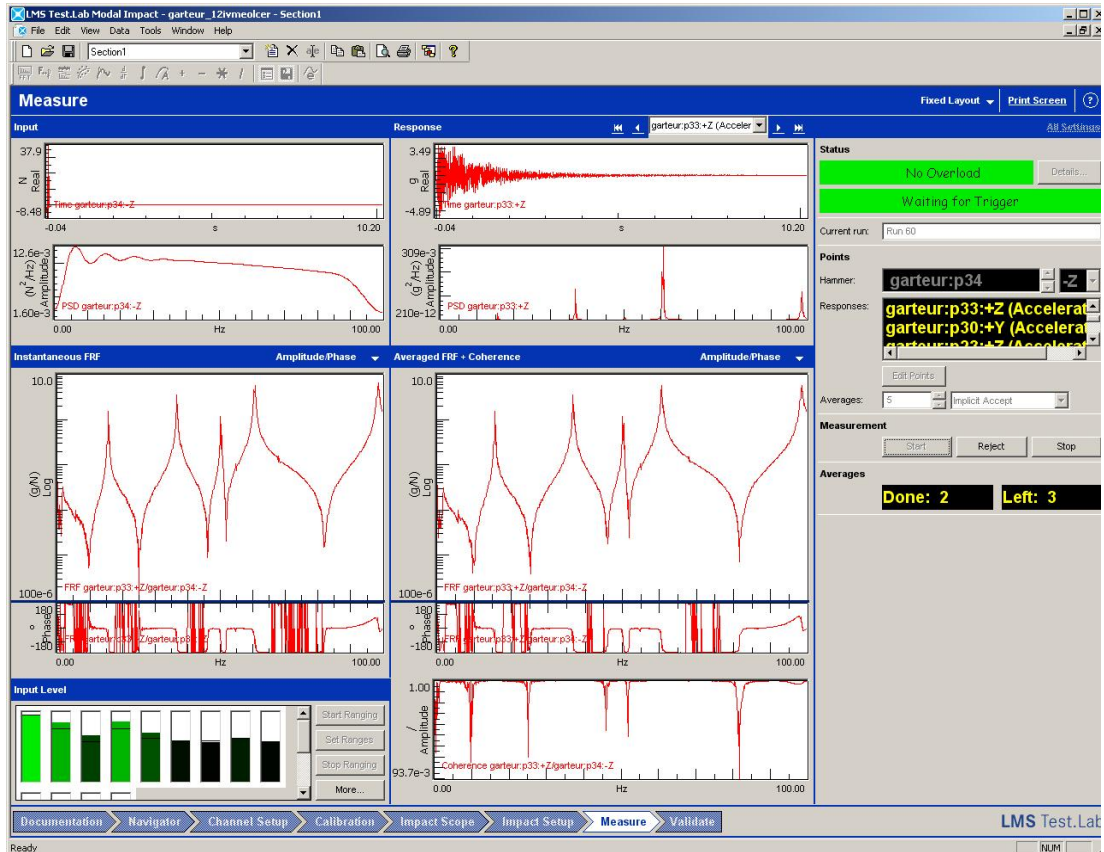


Figure 41. A Screenshot From LMS Modal Testing Software (Excitation and Measurement on z- Axis of Point 34)

After reordering of the FRF values through reciprocity principle, POLYMAX modal analysis software of LMS was used for successive modal analysis.

The stability diagram and chosen stable roots obtained by POLYMAX are given in Figure 42. The model order was chosen to be 150 for modal analysis.

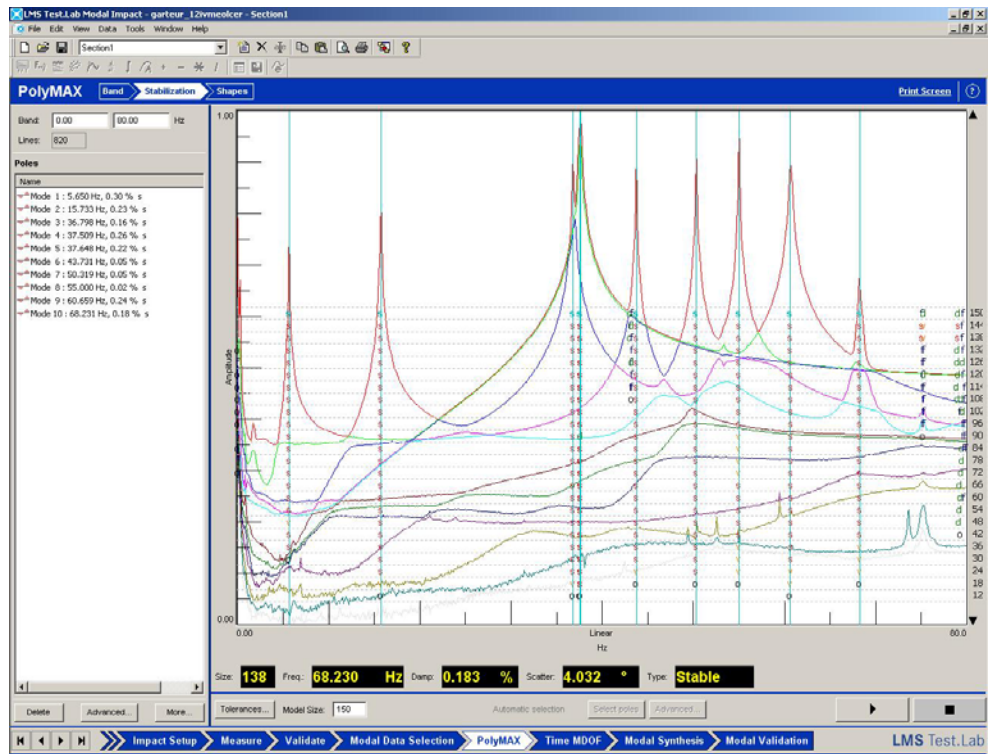


Figure 42. Stability Diagram From POLYMAX

The visual representations of the modes obtained from the above stability diagram and corresponding natural frequencies are given in Figure 43.

The construction and analysis of the finite element model of the test-bed was done by using MSC Patran GUI and MSC Nastran solver respectively.

As the test-bed is composed of strips and the thickness to length ratio of the strips is less than 0.1, the thickness to width ratio of the strips is less than 0.2 (and there are no discontinuities like holes), the strips are modeled as beam elements. The 3-D view of the finite element model is shown in Figure 44.

The thickness of the strips were also taken into account during modeling and the line structure was prepared accordingly. The locations of the strips on the finite element model were the same as the one in the real structure.

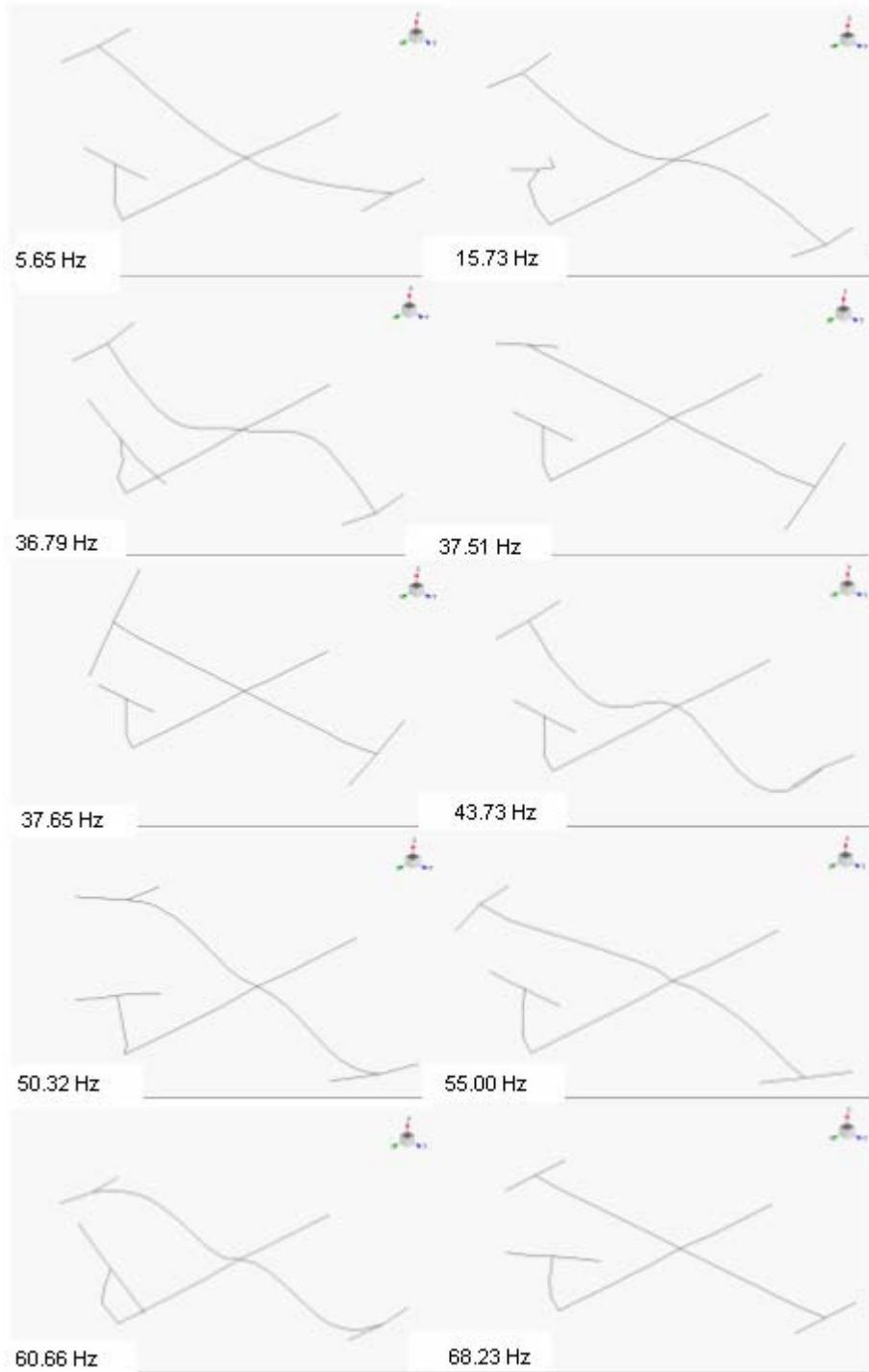


Figure 43. Visual Representations of the First 10 Modes Obtained From POLYMAX

The reason for having broken-line like behaviors in the mode shape representations is the hits that have higher amplitudes in those points.

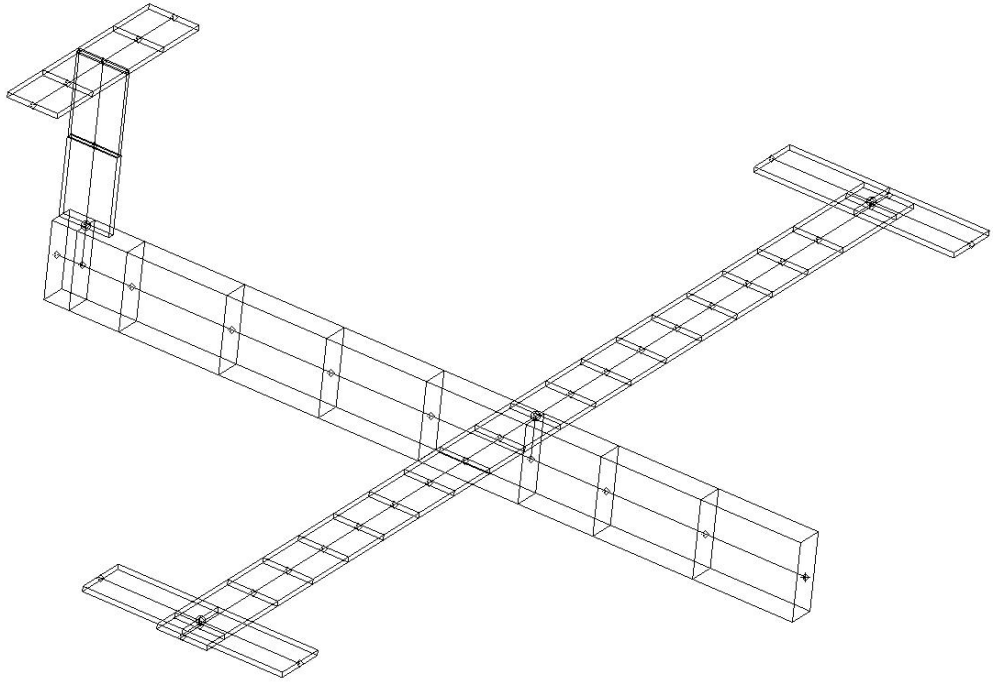


Figure 44. Finite Element Mesh of the Test-Bed Structure (3-D View)

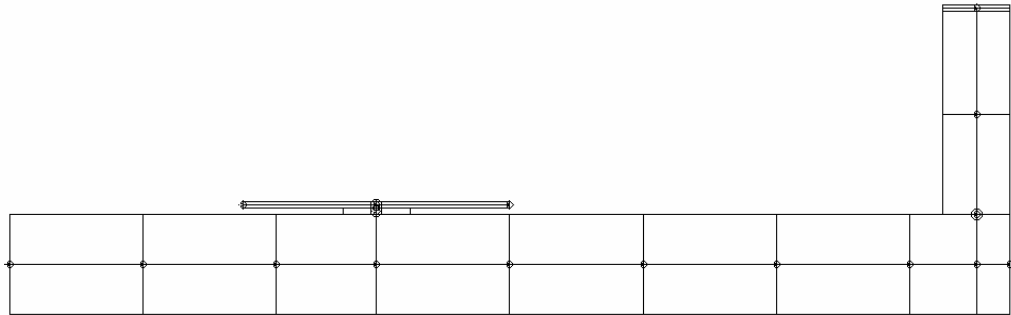


Figure 45. The Locations of the Strips in the Finite Element Model

The differences in the positions of the neutral axes of the beam elements (used for realistic modeling) in z- axis led to discontinuities in the mating junctions of the model. In order to overcome this problem, rigid elements called “*Multi Point Constraint – MPC*” were used between Outer Wing Strips-Wings, Wing-Fuselage

and Fuselage-Vertical Stabilizer. The details of the rigid elements are given in tabulated form in Table 8.

Table 8. MPC Element Details

Parts That MPC Connects	Part That Has the Independent Node	Part That Has the Dependent Node
Outer Wing Strips-Wings (Right Wing)	Wing	Outer Wing Strips
Outer Wing Strips-Wings (Left Wing)	Wing	Outer Wing Strips
Wing-Fuselage	Fuselage	Wing
Fuselage-Vertical Stabilizer	Fuselage	Vertical Stabilizer

The rigid elements conduct the motion on the independent node through the length of the connection. The MPC elements used in the model are shown in Figure 46 in detail.

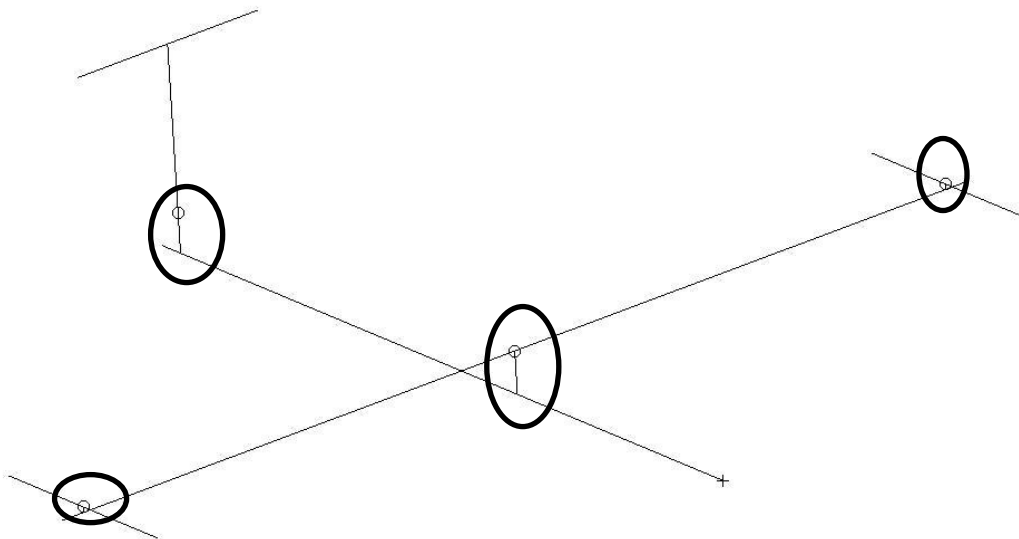


Figure 46. MPC Elements in The Model

The section dimensions of the beam elements are all the same in the original finite element model as they are given in Figure 37. There are 6 more nodes in the finite element model than those in the experimental model. The nomenclature and

positioning of the rest of the nodes are the same for both models (experimental and finite element models). A total of 39 beam elements and 43 nodes (258 degrees of freedom) were used in the finite element model. The beam elements are 3-D 2 noded elements with 6 DOF's at each node. The material properties assigned are tabulated in Table 9.

Table 9. Material Properties Used in the Finite Element Model

Material Property	Value
Young's Modulus (GPa)	70
Density (kg/m^3)	2800
Poisson's Ratio (ν)	0.3

The MAC matrix and natural frequency comparison for the first 10 elastic modes between the experimental model and the original finite element model and the visual representations of the first 10 elastic modes obtained from the original finite element model are given in Figure 47 and Figure 48 respectively.

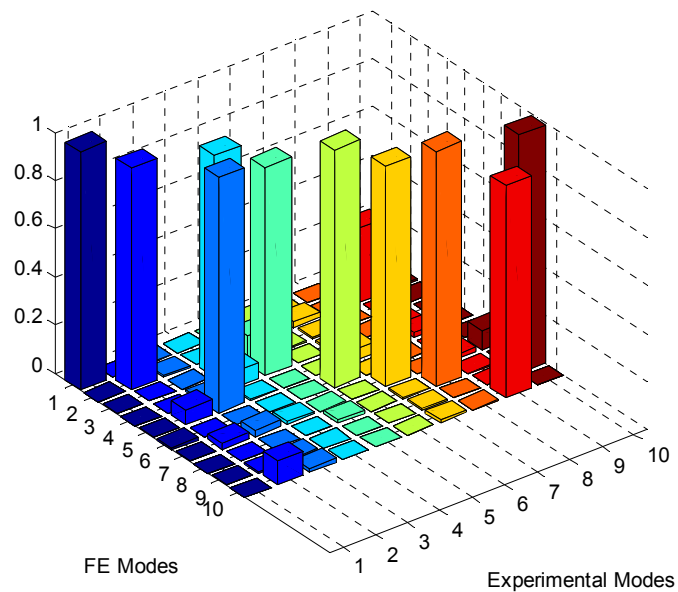


Figure 47. MAC Matrix between the Experimental Model and the Original Finite Element Model

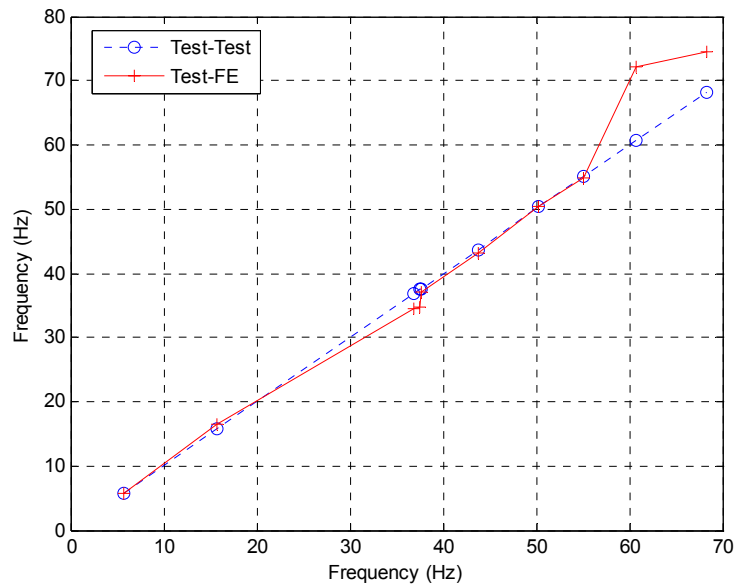


Figure 48. Natural Frequency Comparison between the Experimental Model and the Original Finite Element Model

Through analyzing the original MAC matrix, it is obvious that the ordering of the symmetric and anti-symmetric wing torsional modes and vertical stabilizer torsional mode are wrong. In Table 10, experimental natural frequencies and the correlating finite element model natural frequencies are given.

Table 10. Experimental Modes and Correlating Original Finite Element Model's Modes

Experimental Mode	Natural Frequency (Hz)	Original Finite Element Model Mode	Natural Frequency (Hz)
1	5.65	1	5.66
2	15.73	2	16.54
3	36.79	5	37.05
4	37.51	3	34.57
5	37.65	4	34.67
6	43.73	6	43.17
7	50.32	7	50.35
8	55.00	8	54.75
9	60.66	10	74.43
10	68.23	9	72.16

Good correlation of the mating mode shapes is observed through inspection of the original MAC matrix (a minimum of 80% MAC value for mating pairs), but the natural frequencies are out of order. For this reason, changing the natural frequencies without contaminating the mode shapes is necessary.

In this study, it was tried to accomplish the updating with the minimum possible number of updating parameters. After reviewing the mode shapes of the out-of-order modes, it was decided to choose the parameters which are dominant on wing and vertical stabilizer torsional modes and vertical stabilizer mode about x- axis (it must be noted that the effect of these parameters on the rest of the modes should be low). To do that,

- 2 torsional springs about y axis from the node that node12 is connected with an MPC to the tips of the wings (node 2 for the right wing and node 22 for the left wing)
- a torsional spring about the z axis from node 31 to node 35
- the beam thickness in the y direction of the elements forming the vertical stabilizer

are created or defined as updating parameters. The spring constants are taken as 250000 Nmm/rad and 1000000 Nmm/rad for wings and vertical stabilizers respectively.

After defining the parameters, modal sensitivities of the first 10 modes were calculated using MSC Nastran SOL 200 solver. The iterations were stopped as the natural frequencies calculated by MSC Nastran converged to the experimental natural frequencies. At each step, checks on possible contaminations on the mode shapes were also done.

A total of 6 iteration steps were enough for the parameters to converge. The convergence and the parameter values at each iteration step are given in Figure 50.

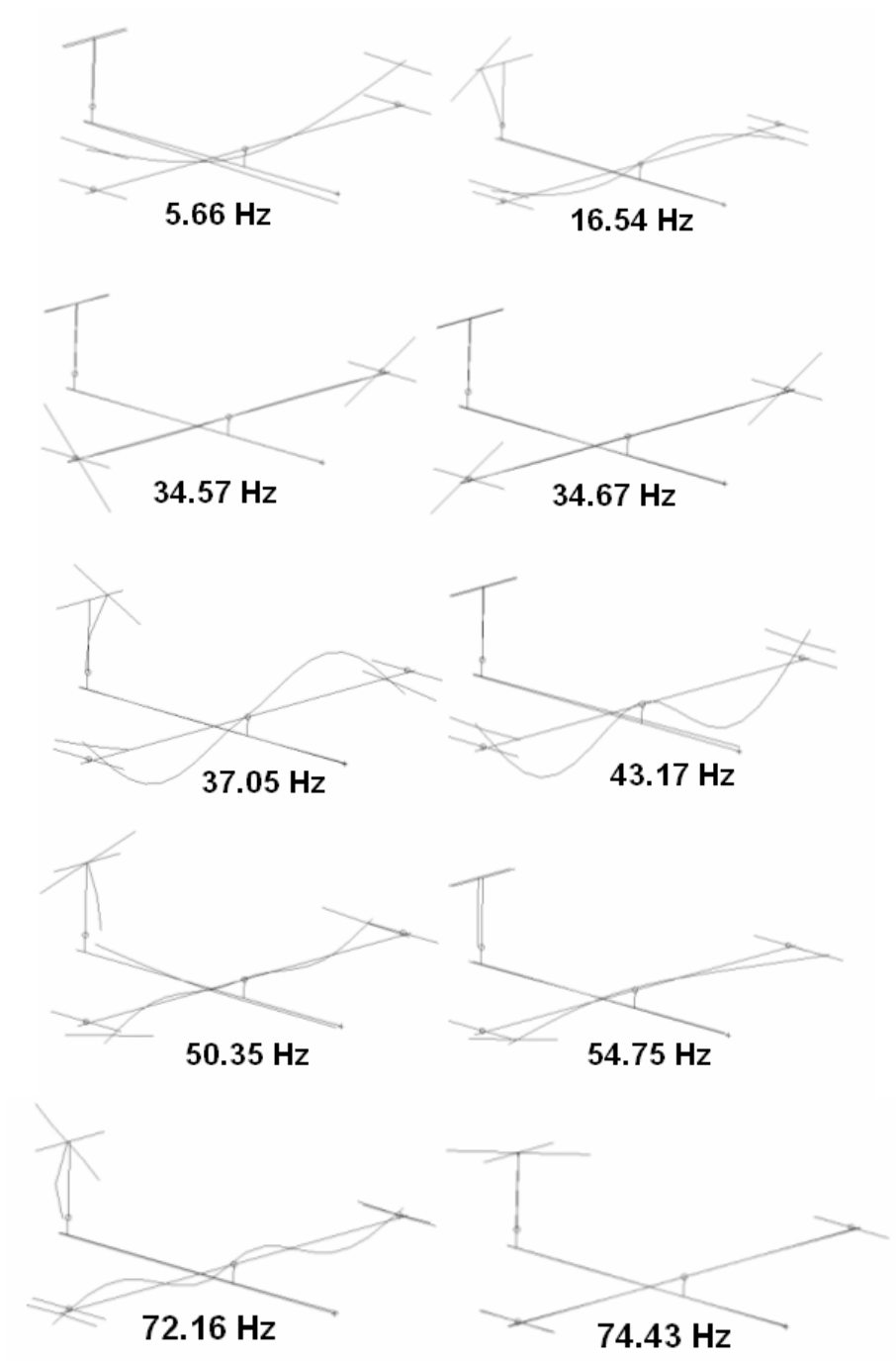


Figure 49. Visual Representations of the First 10 Modes Obtained From the Original Finite Element Model

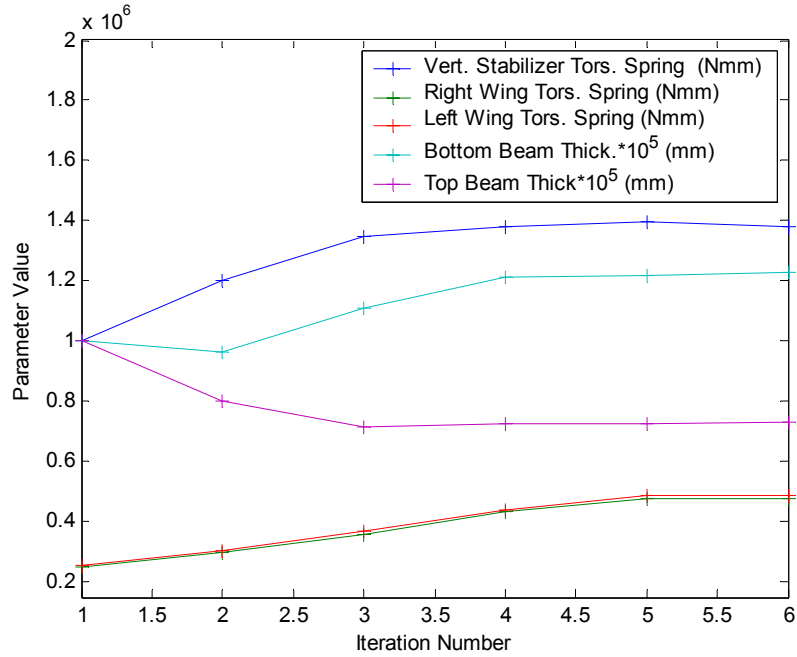


Figure 50. Variation of Parameter Values through the Updating Procedure

The MAC matrix plot after the updating procedure is given in Figure 51. The natural frequency comparison plot and the table containing the experimental and the analytical natural frequencies are given in Figure 52 and Table 11 respectively.

In order to show how the mode shape vectors correlate in detail, mass normalized mode shape value plots (for first ten modes) of the updated finite element model and the experimental model are also given. Although these plots have no physical meaning, they are given in order to show how exactly the experimental and the analytical mode shape values at measurement points fit each other. These plots are given in Figure 53-Figure 62. They show the experimentally obtained mode shape values at the measurement points and the analytically obtained counterparts at the same points. Point FRF values of the experimental, the analytical and the updated models measured at z- direction of node 1 is shown in Figure 63.

The visual representations of the mode shapes obtained from the updated finite element model are given in Figure 64.

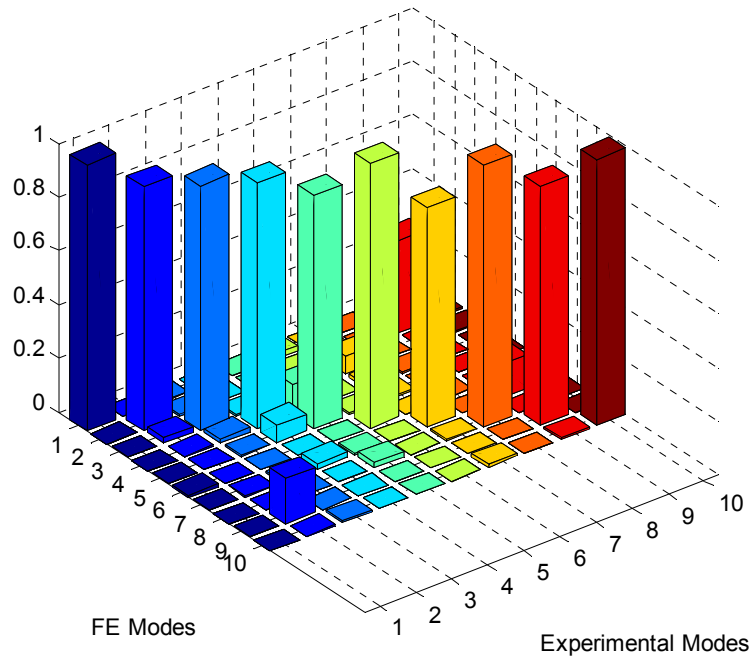


Figure 51. MAC Matrix between the Updated Finite Element Model and the Experimental Model

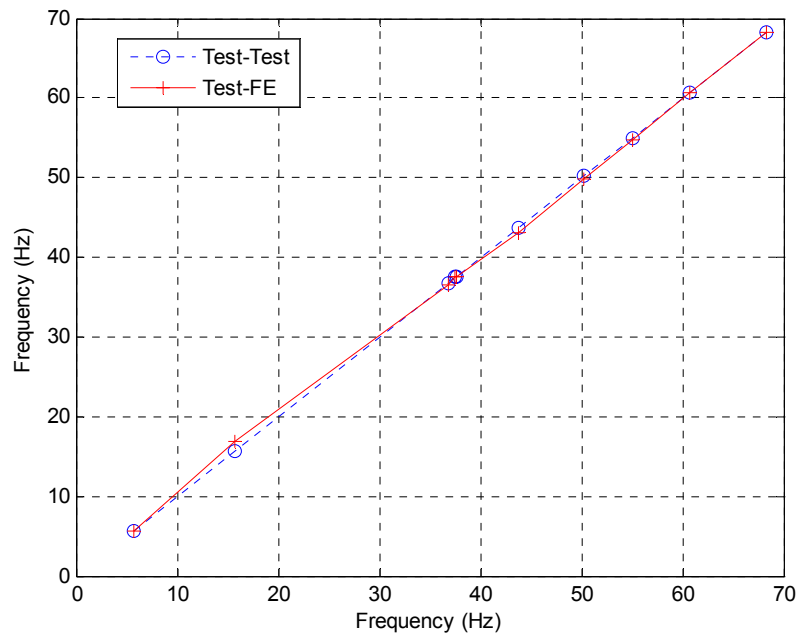


Figure 52. Natural Frequency Comparison between the Updated Finite Element Model and the Experimental Model

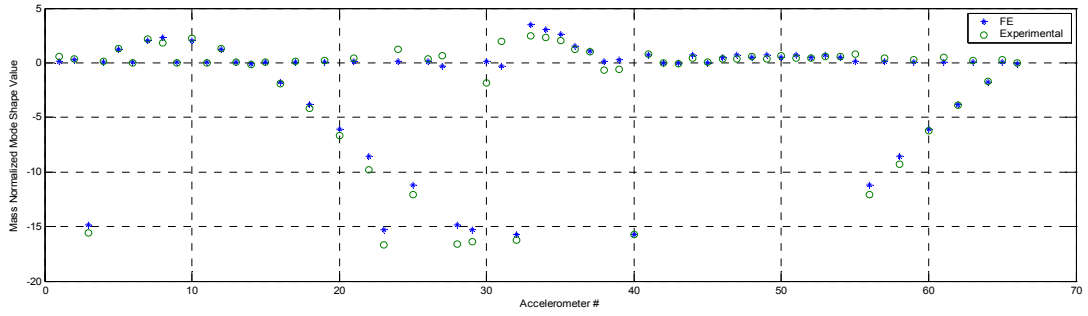


Figure 53. Eigenvector Graphs for 1st Correlating Mode Pair

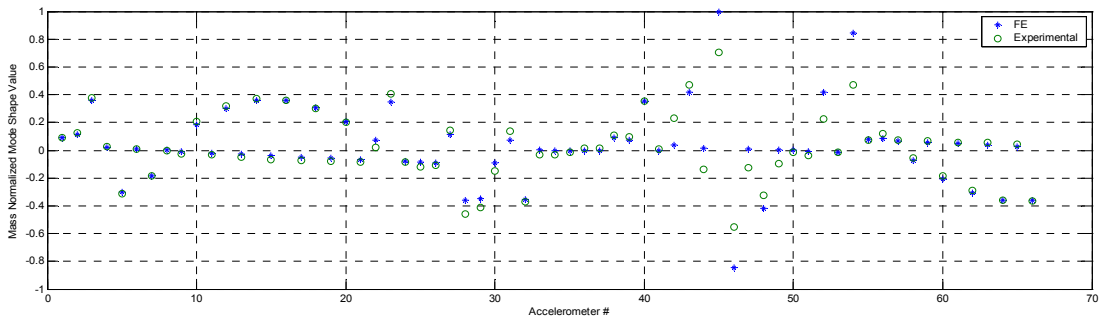


Figure 54. Eigenvector Graphs for 2nd Correlating Mode Pair

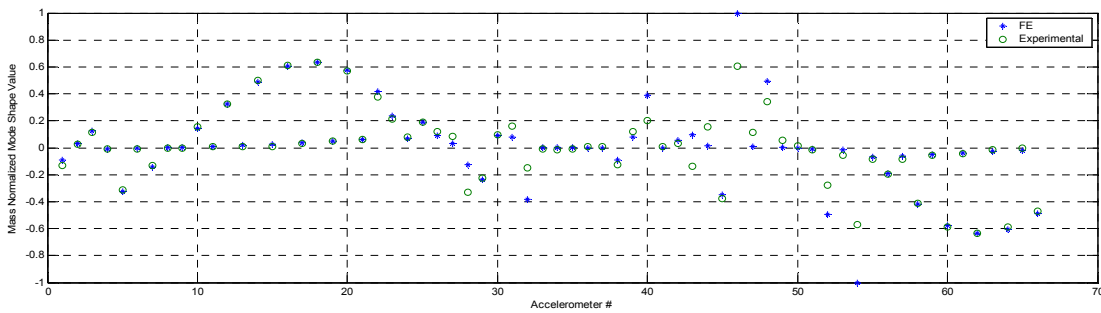


Figure 55. Eigenvector Graphs for 3rd Correlating Mode Pair

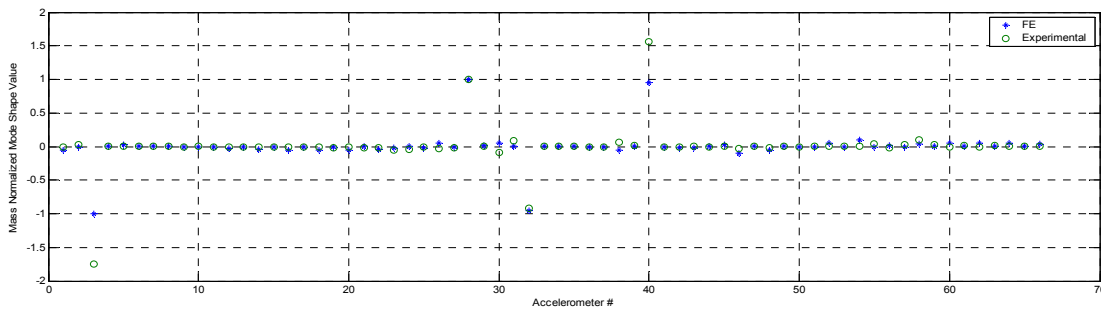


Figure 56. Eigenvector Graphs for 4th Correlating Mode Pair

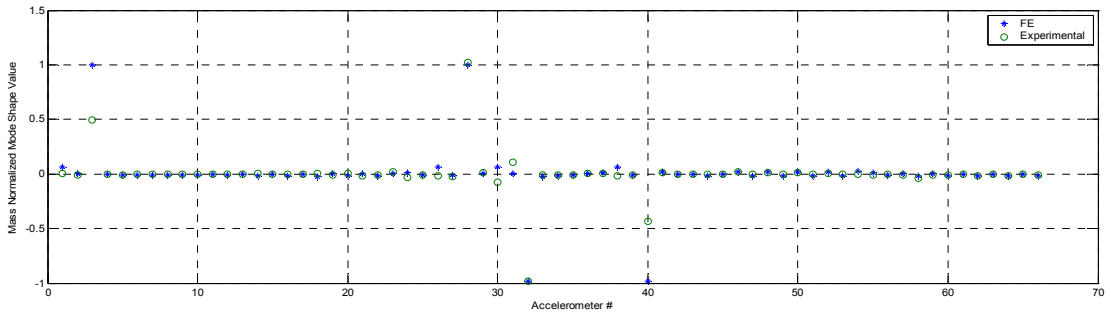


Figure 57. Eigenvector Graphs for 5th Correlating Mode Pair

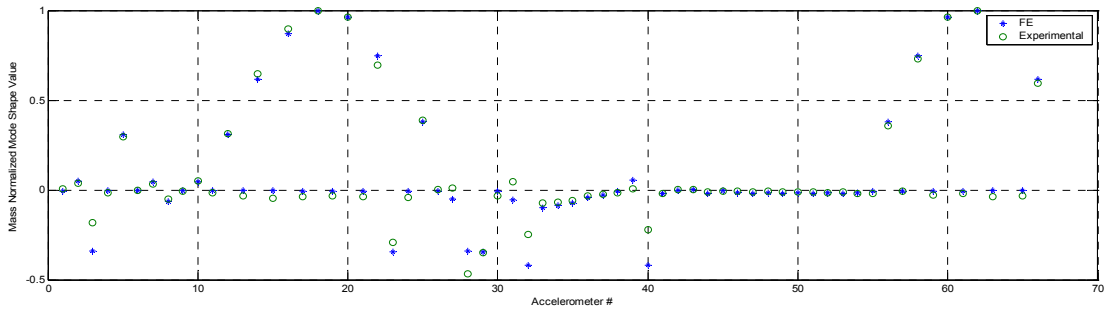


Figure 58. Eigenvector Graphs for 6th Correlating Mode Pair

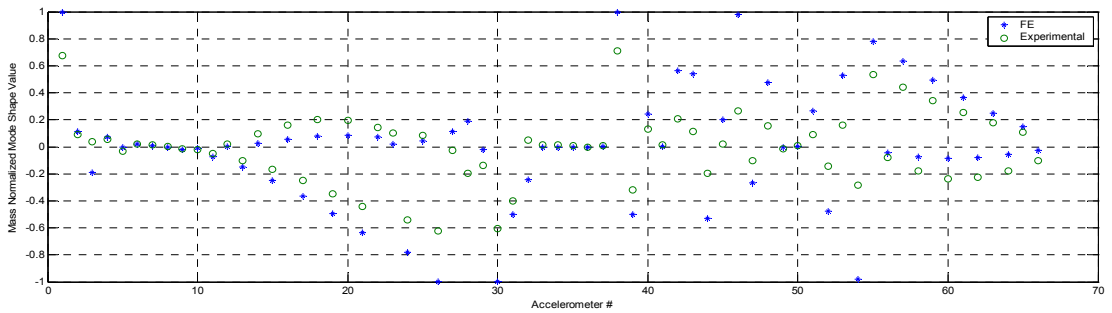


Figure 59. Eigenvector Graphs for 7th Correlating Mode Pair

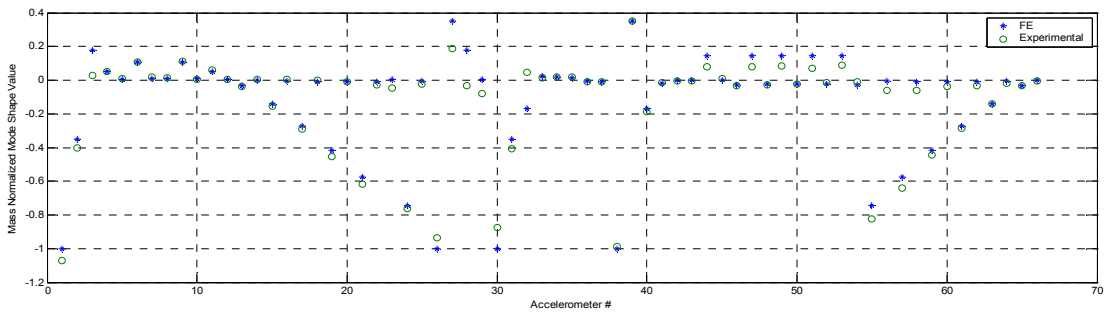


Figure 60. Eigenvector Graphs for 8th Correlating Mode Pair

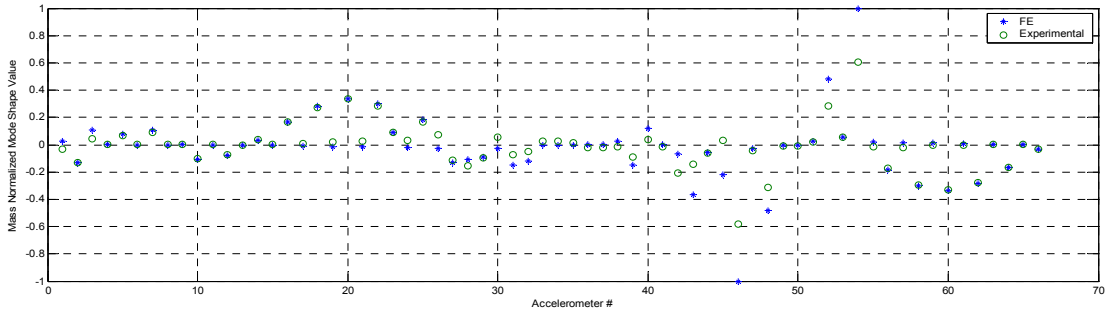


Figure 61. Eigenvector Graphs for 9th Correlating Mode Pair

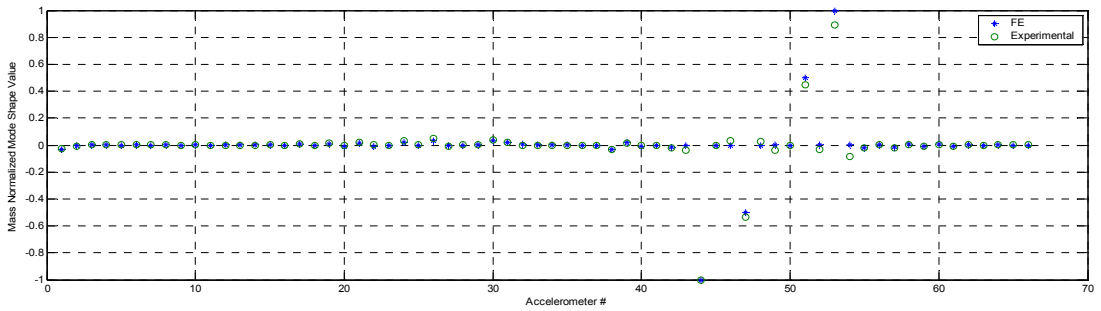


Figure 62. Eigenvector Graphs for 10th Correlating Mode Pair

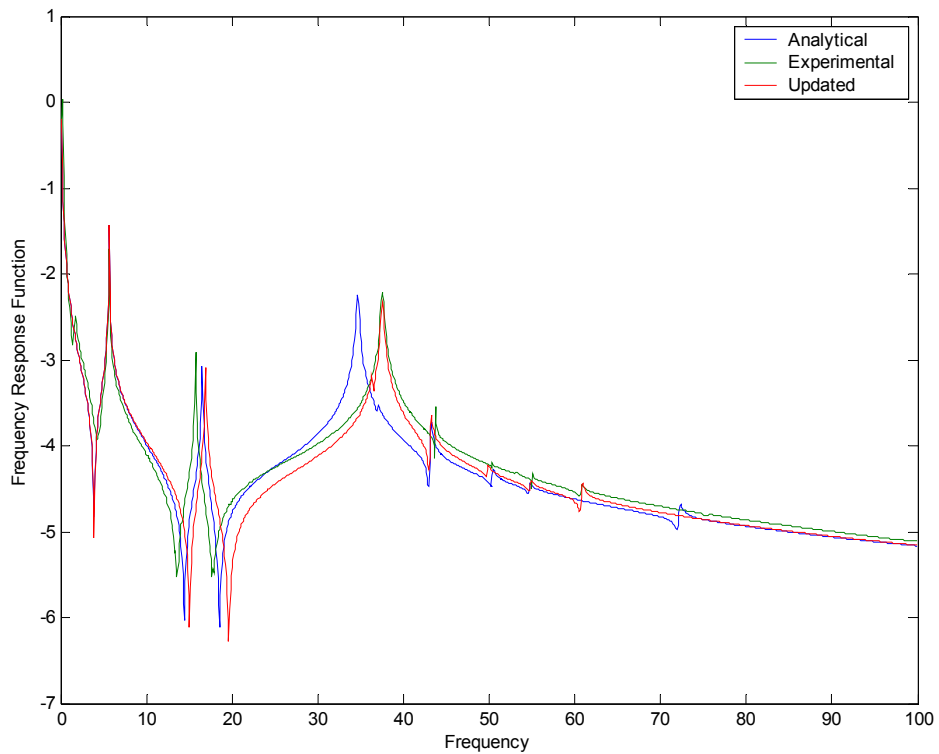


Figure 63. Point FRF Values of Node 1 in z- Direction for the Experimental, the Analytical and the Updated Models

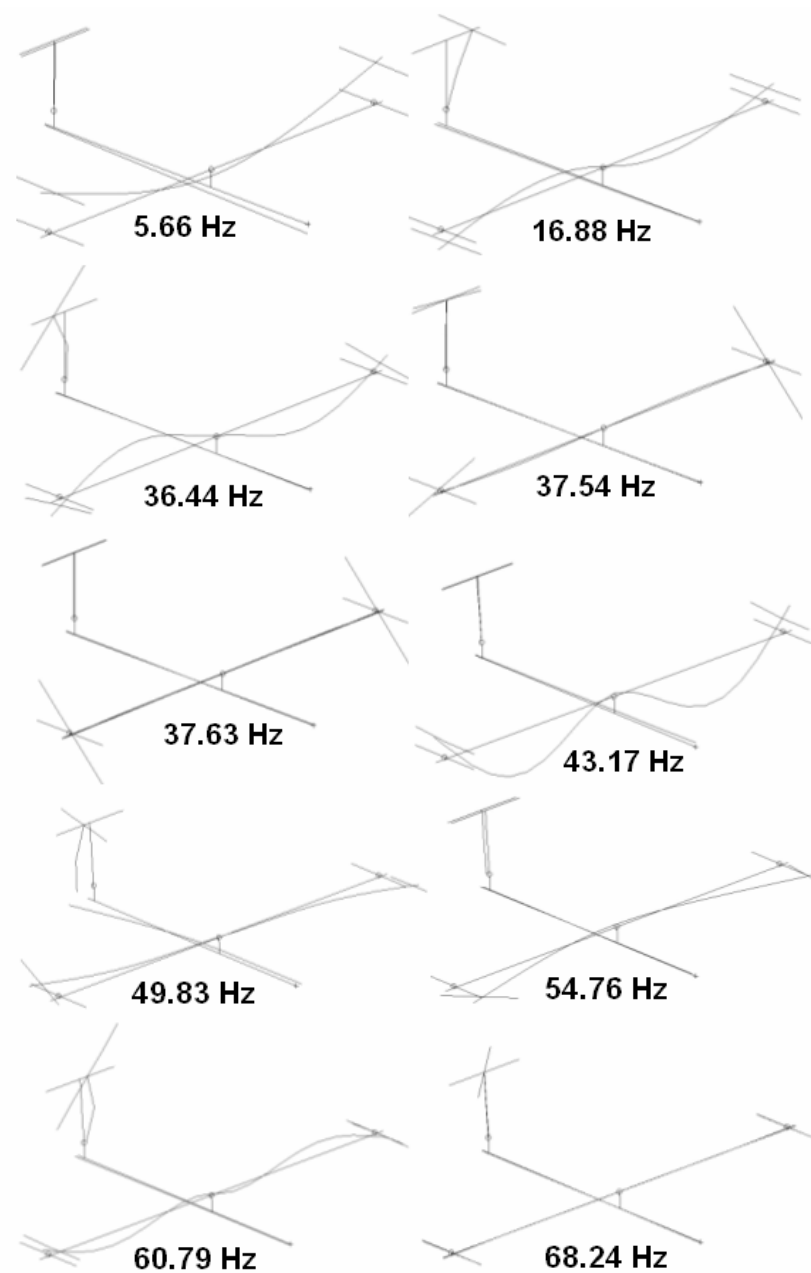


Figure 64. Visual Representations of the First 10 Modes Obtained From the Updated Finite Element Model

The natural frequencies of the first two (symmetric and anti-symmetric) wing torsional modes are raised by adding torsional springs (see Figure 49 and Figure 64). This is the reason for the resonance shifts at about 38 Hz. The vertical stabilizer is bent in the first anti-symmetric wing bending mode. In order to correlate the modes including the bending and torsional motions of the vertical stabilizer, the

beam thickness of the vertical stabilizer is enlarged yielding a higher natural frequency in the first anti-symmetric wing bending mode (about 16 Hz). Although this updating procedure yielded a shift in the resonance value of the first anti-symmetric wing bending mode (that made the correlation worse for that mode), the other modes are brought in a better correlation.

The original finite element model and the experimental model had differences in both natural frequencies and ordering of some modes. After applying the Inverse Eigensensitivity scheme to the parameters selected, the updated model had less errors in natural frequencies and the ordering of the modes were corrected. After reviewing the MAC plot and natural frequency comparison plot given in Figure 51 and Figure 52 respectively, it can be concluded that updating of the selected parameters corrected the errors without contaminating the modes that were originally in good correlation (both in frequency and mode shape vector sense). Also, the plots giving the mode shape values of the experimental and analytical models show that the natural modes from the updated finite element model and those experimentally obtained are in good correlation, and consequently updating of the GARTEUR model by applying the Inverse Eigensensitivity Method is successful.

Table 11. Experimental Modes and Correlating Updated Theoretical Modes from the Finite Element Model

Experimental Mode	Natural Frequency (Hz)	Updated Finite Element Model Mode	Natural Frequency (Hz)	% Absolute Error
1	5.65	1	5.66	0.18
2	15.73	2	16.88	7.3
3	36.79	3	36.44	0.95
4	37.51	4	37.54	0.08
5	37.65	5	37.63	0.05
6	43.73	6	43.17	1.28
7	50.32	7	49.83	0.97
8	55.00	8	54.76	0.44
9	60.66	9	60.79	0.21
10	68.23	10	68.24	0.01

More comments on updating of the GARTEUR model by applying the Inverse Eigensensitivity Method is given in section 6.1.3

5.4 CASE STUDIES ON AN AIRCRAFT MODEL (REAL LARGE STRUCTURE) USING THE INVERSE EIGENSENSITIVITY METHOD

In this case study, the finite element model of a real fighter aircraft is updated using the Inverse Eigensensitivity Method by using the experimental data obtained from a ground vibration testing.

The finite element model of an aircraft was built in MSC Patran GUI and the modal analyses were carried out in MSC Nastran solver. The model consists of shell, beam and point (mass) elements and MPC's (multi point constraints) resulting in about 3200 degrees of freedom. 3-D beam elements (for spars, ribs, stiffeners and bulkheads) and constant thickness (quad and triad) shell elements (for the structural skin) are used for the mesh. The mass matrix is forced to be lumped in the translational degrees of freedom. That is, the mass elements for rotational degrees of freedom are taken to be zero.

Models for empty aircraft and aircraft with fuel and external loads are prepared separately.

5.4.1 Updating the Model of the Empty Aircraft

The natural frequency comparison and MAC matrix of the original finite element model and experimentally obtained model are shown in Figure 65 and Figure 66.

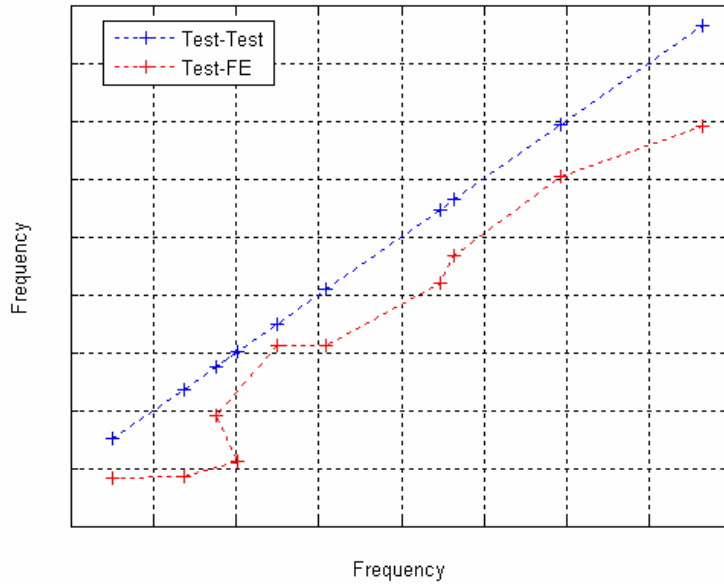


Figure 65. The Natural Frequency Graph for Experimental-Experimental and Experimental-Analytical Model Modes

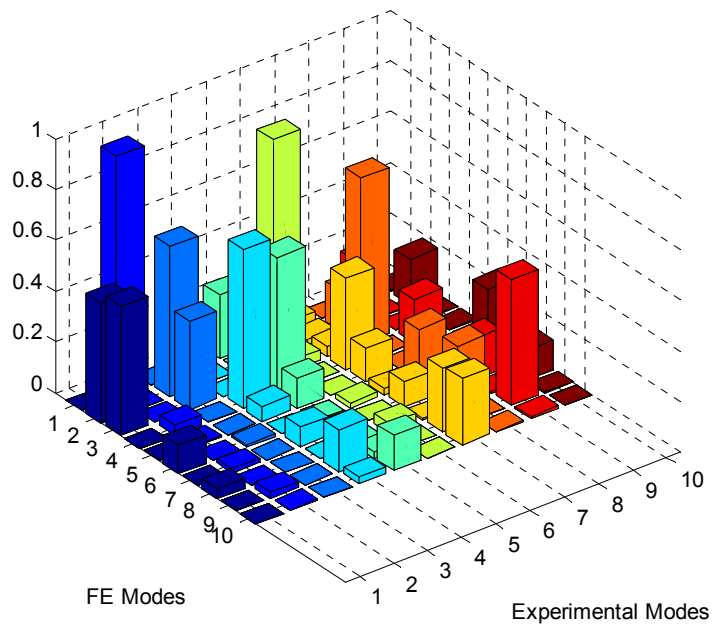


Figure 66. MAC Matrix before Updating Procedure

Results obtained after updating by using the Inverse Eigensensitivity Method are shown in Figure 67 and Figure 68.

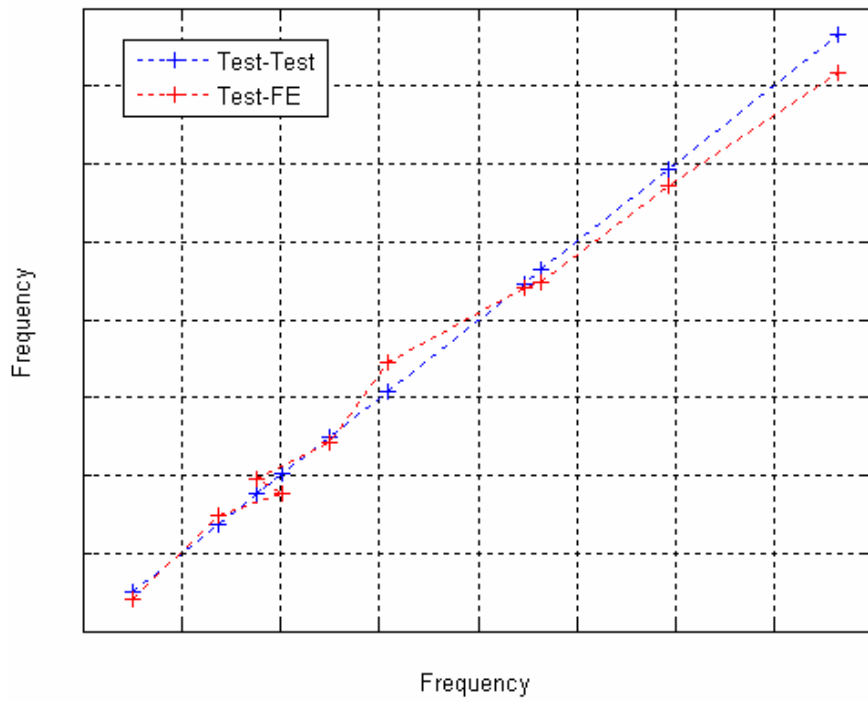


Figure 67. The Natural Frequency Graph for Experimental-Experimental and Experimental-Analytical Model Modes (for Correlating Pairs)

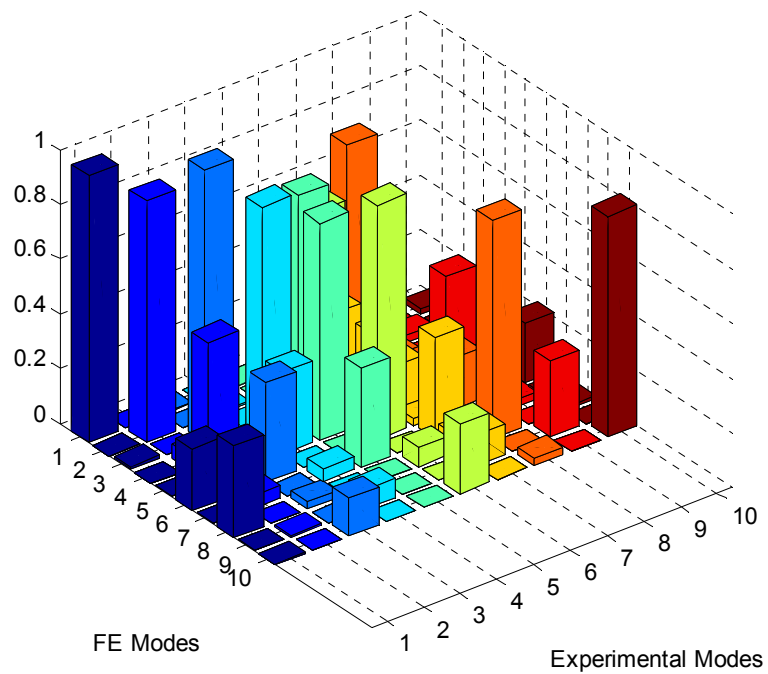


Figure 68. MAC Matrix After Updating Procedure

In Figure 69-Figure 74, are shown the comparison of the mass normalized mode shape values of the experimental model and the updated analytical model for the first 6 modes. The experimental eigenvector values are scaled with respect to the maximum value of the analytical eigenvector for better visualization.

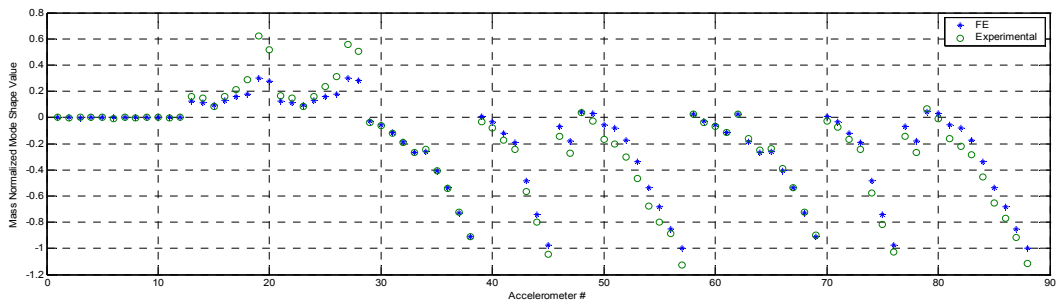


Figure 69. Eigenvector Graphs for 1st Correlating Mode Pair

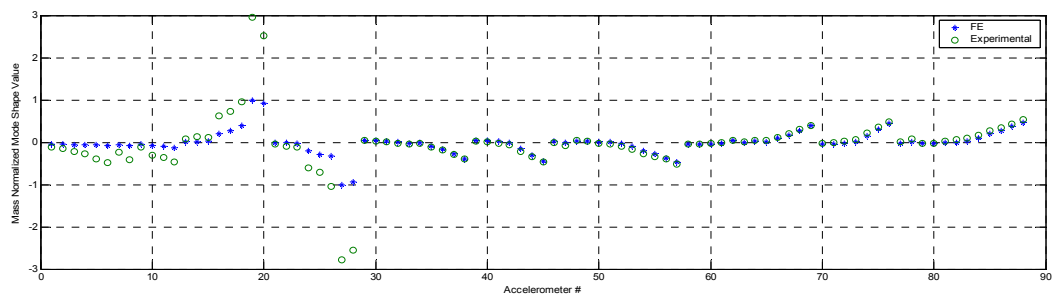


Figure 70. Eigenvector Graphs for 2nd Correlating Mode Pair

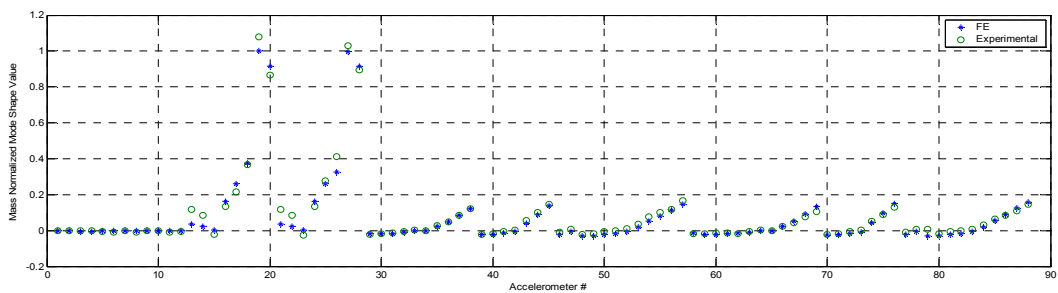


Figure 71. Eigenvector Graphs for 3rd Correlating Mode Pair

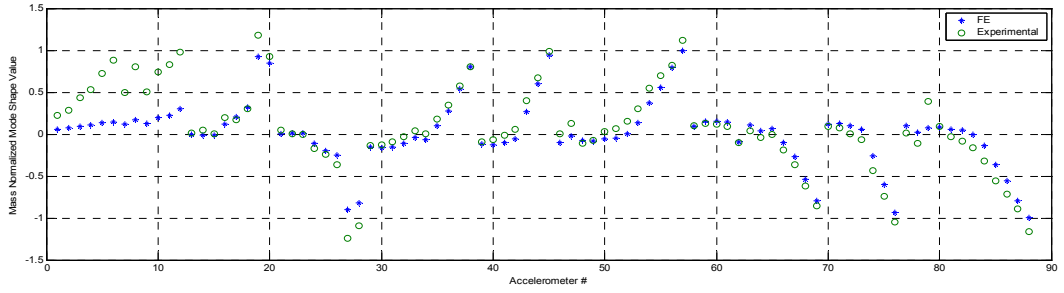


Figure 72. Eigenvector Graphs for 4th Correlating Mode Pair

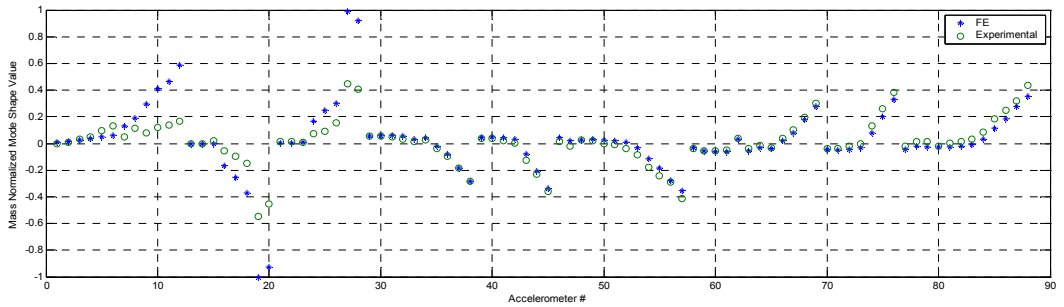


Figure 73. Eigenvector Graphs for 5th Correlating Mode Pair

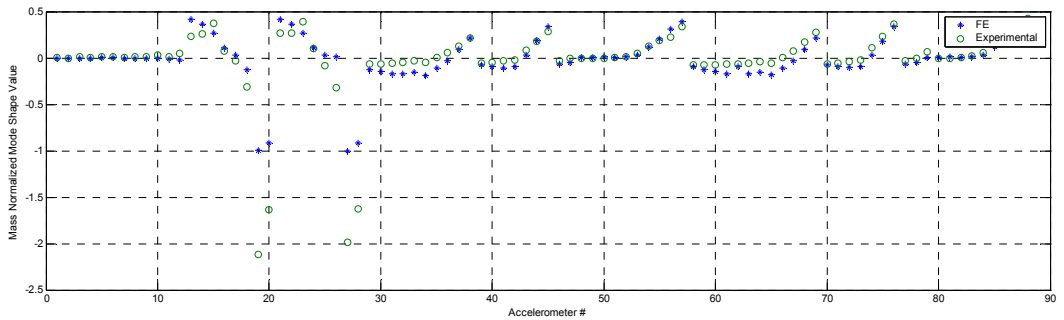


Figure 74. Eigenvector Graphs for 6th Correlating Mode Pair

Point FRF values for the experimental, the analytical and the updated models are shown in Figure 75.

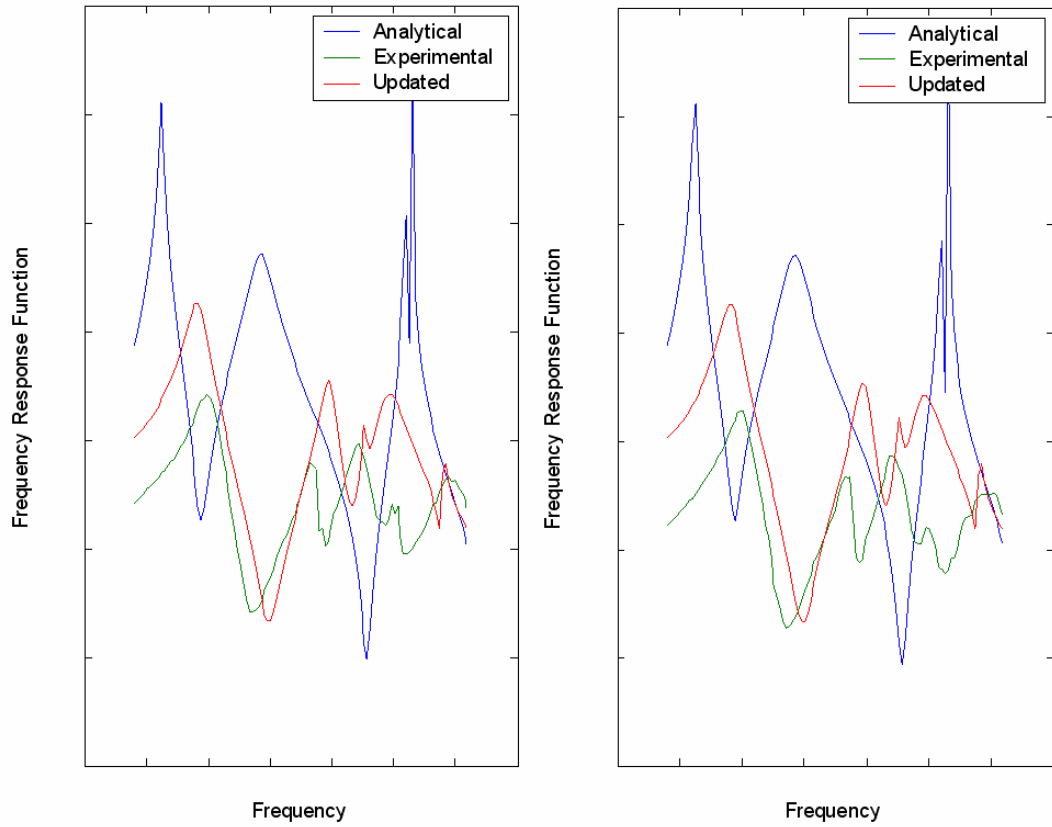


Figure 75. Point FRF Curves for the Empty Aircraft: Measured (Experimental) and Calculated (Analytical and Updated Models) at the Right and the Left Wing Tips

5.4.2 Updating of the Fully Loaded Aircraft

The natural frequency comparison and MAC matrix of the original finite element model and experimental model are in Figure 76 and Figure 77.

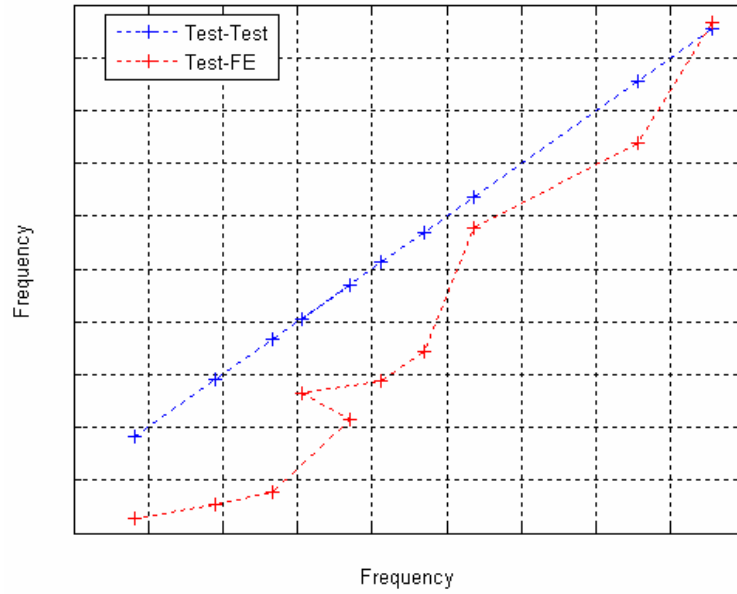


Figure 76. The Natural Frequency Graph for Experimental-Experimental and Experimental-Analytical Model Modes

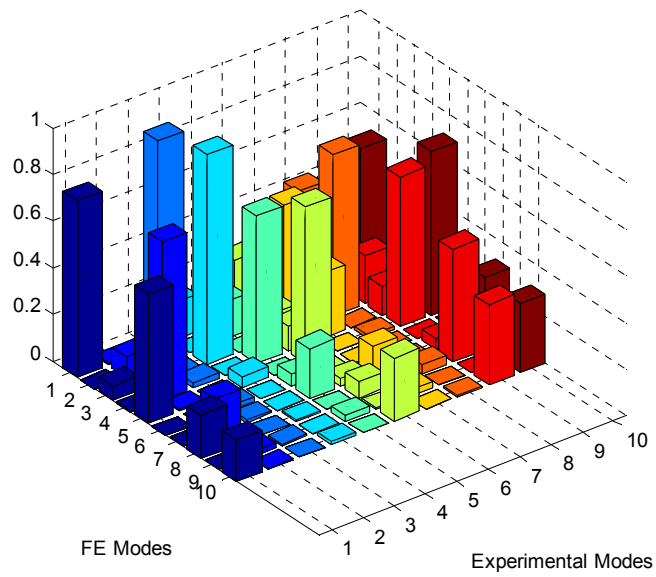


Figure 77. MAC Matrix before Updating Procedure

Results obtained after updating by using the Inverse Eigensensitivity Method are shown in Figure 78 and Figure 79.

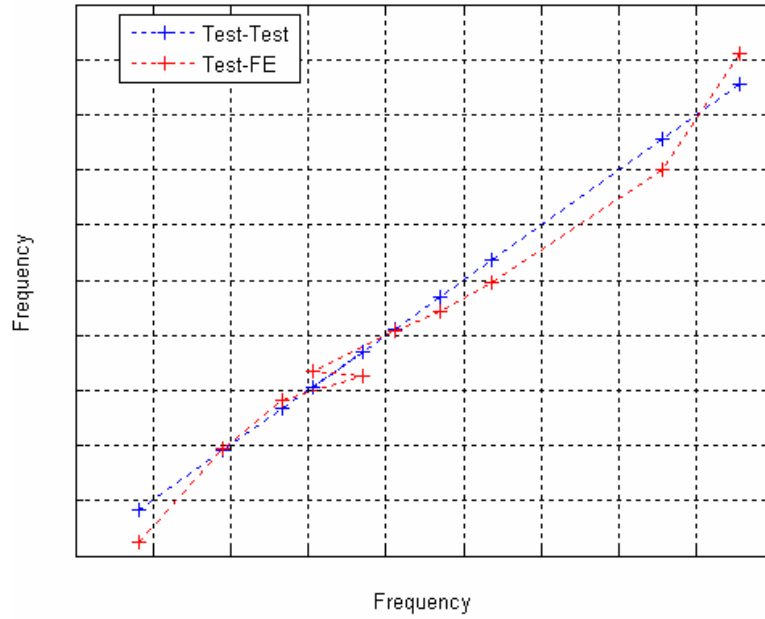


Figure 78. The Natural Frequency Graph for Experimental-Experimental and Experimental-Analytical Model Modes (for Correlating Pairs)

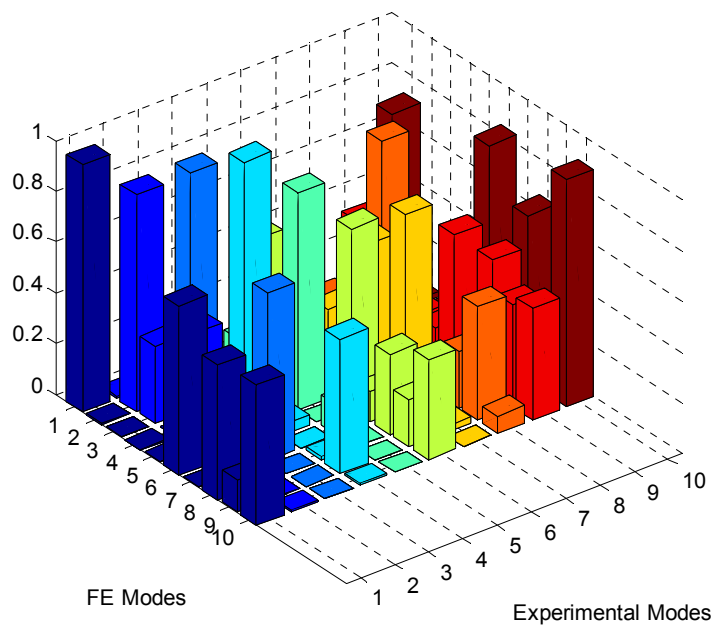


Figure 79. MAC Matrix after Updating Procedure

In Figure 80-Figure 84, are shown the comparison of the mass normalized mode shape values of the experimental model and the updated analytical model for the first 5 modes. The experimental eigenvector values are scaled with respect to the maximum value of the analytical eigenvector for better visualization.

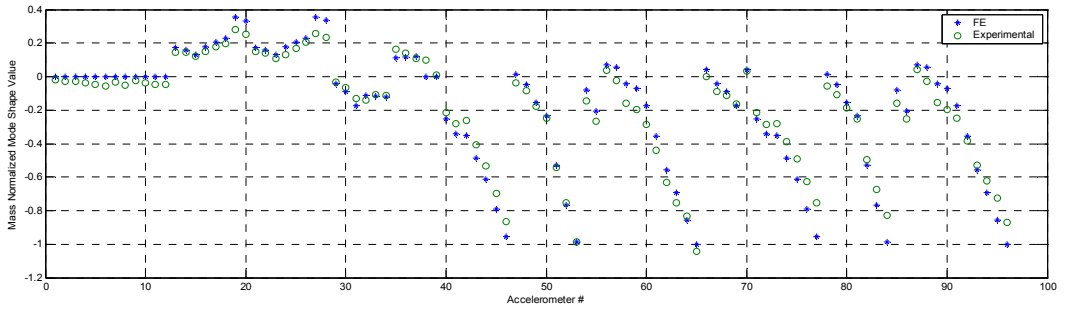


Figure 80. Eigenvector Graphs for 1st Correlating Mode Pair

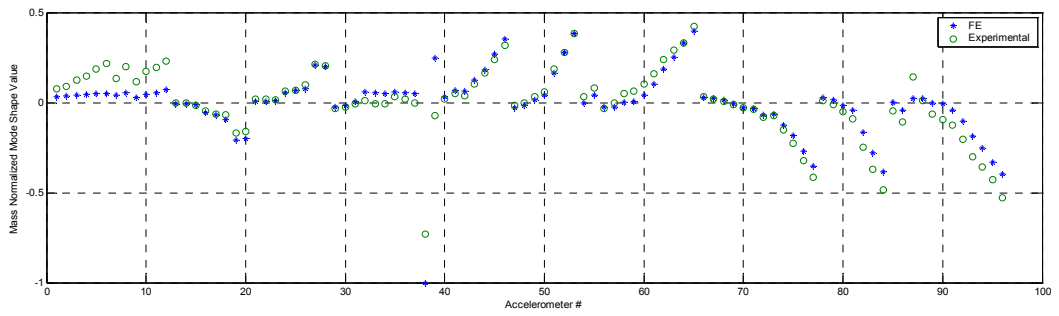


Figure 81. Eigenvector Graphs for 2nd Correlating Mode Pair

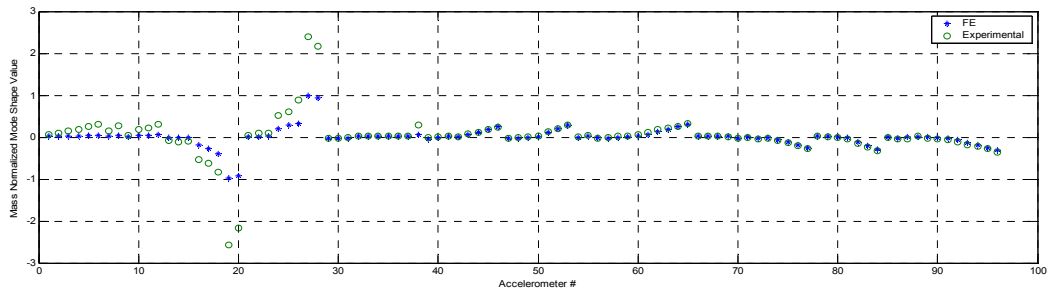


Figure 82. Eigenvector Graphs for 3rd Correlating Mode Pair

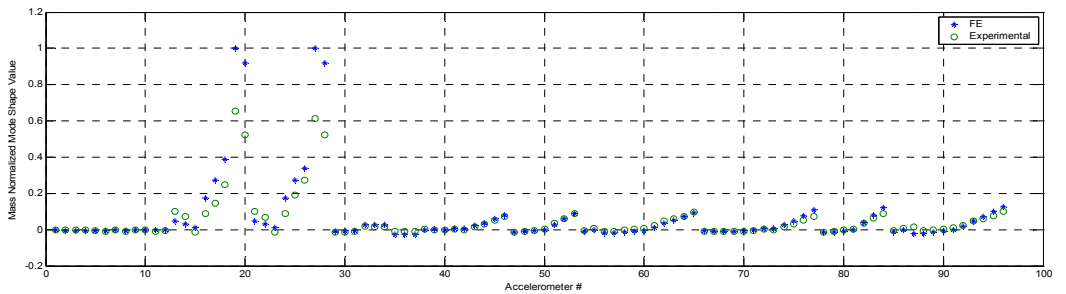


Figure 83. Eigenvector Graphs for 4th Correlating Mode Pair

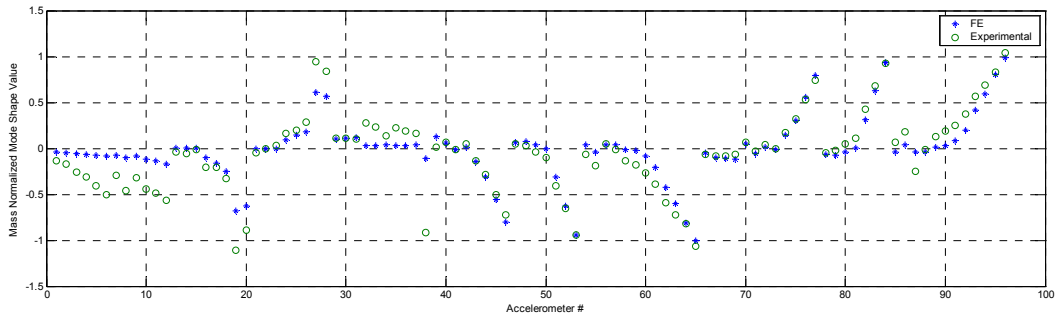


Figure 84. Eigenvector Graphs for 5th Correlating Mode Pair

Point FRF Values for the experimental, the analytical and the updated models are shown in Figure 85.

If the updated results for the real aircraft are examined, it is observed that the maximum absolute values of error for natural frequencies are below 5%. Examining the MAC matrices, it is seen that MAC values of over 80% are obtained for the first 7-8 modes. With these results, after examining the eigenvector value plots of correlating modes, it is concluded that the experimental and analytical models are in good agreement after updating, as far as the first 7-8 modes are concerned.

On the other hand, for the modes for which MAC values are relatively low, the character of the correlating modes seem to be in good correlation if the eigenvector plots are examined. The low MAC values are due to the fact that, experimental mode shape results (obtained from measured FRF values) are not in good condition for frequency values above 25 Hz.

The experimental and the analytical results obtained for the first 10 degrees of freedom in the eigenvalue plots do not seem to be in good agreement in almost all of the modes. Special care was taken on this part of the aircraft but no satisfactory results were obtained. It is believed that the shaker placed in this area contaminates the experimental data.

The reason why off-diagonal terms in MAC matrices are not “0” is the accelerometer placement resolution. The placement resolution is not fine enough for the formulation of MAC to distinguish similar modes. That is, the modes in

which the wing of the aircraft has a first wing bending like behavior will yield off-diagonal terms in MAC matrix which are not zero as the number of accelerometers found on parts other than wings are not enough to have eigenvectors that can sufficiently distinguish the behavior of the modes.

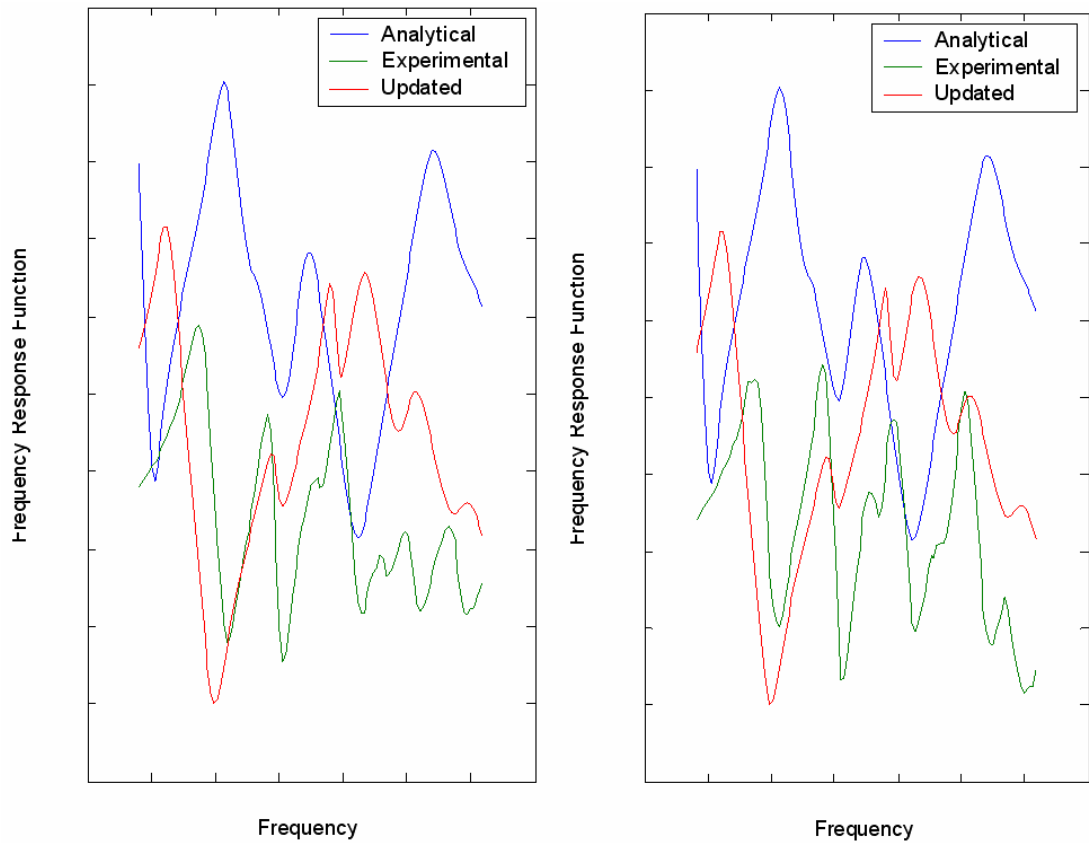


Figure 85. Point FRF Curves for the Fully Loaded Aircraft: Measured (Experimental) and Calculated (Analytical and Updated Models) at the Right and the Left Wing Tips

Some modes are out of order in the two models (see modes 4 and 5 in Figure 76 and Figure 78). Effort was made to keep the experimental order in the analytical model but as iteration numbers were increased, contaminations in the mode shapes were obtained. So, neighboring but out of order modes were kept in the best position possible without getting them in the correct order.

The given FRF plots of the aircraft are in the stiffness controlled region. The original finite element model is less stiff than the experimental model since the FRF values of the experimental model is lower in magnitude. As the FRF matrix in the stiffness controlled region may be thought to be the inverse of the stiffness matrix, lower magnitudes mean higher stiffness. After updating, the finite element FRF values are also lowered which means that there occurred almost an overall stiffness increase in the finite element model. This can also be seen in the shifts of the first two resonance values of the original analytical model. The resonance values of these two modes are increased. On the other hand, the Young's Modulus values of the fuselage components had decreases in value which yielded a negative shift in the resonance values of the third and fourth modes of the original analytical model.

The (y- axis) values of point FRF plots do not seem to be in good agreement. However, model updating has reduced the differences (both magnitude-wise and frequency-wise) which can be seen from the comparison of these values with the original FRF values. The reason for the remaining discrepancy between the updated FRF data and experimental data is the starting finite element model itself. If a better model had been constructed for the aircraft at the very beginning, a more successful updating would have been obtained.

After examining the natural frequency values, MAC matrices and eigenvector plots of correlating modes, it was concluded that the updating procedure of the real aircraft satisfies the practical needs which are to have a finite element model that has the similar natural frequencies and mode shapes in the frequency band 0-20 Hz.

CHAPTER 6

DISCUSSION, CONCLUSIONS AND RECOMMENDATIONS FOR FUTURE WORK

6.1 DISCUSSION

The main objectives of this thesis are to investigate the model updating techniques that are used to correlate the experimental and the analytical models and to decide the methods that are the best for updating of large structural models.

Case studies on computationally generated experimental models are used in order to evaluate the efficiencies of direct methods (namely the Lagrange Multiplier Method, the Error Matrix Method, the Direct Matrix Updating Method and the Matrix Mixing Method), the Response Function Method and the MCI Minimization Method which is a new method developed in this thesis.

On the other hand, case studies on real structures one of which is a real aircraft are solved with the Inverse Eigensensitivity Method.

In this section, discussions about the case studies examined are given.

6.1.1 Discussion on Case Studies Performed Using Direct Methods

The six DOF mass-spring system is analyzed with all of the direct methods (namely the Lagrange Multiplier Method, the Error Matrix Method, the Direct Matrix Updating Method and the Matrix Mixing Method) investigated in this study. As it can be seen from the point FRF plots given, all of the methods except the Error Matrix Method yield exact solutions once the required number of experimental

values are supplied. The error in Error Matrix Method arises from the linearization procedure (omitting the second and higher order terms).

Although the direct methods seem to yield direct solutions and thereby seem to be the first candidate for updating procedures, they also yield system matrices without realistic connection behavior.

6.1.2 Discussion on Case Studies Performed Using with Miscorrelation Index (MCI) Minimization

The new error localization method (MCI Method) and the updating technique (the so called MCI Minimization Method) developed in this thesis are investigated through the case studies. The error localization technique depends on the fact that in an ideally correct analytical model the dynamic stiffness matrix will be the inverse of the experimental model receptance matrix. Based on this fact, the numerical values obtained by multiplication of these two matrices shall yield an identity matrix (or using the analytical dynamic stiffness matrix and a column of the experimental receptance matrix one will yield a vector having 1 in one element and all zeros elsewhere). Although the localization technique is successful for locating the error, the numerical values obtained do not reflect the degree of error connected to a single DOF. On the other hand, if the error in one DOF is increased, the MCI values are also increased.

The model updating method (MCI minimization) developed depends on the minimization of the error locating index MCI. Since these numerical values are non-zero if an error between the theoretical and experimental models exists, trying to minimize these values would yield an updated system that will yield responses similar to those of the experimental model. However, there is a possibility of having the 'trivial solution' that yields '0' MCI values but having system matrices with elements close to null. This case occurs if the updating parameters can not reflect the error behavior present or if there is too much noise in the experimental data. If this is the case, weighting or using penalty functions in the solution step may yield meaningful system matrices.

The two case studies performed are different in the sense that, in the mass-spring model all the parameters in the system matrices are updated. In the second case, where a free-free beam model is analyzed, the updating parameters are used in order to update the individual element matrices. Results from both updating cases are successful. In the first case study, expanded experimental data is used for updating the parameters, on the other hand, all the experimental data is assumed to be available for the second case study.

For the six DOF mass-spring system example solved with this method, although half of the degrees of freedom are not measured, the updating procedure yields reliable results thus indicating that the method is capable of handling cases with incomplete measured data.

In the example for a beam model hung with soft springs solved with this method, effort was made to simulate soft springs in the experimental response data. However, the updating scheme based on updating all the element system matrices did not yield any similar behavior between the experimental and analytical responses when the updating frequencies were chosen close to the static case. For this reason, the rigid body modes in the analytical model were replaced with 2 elastic modes in the experimental model. If one chooses the updating frequencies away from these 'elastic mode' frequencies, the updating algorithm fits the experimental data in the regions relatively away from these frequencies. The agreement between the experimental response and the updated analytical response start at frequencies above 10 rad/s in the examined case studies.

6.1.3 Discussion on the Updating of the Scaled Aircraft Finite Element Model

As can be seen from the MAC matrix plot, the mode shape vectors and natural frequency rankings of the two models are in good correlation. In order to conclude whether the converged model is equivalent to the experimental model (apart from damping), the natural frequency comparison plot should also be investigated. This plot indicates that almost the same natural frequencies are obtained from the two models.

As both the mode shape and natural frequencies of the updated finite element and experimental models are in good agreement, it is concluded that the applied Inverse Eigensensitivity updating procedure is successful. This method is capable of coping with out-of-order modes in the two models.

6.1.4 Discussion on the Updating of the Real Aircraft Finite Element Model

If the updated results for the real aircraft are examined, it is observed that the maximum absolute values of error for natural frequencies are below 5%. Examining the MAC matrices, it is seen that MAC values of over 80% are obtained for the first 7-8 modes. With these results, after examining the eigenvector value plots of correlating modes, it is concluded that the experimental and analytical models are in good agreement after updating, as far as the first 7-8 modes are concerned.

On the other hand, for the modes for which MAC values are relatively low, the character of the correlating modes seem to be in good correlation if the eigenvector plots are examined. The low MAC values are due to the fact that, experimental mode shape results (obtained from measured FRF values) are not in good condition for frequency values above 25 Hz.

The experimental and the analytical results obtained for the first 10 degrees of freedom in the eigenvalue plots do not seem to be in good agreement in almost all of the modes. Special care was taken on this part of the aircraft but no satisfactory results were obtained. It is believed that the shaker placed in this area contaminates the experimental data.

The reason why off-diagonal terms in MAC matrices are not "0" is the accelerometer placement resolution. The placement resolution is not fine enough for the formulation of MAC to distinguish similar modes. That is, the modes in which the wing of the aircraft has a first wing bending like behavior will yield off-diagonal terms in MAC matrix which are not zero as the number of accelerometers found on parts other than wings are not enough to have eigenvectors that can sufficiently distinguish the behavior of the modes.

Some modes are out of order in the two models (see modes 4 and 5 in Figure 76 and Figure 78). Effort was made to keep the experimental order in the analytical model but as iteration numbers were increased, contaminations in the mode shapes were obtained. So, neighboring but out of order modes were kept in the best position possible without getting them in the correct order.

After examining the natural frequency values, MAC matrices and eigenvector plots of correlating modes, it was concluded that the updating procedure of the real aircraft satisfies the practical needs which are to have a finite element model that has the similar natural frequencies and mode shapes in the frequency band 0-20 Hz.

Also, updating of the finite element model of the real aircraft was tried to be performed by using the Response Function Method. However, the number of the parameters and the number of the equations led to unrealistic analysis times. On the other hand, problems with the formulation have been faced when the number of the parameters were tried to be reduced. Therefore, usage of this method with the real aircraft case was omitted.

6.2 CONCLUSIONS

The direct methods, which yield exact results, are only recommended to be used for small mass-spring systems as they contaminate the connection data in the finite element models. The modal properties can be exactly obtained by using these methods but the static responses obtained from the updated models by using these models will be more or less different from those of the real structures.

For the case of indirect methods, there are two main alternatives used by today's researchers:

- The Response Function Method
- The Inverse Eigensensitivity Method

Both methods are used for obtaining the updated model for the real aircraft case. However, the coefficient matrix extraction for the Response Function Method needs complicated programming loops and if the number of updating frequency points and the number of updating parameters are chosen to be large, the loop requires unrealistic computation time. For the case of updating the aircraft model, the estimated computation time was about a couple of months, so although the method is programmed to be used, it was not applied to the aircraft model (the number of updating parameters was several thousands and if that was decreased feasible estimated times would be obtained). Furthermore, methods that contaminate the finite element model like model reduction and mode shape expansion are necessary for the Response Function Method. Instead of dealing with complications other than the model updating technique itself, the Inverse Eigensensitivity Method was chosen to be the updating procedure for the aircraft.

By the use of the MSC Nastran finite element software, the updating of the aircraft with the Inverse Eigensensitivity Method was accomplished relatively easily. The definitions of the updating parameters and updating responses were done easily and the coding was not that complicated compared to the Response Function Method.

For the case of aircraft structures, where the model includes beam and shell elements and point masses, the updating can easily be done with the Inverse Eigensensitivity Method using MSC Nastran because of its simplicity in defining the parameters and coding.

The only disadvantage of using the Inverse Eigensensitivity Method is not being able to update the damping properties. This could have been accomplished if the Response Function Method was used. However, the results obtained with the Inverse Eigensensitivity Method are reliable enough for the upcoming analyses, so it is concluded in this thesis that this method can be used for updating mathematical models obtained by finite element software for large structures.

The MCI minimization routine proposed in this study is also a reliable method for updating routine. The biggest advantage of this method is that there is no need for

calculation of the analytical FRF data (unlike the case in the Response Function Method). However, as coordinate incompatibility is always present, there is a need for calculation of the analytical modal data for expansion processes.

Finally, after investigation of the current model updating techniques and studies on the real aircraft case, the Response Function Method and the Inverse Eigensensitivity Method are concluded as the most promising methods for the updating of aircraft structural models. But if the magnitudes in the FRF data and the damping properties are not of primary concern (correlation of mode shapes and natural frequencies are the primary objectives) the Inverse Eigensensitivity Method should be selected as the updating method.

6.3 RECOMMENDATIONS FOR FUTURE WORK

The main method used in this study is the Inverse Eigensensitivity Method. Although, the studies have been carried out using computer programs, inputting the new values of the updating parameters to MSC Nastran was a time consuming activity. Writing a computer code that can drive MSC Nastran, so that the iterations are done without any interruption in the code is recommended for the future work.

Also, work on weighting the equations (as there can be two or three orders of magnitude difference between sensitivities of natural frequencies and mode shapes) will facilitate the convergence of the updating process. At least, some rules of thumb can be generated for the weighting matrix that is going to be used in sensitivity based model updating processes.

REFERENCES

- [1] S. Z. Rad, *Methods For Updating Numerical Models In Structural Dynamics*. PhD Thesis, Department of Mechanical Engineering, Imperial College of Science, Technology and Medicine, 1997
- [2] D. J. Ewins, *Modal Testing 2*, Research Studies Press, 2000
- [3] N. M. M. Maia, J. M. M. Silva et al., *Theoretical and Experimental Modal Analysis*. Research Studies Press LTD. ISBN 0 86380 208 7, 2000
- [4] M. Baruch, Y. Bar Itzhac, *Optimization Weighted Orthogonalization of Measured Modes*. AIAA Journal, 16(4), 346-351, 1978
- [5] A. Berman, *Mass matrix correction Using an Incomplete Set of Measured Modes*. AIAA Journal, 17(1), 1147-1148, 1979
- [6] B. Caesar, *Update and Identification of Dynamic Mathematical Models*. Proc. of the 4th IMAC, 394-401, Los Angeles, California, 1986
- [7] J. Sidhu, D. J. Ewins, *Correlation of Finite Element and Modal Test Studies of a Practical Structure*. Proc. of the 2nd IMAC, 756-762, Orlando, Florida, 1984
- [8] H. P. Gypsin, *Critical Application of the Error Matrix Method for Localization of Finite Element Modeling Inaccuracies*, Proc. of 4th Int. Modal Analysis Conference, K.U. Leuven, 1339-1351, 1986
- [9] M. Link, *Identification of Physical System Matrices Using Incomplete Vibration Test Data*, Proc. of the 4th Int. Modal Analysis Conference, 386-393, 1986
- [10] B. Caesar, *Updating System Matrices Using Modal Test Data*. Proc of the 5th IMAC 453-459, London, England, 1987
- [11] M. Link, M. Weiland, J. M. Bassagan, *Direct Physical Matrix Identification as Compared to Phase Resonance Testing: An Assessment on Practical Application*. Proc of the 5th IMAC 453-459, London, England, 1987
- [12] Lin, R. M., D. J. Ewins, *Model Updating Using FRF Data*, 15th International Seminar on Modal Analysis, Leuven, Belgium, 141-162, 1990

- [13] P. O. Larsson, P. Sas, *Model Updating Based on Forced Vibration Testing Using Numerically Stable Formulations*, 10th International Modal Analysis Conference, San Diego, USA, 1992
- [14] Lammens, S., *Frequency Response Based Validation of Dynamic Structural Finite Element Models*, Ph. D. Thesis, Katholieke Universiteit, Department Werktuikkunde, Leuven, Belgium, 1995
- [15] W. J. Visser, M. İmregün, *Updating Finite Element Models Using Complex Frequency Response Function Data*, Proc. of the 9th Int. Modal Analysis Conference, Firenze, Italy, 1991
- [16] W. J. Visser, M. İmregün, *A Technique to Update Finite Element Models Using Frequency Response Data*, Proc. of the 9th Int. Modal Analysis Conference, Firenze, Italy, 1991
- [17] R. L. Fox, M. P. Kapoor, *Rate of Change of Eigenvectors and Eigenvalues*, *AIAA Journal* 12(6), 2426-2429, 1968
- [18] D. Göge, 2003, *Automatic Updating of Large Aircraft Models Using Experimental Data From Ground Vibration Testing*, *Aerospace Science and Technology* 7 33-45, 2003
- [19] M. İmregün, W. J. Wisser, *A Review of Model Updating Techniques*, *Shock and Vibration Digest*, Vol. 23, No. 1, pp. 19-20, 1991
- [20] J. E. Mottershead, C. Mares, M. I. Friswell, S. James, *Selection and Updating of Parameters for an Aluminum Space-Frame Model*, *Mechanical Systems and Signal Processing*, Volume 14, Number 6, pp. 923-944(22), 2000
- [21] H. Grafe, *Model Updating of Large Structural Dynamic Models Using Measured Response Functions*, PhD Thesis, Department of Mechanical Engineering, Imperial College of Science, Technology and Medicine, 1998
- [22] W. J. Visser, *Structural Dynamic Model Updating Using Eigensensitivity Analysis*, PhD Thesis, Department of Mechanical Engineering, Imperial College of Science, Technology and Medicine, 1992
- [23] A. Karaman, *Updating Finite Element Models for Dynamic Analysis of Structures*, MSc Thesis, Middle East Technical University, 1994

- [24] M. I. Friswell, J. E. Mottershead, *Finite Element Model Updating in Structural Dynamics*, Kluwer Academic Publishers, 1995
- [25] R. J. Guyan 1965 *Reduction of Stiffness and Mass Matrices*. AIAA Journal. Vol. 3, No. 2, p. 380, 1965
- [26] J. C. O'Callahan, *A procedure for an improved reduced system (IRS)*. Proc. of the 7th IMAC, 17-21, Las Vegas, Nevada, 1989
- [27] P. E. McGowan, A. F. Angelucci, M. Jaweed, *Dynamic Test Analysis Correlation Using Reduced Analytical Models*. AIAA Journal, p. 1711-1721, 1992
- [28] J. C. O'Callahan, P. LI, *SEREP Expansion*. Proc. of the 13th IMAC, 1258-1264, Nashville, Tennessee, 1995.
- [29] R. L. Kidder, *Reduction of Structural Frequency Equations*. AIAA Journal Vol. 11 No. 6, 1973
- [30] R. J. Allemang, L. D. Brow, *A Correlation Coefficient for Modal Vector Analysis* Proc. of the 1st IMAC, 110-116, Orlando, Florida, 1982
- [31] N. A. J. Lieven, D. J. Ewins, *Spatial Correlation of Mode Shapes, The Coordinate Modal Assurance Criterion (COMAC)*. Proc. Of the 6th IMAC, 690-695, Kissimmee, Florida, 1988
- [32] W. P. Targoff, *Orthogonality Check and Correction of Measured Modes*, AIAA Journal, 14, 164-167, 1976
- [33] A. Berman, E. J. Nagy, *Improvement of a Large Analytical Model Using Test Data*. AIAA Journal, 21(8), 1168-1173, 1983
- [34] F. S. Wei, *Structural Dynamic Model Improvement Using Vibration Test Data*. AIAA Journal, 28(1), 1686-1688, 1990
- [35] J. S. Fuh, S. Y. Chen, *System Identification of Analytical Models of Damped Structures*. AIAA Journal, 30(2), 384-392, 1984
- [36] 1984W. Heylen, P. Sas, *Review of Model Optimisation Techniques*. Proc. of the 5th IMAC, 1177-1182, London, England, 1987
- [37] J. He, D. J. Ewins, *Location of Damping Elements in a Vibration Structure*. Proc. of the 11th International Seminar on Modal Analysis, Paper No. A2-4, Leuven, Belgium, 1986

- [38] G. Zhang, G. Lallement, *Dominant Error Localisation in a Finite Element Model of a Mechanical Structure*. Mechanical Systems and Signal Processing, 1(2), 141-149, 1987
- [39] N. A. J. Lieven, D. J. Ewins, *Error Location and Updating Finite Element Models Using Singular Value Decomposition*. Proc. of the 8th IMAC, 768-773, Kissimmee, Florida, 1990
- [40] J. M. W. Lee, G.R. Parker, Application of Design Sensitivity Analysis to Improve Correlations Between Analytical and Test Modes, MSC 1989 World Users' Conference Proceedings, Los Angeles, California, USA, 1989
- [41] M. İmregün, K. Y. Şanlıtürk, D. J. Ewins, Finite Element Model Updating Using Frequency Response Function Data – II. Case Study on a Medium-Size Finite Element Model, Mechanical Systems and Signal Processing, Volume 9, Number 2, pp. 203-213(11), 1995
- [42] S. Lammens, M. Brughmans, J. Leuridan, P. Sas, *Application of a FRF Based Model Updating Technique for the Validation of Finite Element Models of Components of the Automotive Industry*, MSC 1995 World Users' Conference Proceedings, Universal City, CA, 1995
- [43] M. B. Özer, H. N. Özgüven, T. J. Royston, *Identification of Structural Non-Linearities Using Describing Functions and Sherman-Morrison*, Proceedings of the 23rd International Modal Analysis Conference, pp.199-212, Orlando, Florida, January 30 - February 3, 2005
- [44] A. M. Kabe, *Stiffness Matrix Adjustment Using Modal Data*, AIAA Journal 23, 1431-1436, 1985

APPENDIX A

Least-Squares Regression

For a linear system of equations in the form of $\{p\} = [A]^+ \{\delta\}$, if the number of equations is more than the number of unknowns, the problem is said to be over-determined. In such a case, the solution is obtained by a least-squares solution.

For the system

$$\sum_{j=0}^n a_{kj} x_j = b_k \quad (0 \leq k \leq m) \quad (\text{A.1})$$

if $m > n$, then the problem is over-determined. If $(x_0, x_1, x_2, \dots, x_n)$ are substituted on the left hand side, the difference between the two sides of the k^{th} equation is termed as the k^{th} residual. Ideally, all residuals should be equal to zero. If it is not possible to select $(x_0, x_1, x_2, \dots, x_n)$ so as to make all residuals zero, the system is said to be inconsistent or incompatible. In this case, an alternative is to minimize the sum of the squares of the residuals. So, we are led to minimize the expression

$$\phi(x_0, x_1, x_2, \dots, x_n) = \sum_{k=0}^m \left(\sum_{j=0}^n a_{kj} x_j - b_k \right)^2 \quad (\text{A.2})$$

by making an appropriate choice of $(x_0, x_1, x_2, \dots, x_n)$.

The least-squares solution equations are obtained by taking partial derivatives with respect to the x_i and equating them to zero.

$$\sum_{j=0}^n \left(\sum_{k=0}^m a_{ki} a_{kj} \right) x_j = \sum_{k=0}^m b_k a_{ki} \quad (\text{A.3})$$

This is a linear system of just $n+1$ equations involving $n+1$ unknowns $(x_0, x_1, x_2, \dots, x_n)$. It can be shown that this system is consistent, provided that the column vectors in the original coefficient array are linearly independent. This system can be solved, for instance by Gauss elimination. The solution of system represented by Eq. (A.3) is then the best approximate solution to equation Eq. (A.1) in the least-squares sense.

For the system $\{p_n\} = [A_{m \times n}]^+ \{\Delta_m\}$, the Gauss elimination is applied to

$$\sum_{j=0}^n \left(\sum_{k=0}^m A_{ki} A_{kj} \right) \Delta_k = \sum_{j=0}^n p_j A_{kj} \quad (\text{A.4})$$

APPENDIX B

Assigning System Matrices to Finite Element Models Built in MSC Patran

Structures for which modal data are available, can be described using system matrices by using the orthonormal equations that can be expressed as:

$$[K] = ([\phi]^T)^{-1} [\cdot \cdot \omega_r^2 \cdot \cdot] ([\phi])^{-1} \quad (B.1)$$

$$[M] = ([\phi]^T)^{-1} [I] ([\phi])^{-1} \quad (B.2)$$

$$[C] = ([\phi]^T)^{-1} [\cdot \cdot c_r \cdot \cdot] ([\phi])^{-1} \quad (B.3)$$

In order to be able to calculate the system matrices, the mode shape matrices must be square. This condition necessitates either the mode shape data to be reduced to the size of the number of the modes that are calculated by modal analysis or expanding the mode shape data in a fashion that the number of the modes will be equal to the number of degrees of freedom. The second case is more beneficial in the sense that the analyst will have more degrees of freedom that can define the motion. However, the analyst shall synthesize pseudo-modes that are orthogonal to all the other modes (calculated or synthesized).

After synthesizing orthogonal pseudo-modes one can calculate the system matrices by using Eq. (B.1), Eq. (B.2) and Eq. (B.3).

In order to input the finite element system matrices that are built in an environment other than MSC Patran, the element matrices should be saved in a file in a format that defines each element of the matrices by 16 characters (which corresponds to

12 significant digits). This is necessary to avoid the ill-conditioning of the system matrices calculated by using synthesized orthogonal pseudo-modes; because, when the elements of matrices are represented by a smaller number of digits, inaccurate results are obtained. However, experience shows that having the system matrices defined by 16 characters (for each element) yields the same eigenvalue problem solution for the mathematical model itself and MSC Nastran model.

The calculated system matrices should be saved as a text document in the format defined by “*MSC NASTRAN Quick Reference Guide - Bulk Data Entry - DMIG*”. Given below is an example format that defines the system matrices as a bulk data entry for MSC Nastran.

```

DMIG  KMAT      0   6   2   2
DMIG* KMAT              10      3
*          10          3 9.587453525D+8
DMIG* KMAT              100     3
*          10          3 -7.664488759D+8
*          100         3 1.771983160D+9
...
...
DMIG  MMAT      0   6   2   2
DMIG* MMAT              10      3
*          10          3 2.284211654D+3
DMIG* MMAT              100     3
*          10          3 -4.442938415D+3
*          100         3 1.333789877D+4
DMIG* MMAT              101     3
*          10          3 -6.830911917D+2
*          100         3 2.947263170D+3
*          101         3 2.165343810D+3
...
...

```

In the example given above, the entries having “KMAT” and “MMAT” as headers define stiffness and mass entries respectively. The integers values other than 16 character ones, define the connectivity data. A “*” sign at the beginning of a line indicates that the degree of freedom given in that line shall connect to the degree of freedom given above in the line with a header “DMIG* KMAT” or “DMIG* MMAT”. For example, the expression

```
DMIG* KMAT           100      3
*           10           3 -7.664488759D+8
```

yields a stiffness value of “-7.664488759D+8” between the 3rd degree of freedom of node 100 and 3rd degree of freedom of node 10.

After defining the system matrices in the format defined above, the related text file should be saved as “file_name.bdf”.

An important point here is that, the node numbers given in “file_name.bdf” shall also be defined in the MSC Nastran finite element model. The finite element model that is built in MSC Patran should include the points that coincide with the accelerometer points and nodes should be defined on each point with numbers coinciding with numbers in the file “file_name.bdf”. After creating the nodes, point mass elements with a magnitude of zero should be created on each node in order to assemble the mass matrix. For the stiffness matrix, spring elements should be placed between each node that are defined for the degrees of freedom found in the stiffness matrix.

For the degrees of freedom for which no measurements are present, null displacement boundary conditions are applied as these degrees of freedom will not be present in the system matrices.

After creation of the finite element model that is composed of point masses and springs, the file containing the numerical data for system matrices, “file_name.bdf” should be entered to the finite element code. In order to do this, the command

INCLUDE 'file_name.BDF'

SHOULD BE ENTERED TO THE "ANALYSIS-DIRECT TEXT INPUT-BULK DATA SECTION" OF THE MSC PATRAN GUI. ALSO, THE COMMANDS

K2GG=KMAT

M2GG=MMAT

should be entered to the "Analysis-Direct Text Input-Case Control Section". This command will indicate that the headers KMAT and MMAT will define the stiffness and mass matrices respectively. The file "file_name.bdf" must be found under the Nastran working directory.

After this point, the system matrices are defined in MSC Patran GUI. With necessary actions needed for MSC Nastran solver (like defining subcase parameters), either static or modal analysis can be performed using this finite element model.

APPENDIX C

Obtaining the Modal Sensitivities Using MSC Nastran SOL200

The MSC Nastran finite element solver is able to calculate the sensitivities of some design responses (modal variables such as natural frequency and mode shape value are called as “modal responses” in MSC Nastran) with respect to selected design parameters by using the solver SOL 200.

Modal sensitivity in MSC Nastran can be briefly defined as the amount of change in the design response with a unit change in the design parameter.

As is the case for other indirect methods, a least-squares solution is followed for most of the time. The updating parameters will be recomputed for each iteration step and the least-squares solution will be repeated (this procedure will be followed until the updating parameter values converge). An important point about using the sensitivity values is that, the linear extrapolation is valid when the absolute value of the parameter changes is below 10%. The reason for that is the non-linear behavior of the modal responses against modeling changes and misleading effect of sensitivity values under large parameter changes. Enveloping the parameter changes will facilitate the convergence of the solution. For that issue, non-linear least squares solver function of MATLAB program is outstanding. The lower and upper boundaries of the parameter values can be set separately by this command which is embedded in MATLAB. Below is given the command and the related parameters.

*pf=lsqnonlin(@(x) [S*x-res_vek], IV*po, LB*po, UB*po)*

For the above command line, pf is the final parameter vector, po is the initial parameter vector, S is the modal sensitivity matrix, res_vek is the multiplication of the inverse of the modal sensitivity matrix and modal difference vector, IV is the starting point for iterations for non-linear least squares solver, LB is lower bound (ratio) for updating parameter vector, UB is the upper bound (ratio) for the updating parameter vector.

Convergence problems arise if there are more than 2 orders of magnitude difference between different rows of the sensitivity matrix (for example, convergence problems have been faced if no weighting have been applied for an analysis where both eigenvalue and eigenvector sensitivities are used). In order to overcome this difficulty, weighting of the equations are necessary. Weighting is accomplished by a matrix (called the weighting matrix) which is diagonal in form (off-diagonal terms are zeros) and yields the participation factor of each equation in the final solution. There are no definite ways (although there are some rules of thumb) to define the weighting matrix and the analyst should define the values in the weighting matrix through inspection of the sensitivity values.

If there are different mode sets in the two models under consideration and/or if the ranking of the correlating modes in two models are different, then it is crucial to put the sensitivity matrix and the modal response difference vector in order (the equations must be set for correlating modes). The modes can be correlated through inspection of the mode shape animations and/or by examining the MAC matrix. If there are missing modes in a model (usually due to modes that are not excited and/or modes that can not be calculated by finite element analysis and that seem to be the mathematical modes in the modal analysis of the test results), these modes should be ignored (even though they continue to appear in the theoretical model).

Before starting the calculation of the sensitivity values by using the MSC Nastran SOL 200 solver, a finite element model is needed for which mesh, element properties and necessary boundary conditions are all defined. After preparation of the model, it is possible to calculate the sensitivity values by using the MSC Patran 2004 r2 GUI.

First of all, it is necessary to enter the “*Model Variables*” submenu under the “*Tools*” menu. The screenshot of the GUI for this command is shown in Figure 86.

After choosing this submenu, the screen shown in Figure 87 will appear. Available updating properties will appear on the right hand side of the screen if “*Create*” is selected under “*Action*” process and “*Variable*” under “*Object*” process. Available updating parameters are tabulated in Table 12.

After selection of any of the possible specifications defined above, possible parameters become visible on the screen. For example, if it is desired to define the beam dimensions, the screen will become as given in Figure 87.

The box, in which beam section type is set, filters and re-orders the available parameters for the type chosen. After selection of the section from the box in which section names are found, the desired property should be selected. After this point, the software assigns a name for the property. If “*Apply*” is pressed at this point, the parameter is saved in the database file. More than one section can be selected under the section name box. As the software does nomenclature of the updating properties automatically there are no misleading effects in defining the parameters by this way (which is very time saving).

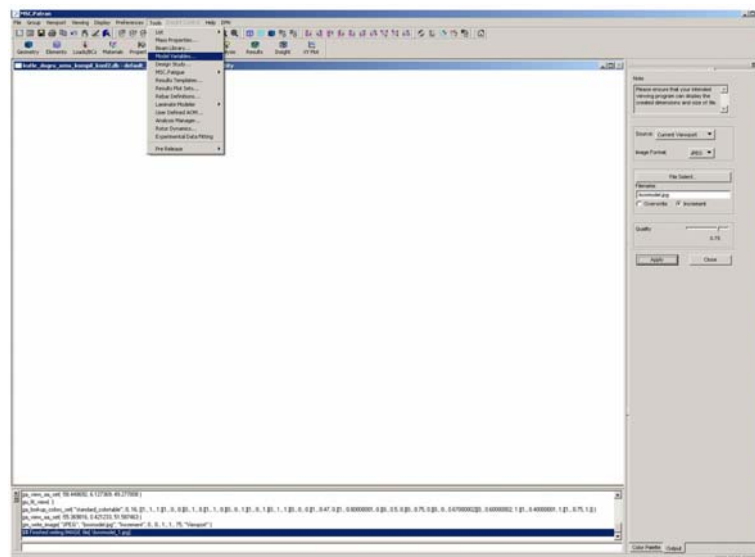


Figure 86. “*Model Variables*” Submenu in MSC PATRAN 2004 r2 GUI

Table 12. Possible Parameters for which Sensitivities can be Calculated

Specification	Possible Parameters
<i>Value</i>	Model Value
<i>Property</i>	Shell thickness, point mass value, spring constant etc
<i>Beam Dimension</i>	Beam element properties (beam height, thickness, width etc.)
<i>Material</i>	Material properties (Young's Modulus, density, Poisson's Ratio etc.)

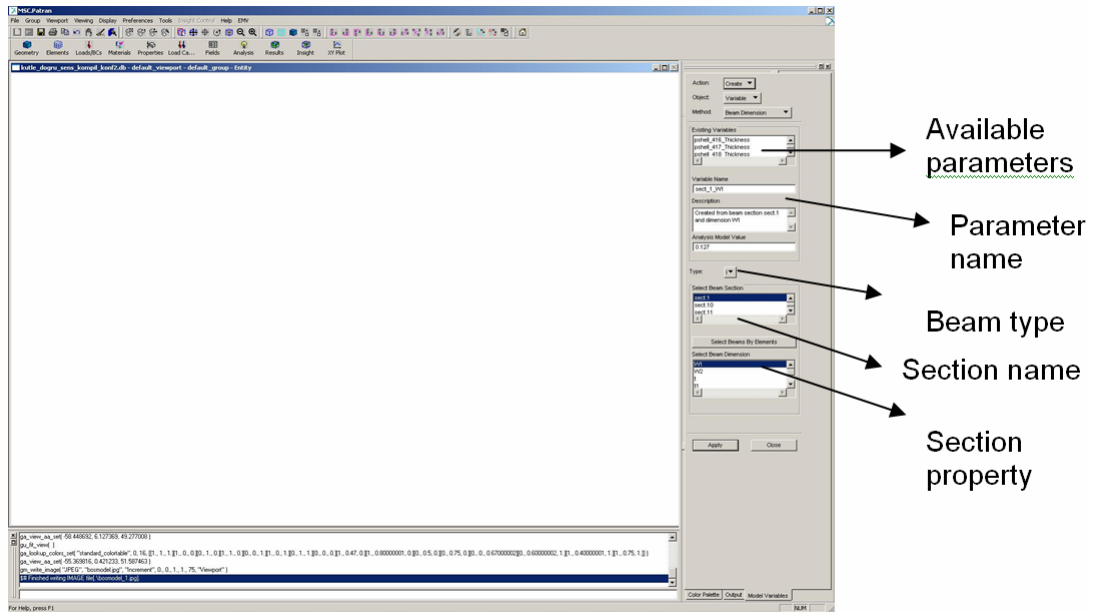


Figure 87. The Screen in MSC PATRAN 2004 r2 GUI in which Beam Dimensions can be Set as Parameters

Setting the material properties as parameters is done in a similar fashion. In Figure 88, the screen of MSC Patran GUI for assigning the material properties as variables is shown.

After defining the variables, the user should enter the “*Design Study*” submenu where updating parameters and design responses are set and these items are

saved under a study. The GUI location of that submenu and the screen that will appear after choosing this submenu are shown in Figure 89 and Figure 90 respectively.

At this point, the desired variables should be selected as updating parameters (undesired ones are omitted). In the resulting result file (with an extension of “f06”) only the sensitivity values of the selected parameters are given. The screen for selecting the parameters is shown in Figure 91.

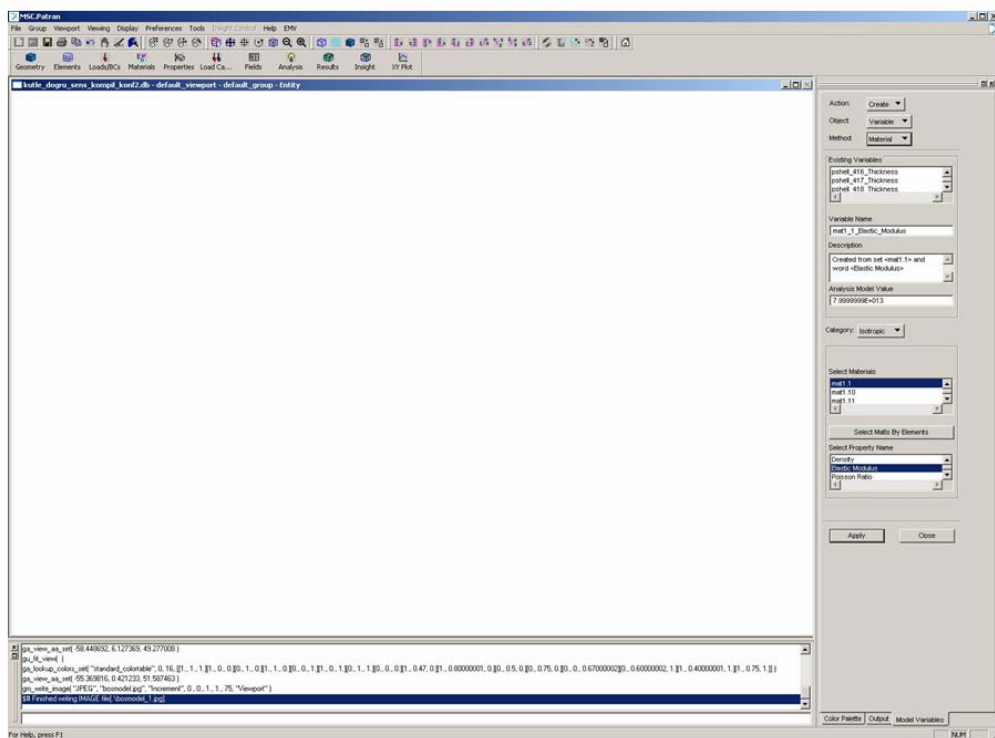


Figure 88. The Screen on which Material Properties are Defined as Design Variables in MSC PATRAN 2004 r2 GUI

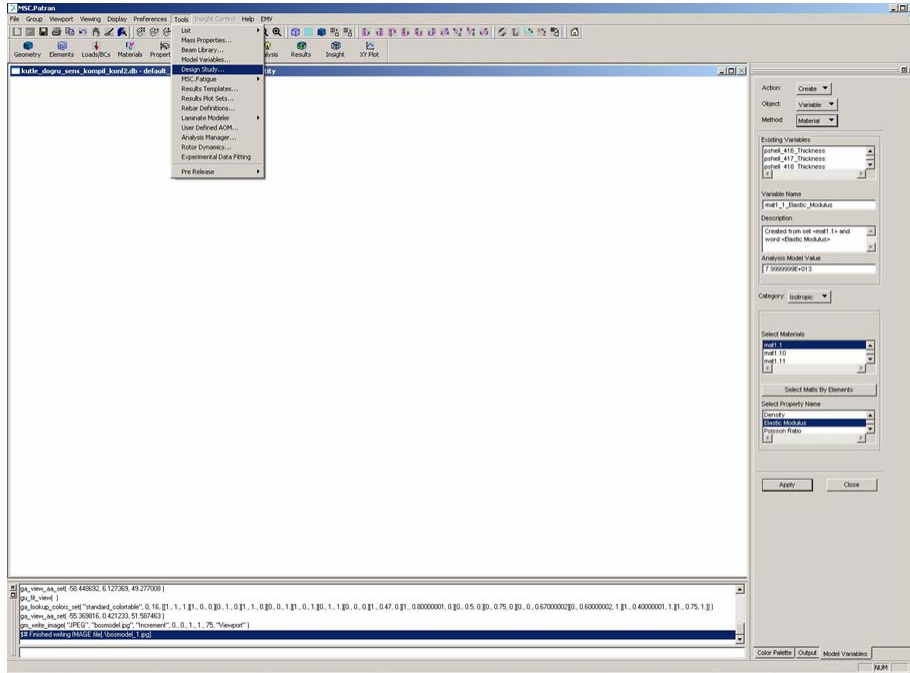


Figure 89. Location of “Design Study” Submenu Under MSC PATRAN 2004 r2

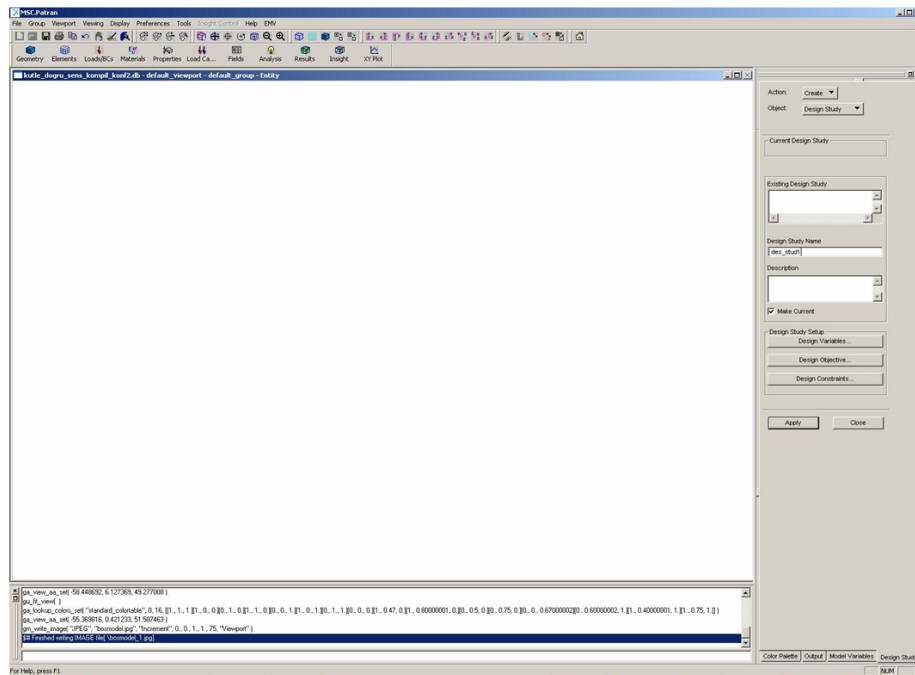


Figure 90. The Screen that Appears After Selection of “Design Study” in MSC PATRAN 2004 r2 GUI

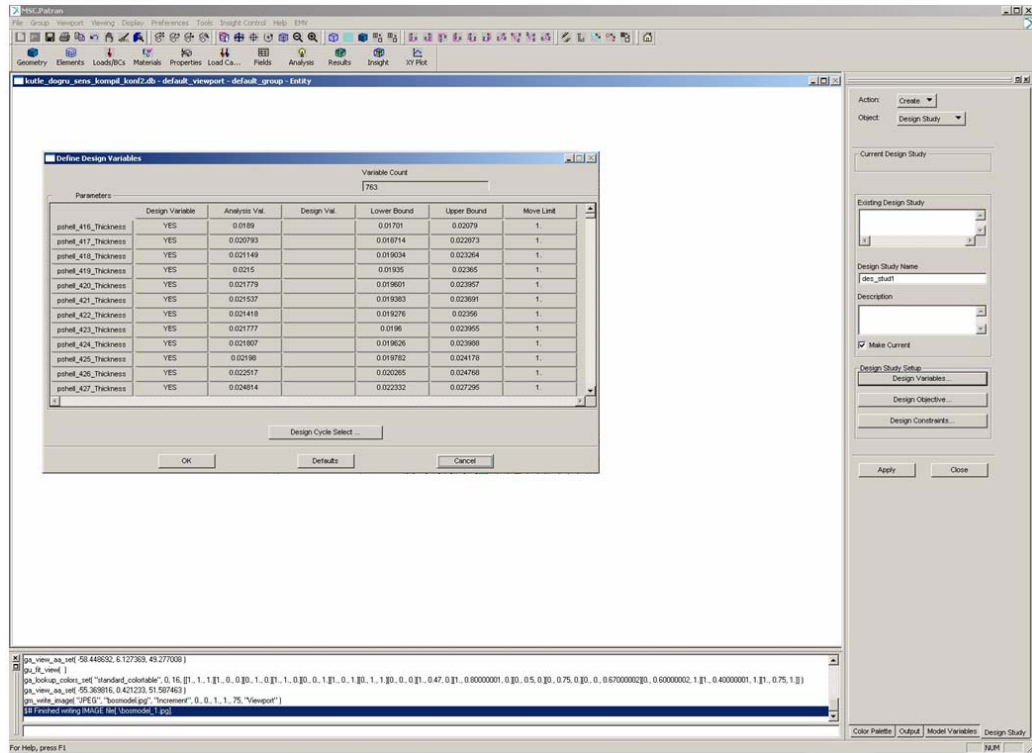


Figure 91. The Screen for Selection of Updating Parameters

MSC Nastran SOL 200 solver is basically designed for design through optimization processes. The optimization process is based on calculating the sensitivities of some basic model responses to model variables and setting the variables in order to reach the desired responses. Sol 200 solver can also output the sensitivity values without any optimization. In order to obtain the sensitivity values, a design objective should be set since the primary objective of the solver is an optimization process. In Figure 92, the GUI screen for selection of the design objective is shown.

After this point, the modal responses for which the sensitivities will be calculated should be chosen. As the sensitivity calculation will be based on modal variables for dynamic finite element model updating procedures, the modal responses that will be chosen will be natural frequencies and eigenvectors.

For selection of the natural frequencies as modal responses, the following should be defined

- The ranking of the mode (among the calculated ones)
- The name of the modal response
- The lower and upper bounds for which the natural frequency is desired to be in (this is for optimization analysis but these values should be in the bulk data file if the sensitivities are to be output). Any two numerical values can be set if the aim is only to obtain the sensitivities.

The screen on which the properties defined above are set is given in Figure 93.

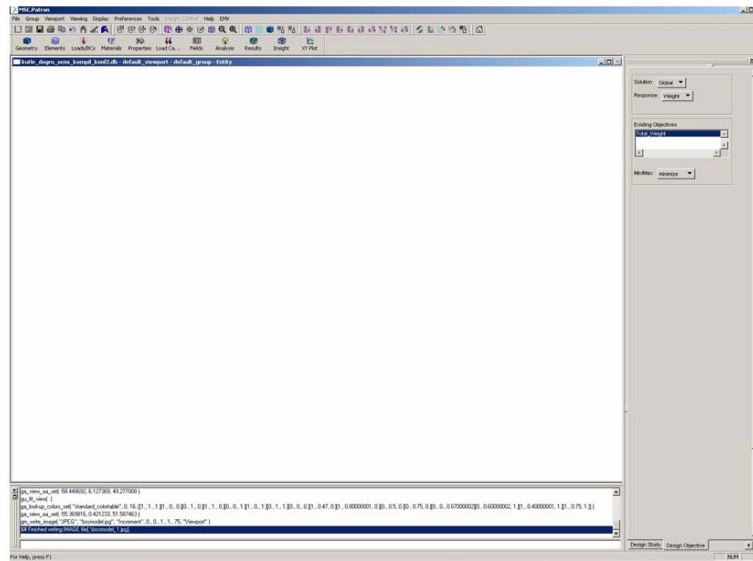


Figure 92. The Screen on which Design Objective is Set in MSC PATRAN 2004 r2 GUI

For the eigenvectors to be set as the modal responses for which the sensitivity values will be calculated, following steps are needed:

- The degree of freedom for which the eigenvector is calculated
- The name of the modal response
- The lower and upper bounds for which the eigenvector value is desired to be in (this is for optimization analysis but these values should be in the bulk data file if the sensitivities are to be output). Any two numerical values can be set if the aim is only to obtain the sensitivities.

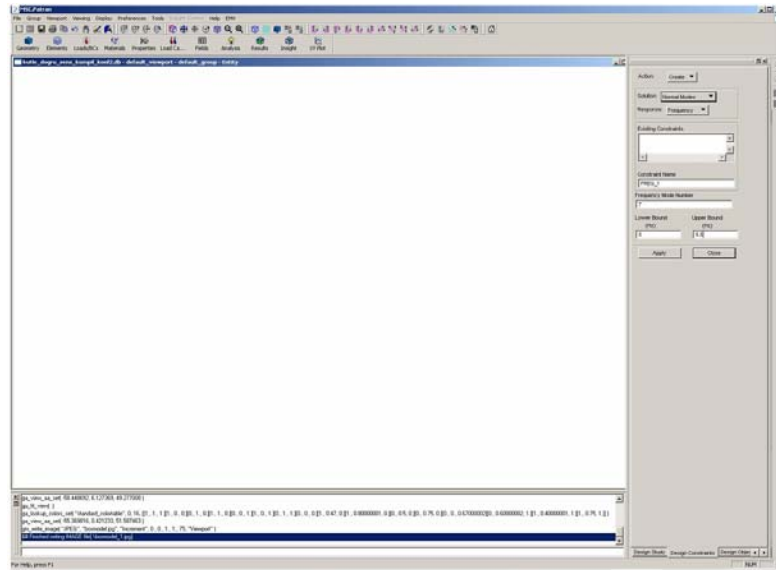


Figure 93. The Screen on which Natural Frequency is Set as a Modal Response for Sensitivity Calculations in MSC PATRAN 2004 r2 GUI

The screen on which the properties defined above are shown is given in Figure 94.

After setting the desired modal responses, the analyst should go back to the “*Design Study*” menu and the design study in which the updating parameters, design objective and modal responses are found, should be saved in the database file.

In order to have the sensitivity values in the output file (*.f06), the analysis type should be chosen as “*Optimization*”. In Table 13, needed sub-menus and entries under “*Analysis*” menu for making a modal sensitivity analysis are given. The screen for these operations is shown in Figure 95.

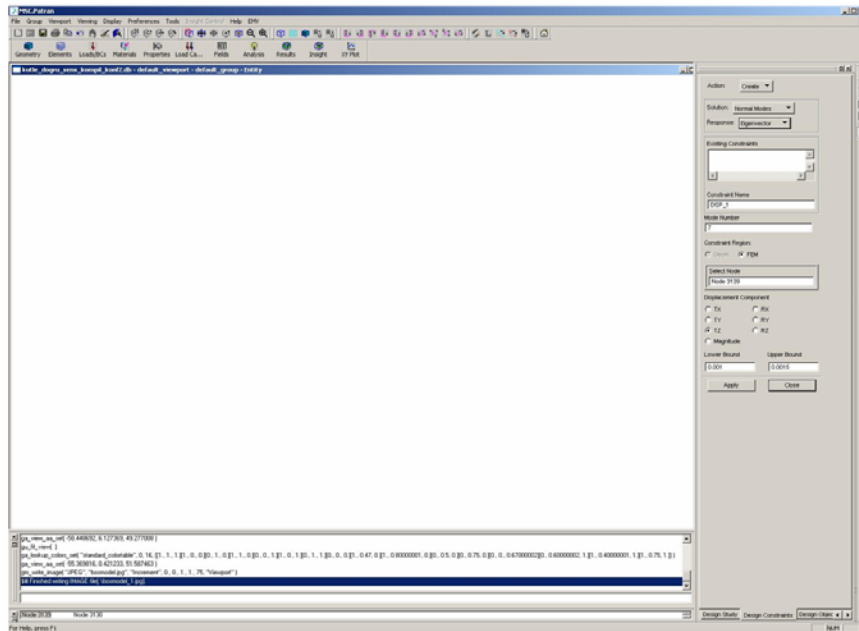


Figure 94. The Screen on which Mode Number, Mode Shape, Node and Degree of Freedom are Selected for Defining Eigenvector as a Modal Response for Sensitivity Calculations in MSC PATRAN 2004 r2 GUI

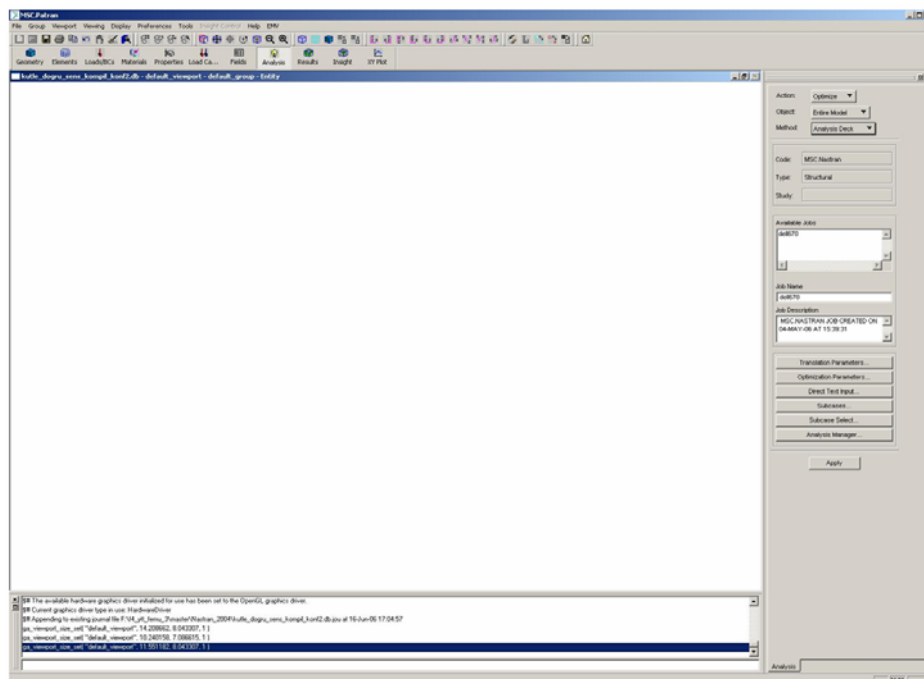


Figure 95. The Screen on which Analysis Settings are Done for a Modal Sensitivity Analysis in MSC PATRAN 2004 r2 GUI

Table 13. Settings for Modal Sensitivity Analysis

Menu	Expression
<i>Action</i>	<i>Optimize</i>
<i>Method</i>	<i>Analysis Deck</i>
<i>Direct Text Input – Case Control Section</i>	<i>DSAPRT(FORMATTED, END=SENS)</i>

The remaining settings shall be done as usual for a modal analysis (the *Subcase* settings) and "Apply" button should be selected for creation of the Nastran input file (*.bdf). The sensitivity values will be output on the result file (*.f06) if the Nastran input file is run with MSC Nastran solver.

Example file formats for weight, natural frequency and eigenvector sensitivities are given in Figure 96, Figure 97 and Figure 98, respectively.

1 Response Type MAY 1, 2006 MSC.NASTRAN 3/24/04 PAGE 588
0 SUBCASE 1

DRESP1 ID=	RESP VALUE	RESPONSE TYPE* WEIGHT	DESIGN VARIABLE	COEFFICIENT	DESIGN VARIABLE	SEID=	COEFFICIENT
1	1.6622E+04	1 SECT_111 7.2520E+00	2 SECT_212 7.2377E+00	3 SECT_313 7.2380E+00			
		4 SECT_214 7.1892E+00	5 SECT_515 7.4042E+00	6 SECT_616 7.4042E+00			
		7 SECT_717 6.2946E+00	8 SECT_818 6.2946E+00	9 SECT_919 6.2946E+00			
		10 SECT_101 6.2946E+00	11 SECT_111 6.2946E+00	12 SECT_122 6.2946E+00			
		13 SECT_133 6.4500E+00	14 SECT_144 4.7322E+00	15 SECT_155 4.7322E+00			
		16 SECT_166 4.7322E+00	17 SECT_177 4.7322E+00	18 SECT_188 4.8074E+00			
		19 SECT_199 5.9332E+00	20 SECT_200 5.9332E+00	21 SECT_211 5.9332E+00			
		22 SECT_222 5.9332E+00	23 SECT_233 5.9346E+00	24 SECT_244 5.9342E+00			
		25 SECT_255 6.0172E+00	26 SECT_266 2.5759E+00	27 SECT_277 1.7401E+00			
		28 SECT_288 2.4839E+00	29 SECT_299 2.4837E+00	30 SECT_300 2.4555E+00			
		31 SECT_311 3.0165E+00	32 SECT_322 1.6254E+00	33 SECT_333 1.6251E+00			
		34 SECT_344 1.6839E+00	35 SECT_355 1.5105E+00	36 SECT_366 1.5112E+00			
		37 SECT_377 1.0734E+01	38 SECT_388 3.0734E+01	39 SECT_399 3.9926E+01			
		40 SECT_400 2.7856E+01	41 SECT_411 2.7876E+01	42 SECT_422 2.4669E+01			
		43 SECT_433 2.7856E+01	44 SECT_444 2.5374E+01	45 SECT_455 2.5160E+01			
		46 SECT_466 7.7252E+00	47 SECT_477 3.8163E+01	48 SECT_488 1.8153E+01			
		49 SECT_499 1.9699E+00	50 SECT_500 1.9699E+00	51 SECT_511 1.4800E+00			
		52 SECT_522 1.4800E+00	53 SECT_533 1.2163E+00	54 SECT_544 1.2163E+00			
		55 SECT_555 1.0427E+00	56 SECT_566 1.0427E+00	57 SECT_577 1.0291E+00			
		58 SECT_588 1.0291E+00	59 SECT_599 1.0233E+00	60 SECT_600 1.0233E+00			
		61 SECT_611 9.3777E-01	62 SECT_622 9.3777E-01	63 SECT_633 9.2545E-01			
		64 SECT_644 9.2545E-01	65 SECT_655 1.5621E+00	66 SECT_666 1.5621E+00			
		67 SECT_677 1.6880E+00	68 SECT_688 1.6880E+00	69 SECT_699 1.2213E+00			
		70 SECT_700 1.2213E+00	71 SECT_711 1.0586E+00	72 SECT_722 1.0586E+00			
		73 SECT_733 9.4885E-01	74 SECT_744 8.4413E-01	75 SECT_755 9.4885E-01			
		76 SECT_766 9.4885E-01	77 SECT_777 8.7838E-01	78 SECT_788 8.7838E-01			
		79 SECT_799 7.9085E-01	80 SECT_800 7.9085E-01	81 SECT_811 7.0045E-01			
		82 SECT_822 7.9085E-01	83 SECT_833 1.2494E+00	84 SECT_844 1.2494E+00			
		85 SECT_855 1.4873E+00	86 SECT_866 1.4873E+00	87 SECT_877 8.6398E-01			
		88 SECT_888 8.6398E-01	89 SECT_899 8.3222E-01	90 SECT_900 8.3222E-01			
		91 SECT_911 6.6927E-01	92 SECT_922 6.6927E-01	93 SECT_933 8.7814E-01			
		94 SECT_944 8.7814E-01	95 SECT_955 6.2922E-01	96 SECT_966 6.2922E-01			
		97 SECT_977 6.0266E-01	98 SECT_988 6.0266E-01	99 SECT_999 5.9944E-01			
		100 SECT_100 5.9944E-01	101 SECT_101 7.9278E-01	102 SECT_102 7.9278E-01			
		103 SECT_103 3.9355E+00	104 SECT_104 3.9355E+00	105 SECT_105 1.6516E+00			
		106 SECT_106 1.6516E+00	107 SECT_107 1.8333E+00	108 SECT_108 1.8333E+00			
		109 SECT_109 1.3961E+00	110 SECT_110 1.3961E+00	111 SECT_111 2.5224E+00			
		112 SECT_112 2.5224E+00	113 SECT_113 9.7694E-01	114 SECT_114 9.7694E-01			
		115 SECT_115 1.2594E+00	116 SECT_116 1.2594E+00	117 SECT_117 1.2594E+00			
		118 SECT_118 1.2594E+00	119 SECT_119 1.2594E+00	120 SECT_120 1.2594E+00			
		121 SECT_121 4.0233E+00	122 SECT_122 4.0233E+00	123 SECT_123 4.0233E+00			
		124 SECT_124 4.0233E+00	125 SECT_125 4.0246E+00	126 SECT_126 4.0233E+00			
		127 SECT_127 4.0246E+00	128 SECT_128 4.0235E+00	129 SECT_129 4.0235E+00			
		130 SECT_130 3.3354E+00	131 SECT_131 3.3339E+00	132 SECT_132 3.7089E+00			
		133 SECT_133 3.7108E+00	134 SECT_134 3.6636E+00	135 SECT_135 3.7089E+00			
		136 SECT_136 3.7089E+00	137 SECT_137 4.2272E+00	138 SECT_138 3.2014E+00			
		139 SECT_139 3.3025E+00	140 SECT_140 2.9059E+00	141 SECT_141 1.1750E+01			
		142 SECT_142 1.1761E+01	143 SECT_143 1.1762E+01	144 SECT_144 1.1760E+01			
		145 SECT_145 1.1815E+01	146 SECT_146 1.6460E+01	147 SECT_147 1.6462E+01			
		148 SECT_148 1.0981E+01	149 SECT_149 1.0981E+01	150 SECT_150 1.0974E+01			
		151 SECT_151 1.0871E+01	152 SECT_152 6.7425E+00	153 SECT_153 6.7449E+00			
		154 SECT_154 6.7480E+00	155 SECT_155 6.7077E+00	156 SECT_156 1.1549E+01			
		157 SECT_157 1.1553E+01	158 SECT_158 1.1464E+01	159 SECT_159 7.6096E+00			
		160 SECT_160 7.6135E+00	161 SECT_161 7.6146E+00	162 SECT_162 4.1815E+00			
		163 SECT_163 4.1790E+00	164 SECT_164 4.1799E+00	165 SECT_165 4.2081E+00			
		166 SECT_166 8.1843E+00	167 SECT_167 8.6201E+00	168 SECT_168 8.6170E+00			
		169 SECT_169 8.6101E+00	170 SECT_170 7.2324E+00	171 SECT_171 7.2355E+00			

Figure 96. Example File Format for Weight Sensitivity Values

Modal Response Type				Mode Number				SUBCASE 1																																																																																																																																																																																																																																																																																																																																																																																																																																																																																					
DRSP1 ID=	B6	RESPONSE TYPE=	FREQ	MODE ID=	ID	SEID=	O	DRSP1 ID=	B6	RESPONSE TYPE=	FREQ	MODE ID=	ID	SEID=	O																																																																																																																																																																																																																																																																																																																																																																																																																																																																														
SUBCASE	RESP VALUE	DESIGN VARIABLE	COEFFICIENT	DESIGN VARIABLE	COEFFICIENT	DESIGN VARIABLE	COEFFICIENT	SUBCASE	RESP VALUE	DESIGN VARIABLE	COEFFICIENT	DESIGN VARIABLE	COEFFICIENT	DESIGN VARIABLE	COEFFICIENT																																																																																																																																																																																																																																																																																																																																																																																																																																																																														
1	1.0142E+01	SECT_113	1.0000E-03	2	SECT_212	7.9705E-04	3	SECT_313	4.9341E-04	4	SECT_414	3.8459E-04	5	SECT_515	3.6898E-04	6	SECT_616	1.6231E-04	7	SECT_717	1.0579E-04	8	SECT_818	-9.1240E-05	9	SECT_919	-2.2393E-04	10	SECT_1020	-1.7584E-04	11	SECT_1121	-1.4588E-04	12	SECT_1222	-1.2298E-04	13	SECT_1323	-3.6366E-04	14	SECT_1424	-2.6859E-04	15	SECT_1525	-3.5901E-04	16	SECT_1626	-3.5901E-04	17	SECT_1727	-3.5901E-04	18	SECT_1828	-4.3072E-04	19	SECT_1929	-7.3834E-04	20	SECT_2030	-8.1214E-04	21	SECT_2131	-9.1762E-04	22	SECT_2232	-3.9797E-04	23	SECT_2333	-4.2502E-04	24	SECT_2434	-4.5674E-04	25	SECT_2535	-4.9770E-04	26	SECT_2636	-1.6547E-04	27	SECT_2737	-1.1051E-04	28	SECT_2838	5.1445E-04	29	SECT_2939	4.7152E-04	30	SECT_3040	7.5801E-04	31	SECT_3141	-1.4863E-05	32	SECT_3242	-4.5079E-05	33	SECT_3343	-7.8894E-05	34	SECT_3444	4.8357E-05	35	SECT_3545	-2.4540E-05	36	SECT_3646	4.6747E-05	37	SECT_3747	3.5377E-05	38	SECT_3848	-5.8895E-05	39	SECT_3949	-1.5929E-04	40	SECT_4050	-1.9707E-04	41	SECT_4151	-1.9707E-04	42	SECT_4252	-2.5198E-05	43	SECT_4353	-1.1357E-04	44	SECT_4454	-1.0573E-04	45	SECT_4555	-1.1357E-04	46	SECT_4656	-3.7469E-05	47	SECT_4757	-9.3347E-05	48	SECT_4858	-9.3347E-05	49	SECT_4959	4.6419E-04	50	SECT_5060	2.4690E-04	51	SECT_5161	6.3197E-04	52	SECT_5262	2.2285E-04	53	SECT_5363	3.7247E-04	54	SECT_5464	8.5424E-05	55	SECT_5565	2.4875E-04	56	SECT_5666	8.7087E-05	57	SECT_5767	4.4013E-04	58	SECT_5868	3.1215E-04	59	SECT_5969	3.1215E-04	60	SECT_6070	1.5892E-04	61	SECT_6171	1.5892E-04	62	SECT_6272	1.3494E-04	63	SECT_6373	6.9301E-05	64	SECT_6474	5.1819E-05	65	SECT_6575	2.5612E-05	66	SECT_6676	2.2123E-05	67	SECT_6777	4.3263E-04	68	SECT_6878	2.4260E-04	69	SECT_6979	4.6995E-04	70	SECT_7080	5.3012E-04	71	SECT_7181	1.0045E-03	72	SECT_7282	6.7098E-04	73	SECT_7383	7.3627E-04	74	SECT_7484	5.0792E-04	75	SECT_7585	4.4941E-04	76	SECT_7686	3.0137E-04	77	SECT_7787	1.6488E-04	78	SECT_7888	1.1076E-04	79	SECT_7989	2.6616E-05	80	SECT_8090	1.7675E-05	81	SECT_8191	-4.8657E-05	82	SECT_8292	-3.2363E-05	83	SECT_8393	-1.6603E-04	84	SECT_8494	-1.6603E-04	85	SECT_8595	-4.1125E-04	86	SECT_8696	-2.9875E-04	87	SECT_8797	-2.3647E-04	88	SECT_8898	-1.7025E-04	89	SECT_8999	-2.5082E-04	90	SECT_9000	-1.7864E-04	91	SECT_9101	-2.2069E-04	92	SECT_9202	-1.5593E-04	93	SECT_9303	-3.3347E-04	94	SECT_9404	-2.3214E-04	95	SECT_9505	-2.3564E-04	96	SECT_9606	-1.7716E-04	97	SECT_9707	-2.6218E-04	98	SECT_9808	-1.8008E-04	99	SECT_9909	-2.7658E-04	100	SECT_10010	-1.8906E-04	101	SECT_10111	-4.0550E-04	102	SECT_10212	-2.7568E-04	103	SECT_10313	-2.7999E-03	104	SECT_10414	-1.9831E-03	105	SECT_10515	-1.2498E-03	106	SECT_10616	-8.8005E-04	107	SECT_10717	-1.4299E-03	108	SECT_10818	-1.0020E-03	109	SECT_10919	-1.1175E-03	110	SECT_11020	-7.8021E-04	111	SECT_11121	-2.0598E-03	112	SECT_11222	-1.4858E-03	113	SECT_11323	-8.3711E-04	114	SECT_11424	-5.7947E-04	115	SECT_11525	-1.1079E-03	116	SECT_11626	-7.6495E-04	117	SECT_11727	-1.1366E-03	118	SECT_11828	-7.8266E-04	119	SECT_11929	-1.1690E-03	120	SECT_12030	-8.0209E-04	121	SECT_12131	1.6367E-03	122	SECT_12232	2.7605E-04	123	SECT_12333	1.1491E-04	124	SECT_12434	8.8552E-05	125	SECT_12535	7.5227E-05	126	SECT_12636	1.2550E-04	127	SECT_12737	2.3712E-04	128	SECT_12838	5.6694E-04	129	SECT_12939	9.7706E-04	130	SECT_13040	1.6193E-03	131	SECT_13141	1.5052E-03	132	SECT_13242	1.9611E-03	133	SECT_13343	2.3719E-03	134	SECT_13444	3.0205E-03	135	SECT_13545	3.8476E-03	136	SECT_13646	4.2965E-03	137	SECT_13747	2.1125E-02	138	SECT_13848	5.7465E-02	139	SECT_13949	5.2080E-04	140	SECT_14050	3.4214E-02	141	SECT_14151	1.7221E-03	142	SECT_14252	3.6704E-04	143	SECT_14353	1.0103E-03	144	SECT_14454	1.7221E-03	145	SECT_14555	2.2440E-03	146	SECT_14656	3.5057E-03	147	SECT_14757	9.9197E-03	148	SECT_14858	9.1597E-03	149	SECT_14959	1.1775E-02	150	SECT_15060	1.5042E-02	151	SECT_15161	1.6248E-02	152	SECT_15262	2.0239E-02	153	SECT_15363	2.9061E-02	154	SECT_15464	4.3140E-02	155	SECT_15565	3.9514E-02	156	SECT_15666	1.4947E-01	157	SECT_15767	2.6770E-01	158	SECT_15868	1.0489E-01	159	SECT_15969	-2.5260E-04

Figure 97. Example File Format for Natural Frequency Sensitivity Values

In order not to change the mass matrix throughout the updating procedure, the weight sensitivities (for which an example file format is given in Figure 96) should be used (if density or geometrical dimensions are chosen as updating properties). The following equation should be inserted in the equation set for natural frequency and eigenvectors.

$$\left\{ S_w^{p1} \quad S_w^{p2} \quad S_w^{p3} \quad S_w^{p4} \right\} \begin{Bmatrix} p1 \\ p2 \\ p3 \\ p4 \end{Bmatrix}_f = \left\{ S_w^{p1} \quad S_w^{p2} \quad S_w^{p3} \quad S_w^{p4} \right\} \begin{Bmatrix} p1 \\ p2 \\ p3 \\ p4 \end{Bmatrix}_o \quad (C.1)$$

In the above expression, p_i is the i^{th} parameter, $S_w^{p_i}$ is the sensitivity of the weight against the i^{th} parameter, $\{ \}_f$ is the final parameter vector and $\{ \}_o$ is the initial parameter vector.

